國立交通大學
電機與控制工程學系
碩士論文

PDMS 在微機電的應用

Application of PDMS in MEMS

研究生：王嘉豪
指導教授：邱一助理教授

中華民國九十三年十月

PDMS 在微機電的應用

Application of PDMS in MEMS

研究生：王嘉豪　　Student：Chia-Hao Wang

指導教授：邱一　　Advisor：Yi Chiu

國立交通大學 電機資訊學院

電機與控制工程學系

碩士論文

A Thesis

Submitted to Department of Electrical and Control Engineering
College of Electrical Engineering and Computer Science
National Chiao Tung University
In Partial Fulfillment of the Requirement
For the Degree of
Master
In

Electrical and Control Engineering

October 2004

Hsinchu, Taiwan, R.O. C

中華民國九十三年十月

中文摘要

近年來，PDMS 相關的研究越來越頻繁了，不論是微流道網路，或者是薄膜、微閥門，PDMS 都展現了製造的方便性以及優良的機械特性。本每研究中將會提出兩個使用 PDMS 來製做的元件，首先是一個在上下電極板中包含有一個 PDMS 結構的軸向靜電致動器。這種致動器使用 PDMS 的彈性，當一個 PDMS 的結構受到上下電極板的擠壓，它會產生一個和壓縮量成非線性的回復力。靜電力的非線性特性會讓一個軸向的靜電力發生 pull in 的現像，而讓可移動的距離只有原間隙的 1/3。但是利用這一個非線性的回復力可以增加軸向致動器的可移動距離。本研究中致動器的可移動距離達到了原間隙的 54%。

第二個元件是使用 PDMS 製做懸臂樑。和一般微機電常用的結構層材料 polysilicon 相比，PDMS 的楊氏系數大約比的小了 5 個數量級，所以這種元件的驅動電壓會很小。此外，適合 PDMS 的製程會能夠經由在製做此元件的過程中發展出來。然而在本研究中並沒有完成此一元件的製做，PDMS 本身的楊氏系數小而讓它不容易懸浮。但是在本研究中以經成功的蝕刻定義了一層旋塗的 PDMS 膜。

Abstract

PDMS is a frequently used material in MEMS applications. Whether the systems such as microfluidic networks or the devices such as membranes and valves, PDMS is easy to fabricate and exhibit excellent mechanical properties. In this study, PDMS will be used to fabricate two devices. The first one is a gap-closing actuator with PDMS posts placed between the electrodes. Such a device employs the elasticity of PDMS. When a small PDMS post is compressed by two parallel plates, it undergoes a large deformation and therefore provides elastic restring force that is nonlinear with the compressive displacement. The nonlinear elastic restoring force of the PDMS post will be used to balance the nonlinear electrostatic force. Because the elastic restoring force is nonlinear, the gap-closing actuator can achieve a larger controllable displacement than the actuator with linear elastic structure. The measured data of this device reveal that the nonlinear elastic restoring of the PDMS posts can extend the controllable displacement of a gap-closing actuator. The controllable displacement achieves the 54% of the original gap.

The second device is PDMS cantilever beams. The Young's modulus of PDMS is about 5 orders less than the polysilicon, which is a common by used structure material in MEMS. Therefore, to actuate such a device, the applied voltage will be much less. Besides, by fabricating such a device, the properties of PDMS can be obtained and the processes suitable for PDMS fabrication will be developed. But the results of the fabrication process reveal that the stiffness of PDMS is too small to suspend itself. However, processes to pattern a spun on PDMS layer was developed successfully.

Acknowledgement

I would like to thank my advisor, Prof. Yi Chiu. In these two years, he gave me a lot of guidance and taught me the right attitude. He also inspired my interest in research, and widened my horizon.

I would also like to thank National Nano Device Laboratories for the providing of the clean rooms and the instruments. I also thank the people who have taught me and helped me in the clean room. I will not accomplish my work without them.

Thank all the people in the PSOC laboratory. They gave me attention and accompany me in my hard time. My life was full of happiness with them.

Thank my parents and families. They encouraged and supported me, so I could keep research with nothing to worry. And my girl friend, she relaxed my when I felt nervous, and also inspired me.

Thanks the teachers and friends of Zen club. They enabled me to concentrate and taught me the meaning of life, thus I am no longer in a maze.

Thank you very much!

Table of Content

List of Figures

List of Tables

Ⅰ、Introduction

MicroElectroMechanical System (MEMS) is a technology employing semiconductor fabrication processes to fabricate miniaturized mechanical devices. Compared with conventional mechanical devices, the miniaturized devices have the characteristics of shorter response time and less power consumption. In addition, MEMS devices and signal processing circuits can be fabricated on the same chip to reduce the noise and signal distortion. In the recent years, MEMS technology has grown from research projects of laboratories to commercially available products such as the Digital Mirror Device of TI and accelerometer of Analog Device.

Actuators are critical devices in MEMS technology. Their main functions are to produce a displacement output to actuate other mechanical structures. According to the principle of actuation, most MEMS actuators can be classified as electrostatic, electro-thermal, electromagnetic, and piezoelectric types. Among those, electrostatic actuators have the advantage of low power consumption, short response time, and compatibility with IC fabrication processes. Therefore the application of electrostatic actuators is widespread. In electrostatic actuators, the electrostatic force is produced by applying a voltage across two closely spaced electrodes. The force acts on the actuator structure and result in displacement. According to the direction of displacement, electrostatic actuators can be classified as laterally and axially driven types, as shown in Figure 1-1.

When a voltage is applied to a laterally driven actuator, the electrodes are displaced perpendicularly to the direction of electric field, as shown in Figure 1-1 (a). The gap between electrodes does not change with displacement. Comb drive actuators, as shown in Figure 1-2, are typical laterally driven electrostatic actuators [1].

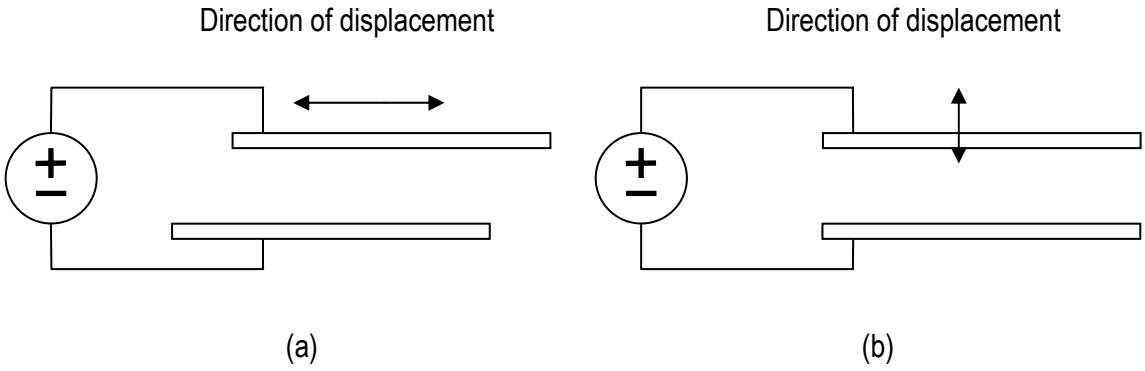

Figure 1-1 (a) Laterally driven actuator. (b) Axially driven actuator.

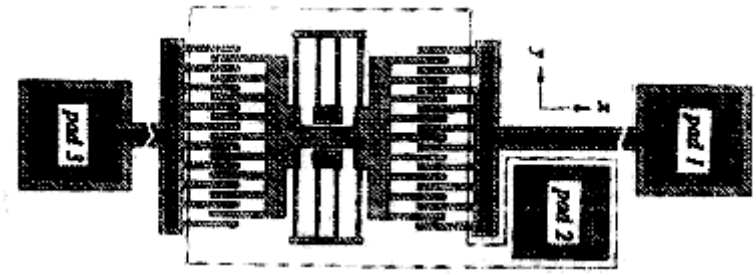

Figure 1-2 Comb drives, the typical laterally driven actuators.

Axially driven actuators are also called gap-closing actuators, as shown in Figure 1-1 (b). In axially-driven actuators, the displacement is in the same direction as the electrostatic field. The driving force in such an actuator is inversely proportional to the square of the gap distance between electrodes ($F \propto 1/d^2$). The nonlinear electrostatic driving force and linear elastic restoring force cause the so-called pull in effect. When the actuator is driven beyond a displacement of one third of the original gap distance, the electrostatic force becomes too large to be balanced by the elastic restoring force. The two electrodes will be brought into contact. Therefore, one third of the original gap distance is the limit of controllable distance. To increase the controllable distance, several strategies have been presented, such as feedback capacitance, current driving, and dimension design. In this study, structures that provide nonlinear restoring force will be used to balance to nonlinear electrostatic

force. Since the electrostatic force and the restoring force are both nonlinear, the behavior of such a device will be more linear.

With regard to the pull-in problem, an innovated micromechanical structure is proposed in this research. In this structure, small elastomer structures are placed between two electrodes to provide additional restoring force. When the elastomer structure is compressed by two parallel plates, it undergoes a large deformation and will provide a nonlinear elastic restoring force. Therefore, it can be used to balance the nonlinear electrostatic force and increase the controllable actuation distance. The elastomer structure is a critical part in this device. It will be compressed by parallel plates through electrostatic force, so it must be very flexible and be able to undergo large deformation. For materials used in IC processes such as polysilicon, silicon dioxide, silicon nitride, aluminum, and other metals, their Young's moduli range from 50GPa to 200GPa. So they can not be taken as the material of elastomer structures.

Polymers such as PDMS, parylene, polyimide, PMMA, and SU-8 are frequently used in MEMS applications. Among the common used polymers in MEMS, PDMS exhibits rubbery elasticity and its elongation at break can achieve 140%. Furthermore, it possesses high chemical stability and various etching agents such as BOE, HF, HNO_3, CH_3COOH, and H_3PO_4 are allowable in the process. Therefore, PDMS will be taken as the material for the elastomer structures in this study. In addition, to investigate the mechanical properties, cantilever beams made of PDMS would also be fabricated in this study.

PDMS (poly-dimethylsiloxane) is a linear polymer. Before curing, it is a viscous liquid, with a linear Si-O backbone and two methyl group attached to each Si atom. Figure 1-3 (a) is the chemical structure of PDMS. After mixed with the curing agent,

cross link reaction takes place. Curing agent include the cross link agent and catalyst. The crosslink agent is the partly hydrogenated PDMS, whose chemical structure is shown in Figure 1-3 (b). When the cross link reaction takes place, the H group on the cross link agent will react with the $CH=CH_2$ group on the terminal of PDMS, and bond them together [2]. Figure 1-3 (c) shows the chemical structure of the cross linked PDMS. Therefore, through the cross link agent, cross linked PDMS forms a three-dimensional network, and PDMS is transformed from viscous liquid to elastomer. Figure 1-3 (d) shows the sketch of the network. PDMS elastomer is extremely flexible at room temperature. The limit of compression and extension of PDMS is far beyond metal and other materials. Therefore, it is widely used in conventional mechanical components such as shock absorbers, bearings, and other structures that require large deformation. Table 1-1 shows elongation of various materials.

Table 1-1 Percent elongation limit of materials [3].

Material	Percent elongation
Aluminum alloys	1-45
Brass	4-60
Copper and copper alloys	4-50
Magnesium alloys	2-20
Nickel	2-50
Nylon	2-100
Polyethylene	15-300
Rubber	100-800

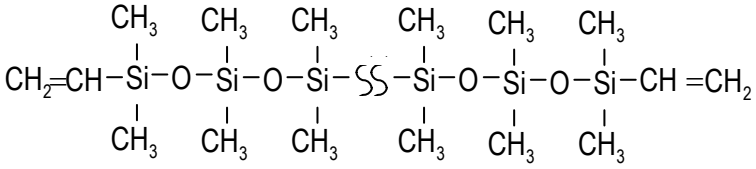

(a)

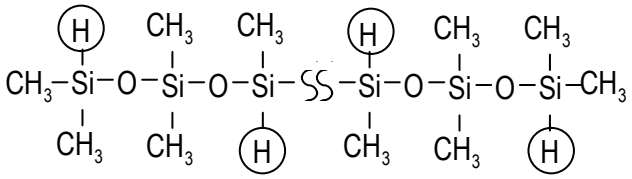

(b)

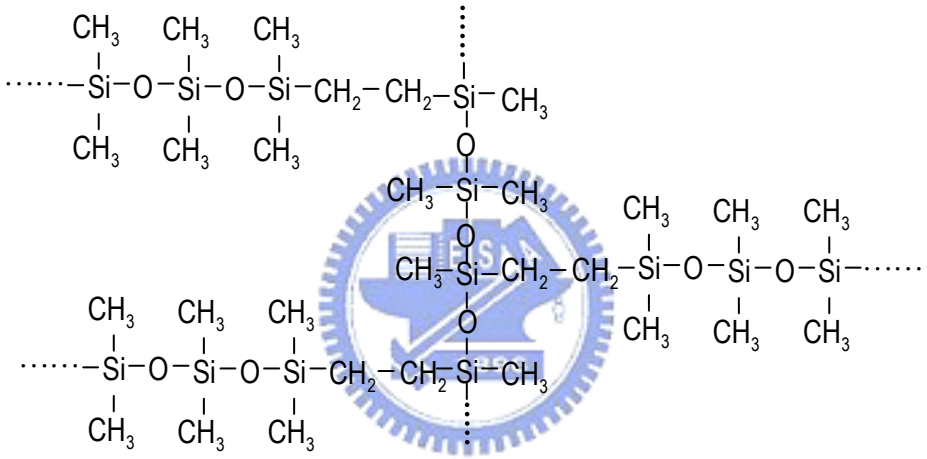

(c)

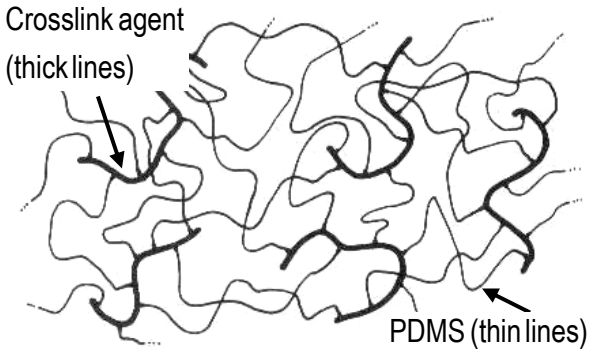

(d)

Figure 1-3 (a) Chemical structure of PDMS, (b) Chemical structure of crosslink agent, (c) Chemical structure of cross linked PDMS, (d) Sketch of network of crosslinked PDMS [2]

1-1 Literature survey

Gap-closing actuator

Gap-closing actuators can be classified as digital control and analog control types. For the digital control type, the input signal has only two states, “high” and “low”, and the output of the device also has two states. Digital control type actuators such as the DMD light switch employ the pull in effect to operate [4]. Figure 1-4 shows the operating concept of DMD. When signal “$\Phi_{address}$” is “high” and “$\overline{\Phi}_{address}$” is “low”, the mirror pulls in with the electrode named “$\Phi_{address}$”, and rotate clockwise. When signal “$\Phi_{address}$” is “low” and “$\overline{\Phi}_{address}$” is “high”, the mirror pulls in with the electrode named “$\overline{\Phi}_{address}$”, and rotate counterclockwise.

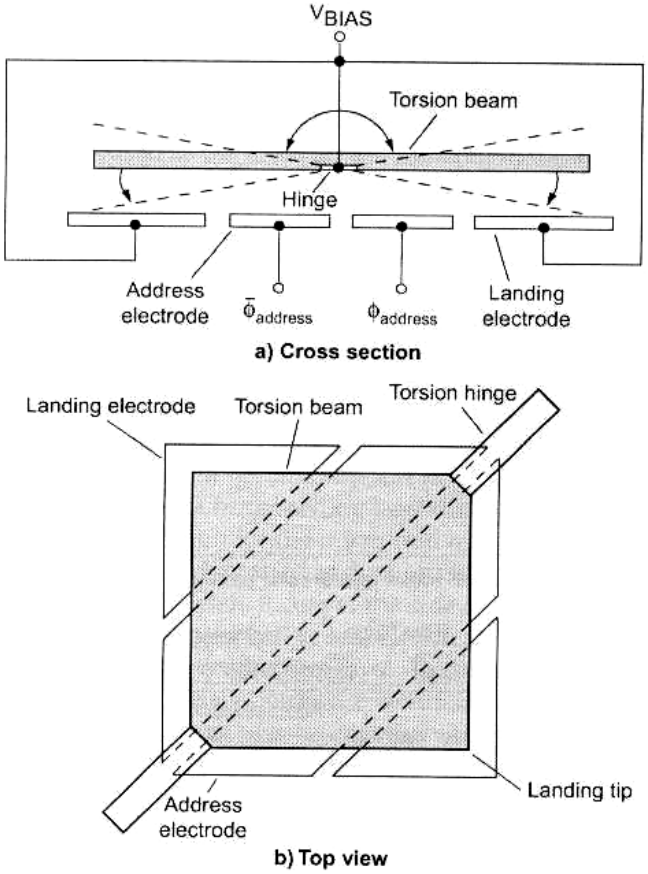

Figure 1-4 The operating concept of DMD [3].

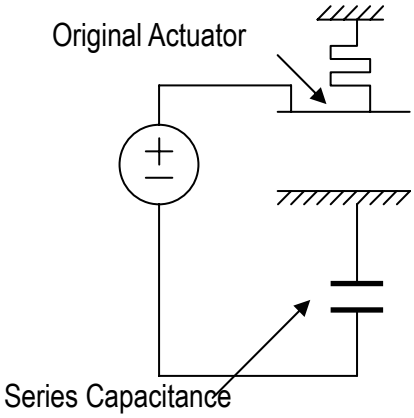

Figure 1-5 Actuator with a series capacitor.

The pull in effect can also be employed to measure air pressure. Raj K. Gupta et al. reported that the pull in time of a gap-closing actuator was sensitive to the ambient air pressure. In their study, fixed-fixed beams were fabricated to be the sensors. It was reported that the pull in time was nearly a linear function of ambient air pressure in the measured range of 0.1 mbar to 1013 mbar. [5].

For analog control gap-closing actuators, only one third of the gap distance can be used due to the pull in effect. Several strategies have been reported to extend this limit. One strategy is to use feedback capacitor to control the actuators. Edward K. Chan et al. employed a series capacitor to provide stabilizing negative feedback [6]. Figure 1-5 shows a device in which a capacitor in series. They reported that the actuator with the series capacitor could go beyond the theoretical limit and reach almost twice the conventional range. However the actuating voltage was higher because the series capacitor divided the voltage.

R. Nadal-Guardia et al. reported two other approaches to control the charge in the actuator by means of current driving [7]. Theoretical equations derived for each method showed that full range of travel could be achieved. Those approaches were

based on the use of current pulses to inject the required amount of charge to fix the position of the movable plate. The first method used a series capacitance to sense the voltage drop produced by the injected charge. The experimental measurement revealed that displacement of 715nm could be achieved with the original gap of 1.5μm. The second approach operated in a open loop configuration. The current source was switched off after injecting the required charge. The experimental measurement revealed that displacement of 870nm could be achieved for the same original gap.

In addition to the approaches that use feedback capacitance or charge controlling to extend the controllable displacement, geometry design to obtain the optimal controllable distance for torsion actuator was also reported. Ofir Degani et al. reported that the relative location of actuating electrodes was an important issue. A new approximated analytical solution was derived for the pull-in angle and pull-in voltage of an electrostatic torsion actuator with rectangular plates [8]. Using those analytical expressions, the optimal design of the torsion actuator and parametric study can be carried out with much less time.

PDMS applications

PDMS is frequently used in microfluidic system due to its bio-compatible property. Because PDMS is cured from liquid, its structure can be formed by molding, and the patterned photoresist is frequently taken as the molds. Molding processes are often used with PDMS due to the low processing temperature and quick turn around time.

Another characteristic of PDMS is that the surface properties of PDMS can be changed by treating it with oxygen plasma. The hydrophobic surface can be converted into hydrophilic. Besides, bonds will from between two surfaces of PDMS if they are

treated with oxygen plasma and then brought into conformal contact. This process can be used to seal the microfluid channels.

David C. Duffy et al. reported a procedure to design and fabricate microfluidic systems in PDMS in less than 24 hours including sealing [9, 10]. The PDMS used in their study was Sylgard 184 from Dow Corning. A network of microfluidic channels (with width >20μm) was designed in a CAD software. The design was converted into a transparency by a high-resolution printer. This transparency was used as a mask in photolithography to create a master in the positive relief photoresist. PDMS cast against the master yielded a polymeric replica containing a network of channels. The surfaces of the replica, and a flat slab of PDMS, were oxidized in oxygen plasma. These oxidized surfaces were sealed tightly and irreversibly when brought into conformal contact. The procedure is shown in Figure 1-6. It was also pointed out that oxidized PDMS also sealed irreversibly to other materials used in microfluidic systems, such as glass, silicon, silicon oxide.

Byung-Ho Jo et al. developed a fabrication technique for building three-dimensional micro-channels in PDMS [11]. The PDMS used in their study is Sylgard 184 from Dow Corning. The process allowed the stacking of many thin (less than 100μm thick) patterned PDMS layers to realize complex 3-D channel paths. The master for each layer was formed on a silicon wafer using an epoxy-based photoresist (SU 8). PDMS was cast against the master producing molded layers containing channels and openings.

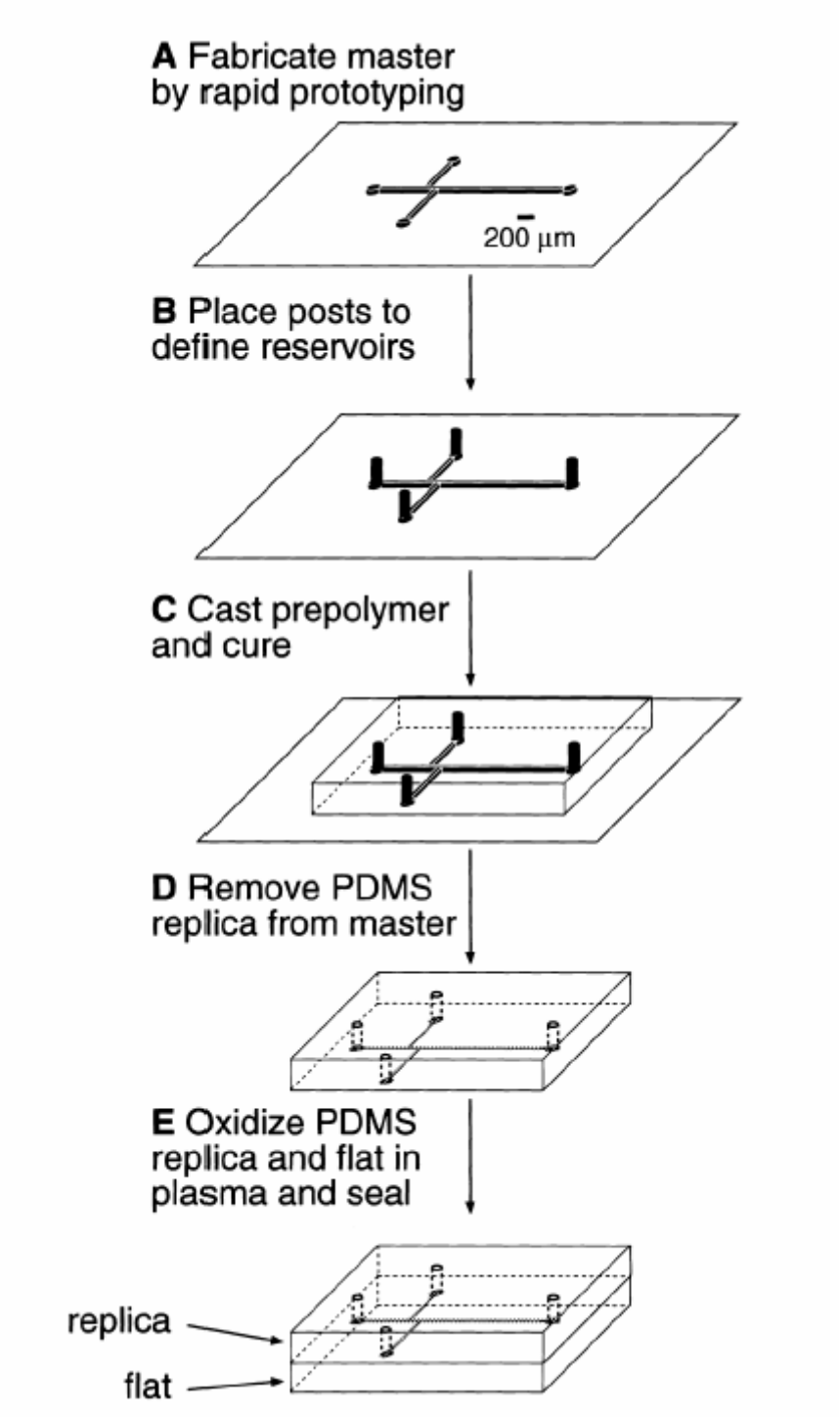

Figure 1-6 The procedure to fabricate a microfluidic system.

J. Garra et al. developed a fluorine-based reactive ion etch (RIE) process to anisotropically dry etch PDMS Sylgard 184 [12]. The technique complements the standard molding procedure. Total gas pressure and the ratio of O_2 and CF_4 were

varied to optimize the etch rate. The RIE recipe developed in their study was 1:3 mixture of O_2 and CF_4 gas, resulting in a highly directional and stable etch rate of approximately 20μm per hour.

For bio-MEMS applications, E. Leclerc et al. developed a three-dimensional PDMS chamber array interconnected by channels for mammalian cell culture [13]. In their research, the device was composed of six stacked PMDS layers with channel networks fabricated on both side of the layers. One side was patterned by SU-8 photoresist molding, and the opposite side was patterned by RIE with an aluminum hard mask. They pointed out that dry etching can be performed with SF_6 for a rate about 0.6μm per minute, and the material kept its biocompatible property despite the dry etching process by plasma treatment.

The mechanical properties of PDMS have also been exploited in various applications; especially, the elasticity has been widely used in mechanical structure. X. Yang et al. employed PDMS to manufacture thermo-pneumatic silicone rubber successfully [14]. In their research, PDMS MRTV 1 is used. Two methods were developed to fabricate PDMS membranes. In Figure 1-7 (a), the silicone rubber was spun on; in Figure 1-7 (b), premixed silicone was poured into the cavities on the wafer front side. By scraping a piece of glass with a flat smooth edge across the wafer, extra silicone was taken away and a layer of silicone was left in the cavity. With regard to the mechanical properties of PMDS, they pointed out that it could sustain elongation as high as 1000%, so very large deflection could be achieved in valve membranes. Besides, sealing of this material on rough surfaces could be very good due to its very low hardness (Shore A 24).

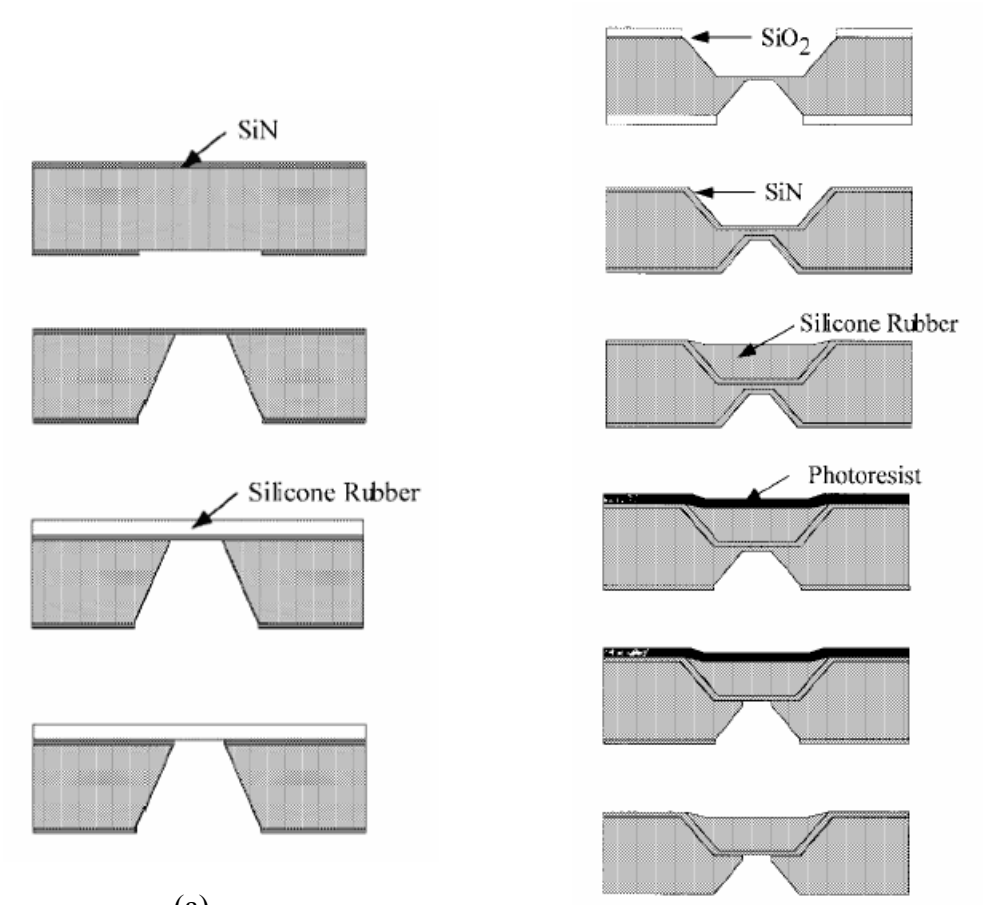

Figure 1-7 (a) Fabrication process for spin-coated silicone rubber membrane (b) Fabrication process for squeegee-coated silicone rubber member.

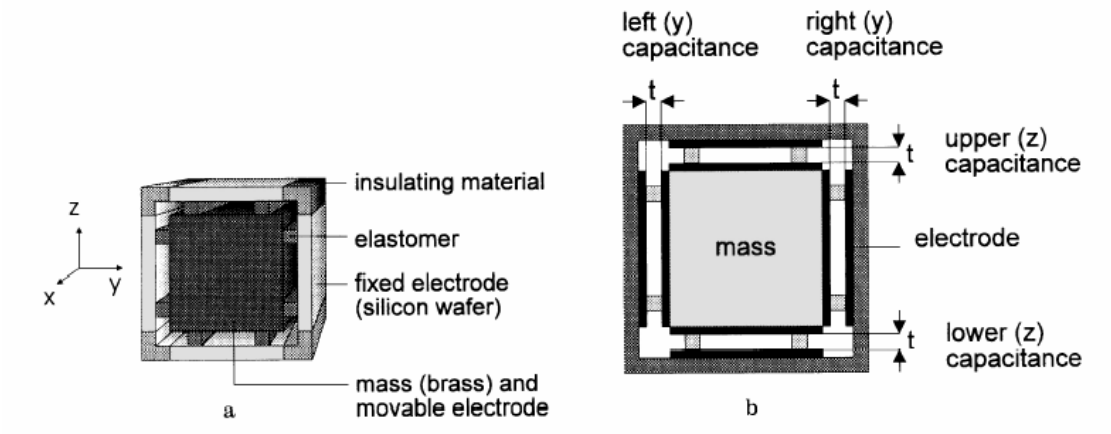

Figure 1-8 Cross-section of the triaxial accelerometer

Lotters et al. reported a triaxial accelerometer that employed PDMS as the spring material and metal as the proof mass to form a spring- mass system [15, 16]. The cross-section of the device is shown in Figure 1-8. They used PDMS PS851 (ABCR) in their research. The PDMS is photocurable, and was patterned with by photolithography.

Referring to the processes of PDMS that have been reported, the processes to produce PDMS posts and PDMS cantilever beams have a roughly outline. The PDMS posts can be produced by molding processes, and the PDMS cantilever beam can be produced by RIE patterning. Further process issues will be discussed later.

1-2 Objective and organization of the thesis

The objectives of this study include:

(a) To develop a nonlinear electrostatic actuator with the PDMS structures placed between two electrodes. With the elastic restoring force of PDMS structures, the controllable displacement of the device can be extended, and the relationship between displacement and applied voltage can be more linear.

(b) To develop PDMS cantilever beams which are actuated by electrostatic force. The mechanical properties of PDMS can be obtained by investigate the behavior of this device.

The fundamental principles of material mechanics, design of PDMS structures and the full device are described in detail in the Chapter 2. The fabrication process, process issues and fabrication results of the actuator with PDMS structures and PDMS cantilever beams are described in Chapter 3. The Measured results and discussion are presented in Chapter 4. The future works are discussed in Chapter 5.

Ⅱ、Principle and Design

In this chapter, basic concepts of material mechanics will be introduced to characterize the mechanical properties of PDMS structures. In the device design, finite element analysis software ANSYS is used to simulate the behavior of the PDMS structure.

2-1 Elasticity

Mechanics of materials deals with the behavior of solid bodies subjected to various types of loading. Elasticity is the property of a solid body to return to its original dimensions upon unloading. In this section, basic concepts of elasticity will be introduced, and properties of various materials will be discussed from the viewpoint of mechanics of materials. The nonlinear elastic restoring force will discussed subsequently.

Stress and Strain

The fundamental concepts in mechanics of materials are stress and strain. These concepts can be illustrated in their most elementary forms by considering a prismatic bar subjected to an axial force. Figure 2-1 shows a prismatic bar in tension, where P is the applied force, L is the original length of the bar, A is the area of the cross section, and L+δ is the length of the bar where P is applied.

The intensity of the force is called the stress and is denoted by the Greek letter σ. If the stress is uniformly distributed over cross section mn, as shown in Figure 2-1 (d), the following expression of the stress can be obtained:

$$\sigma = \frac{P}{A} \tag{2-1}$$

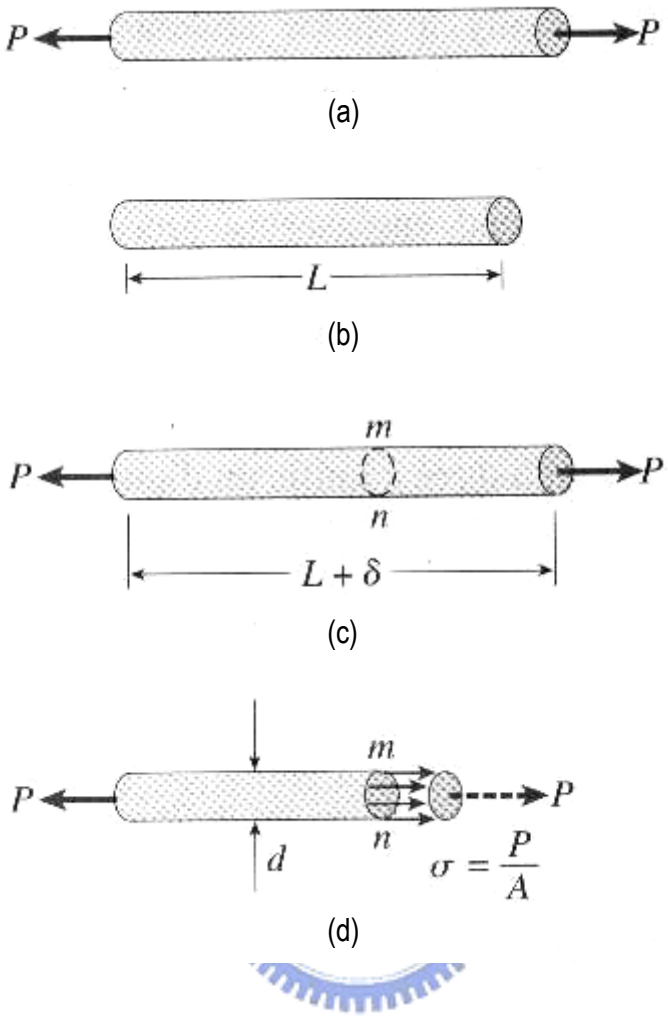

Figure 2-1 Prismatic bar in tension (a) Free-body diagram, (b) Segment of the bar, (c) Segment of a bar after loading, and (d) Normal stress in the bar.

The straight bar will change in length when loaded axially. As shown in Figure 2-1 (c), δ is the elongation after P is applied. The strain is the elongation per unit length, denoted by the Greek latter ε and given by the equation,

$$\varepsilon = \frac{\delta}{L} \tag{2-2}$$

If the bar is in tension, the strain is called a tensile strain; on the other hand, if the bar is in compression, the strain is a compressive strain.

Young's Modulus and Poisson's Ratio

When a material behaves elastically and also exhibits a linear relationship between stress and strain, it is said to be linearly elastic. The linear relationship between stress and strain for a bar is expressed by equation

$$\sigma = E\varepsilon \tag{2-3}$$

where σ is the axial stress, ε is the axial strain, and E is a constant of proportionality known as the modulus of elasticity, or Young's modulus. It represents the stiffness of a material, and is an important mechanical property.

When a prismatic bar is loaded in tension, the axial elongation is accompanied by lateral contraction, as shown in Figure 2-2. Lateral strain at any point in the bar is proportional to the axial strain at the same point if the material is linearly elastic. The ratio of the lateral strain ε' to the axial strain ε is known as Poisson's ratio and is denoted by the Greek letter ν.

$$\nu = -\frac{\text{lateral strain}}{\text{axial strain}} = -\frac{\varepsilon'}{\varepsilon} \tag{2-4}$$

The axial and lateral strains have opposite signs. Therefore, the Possion's ratio always has a positive value. For various materials, Possion's ratios range from 0 to 0.5. Materials with an extremely low value of Poisson's ratio, such as cork, the lateral strain is practically zero. For most metals and many other materials, ν is in the range of 0.25 to 0.35. The theoretical upper limit for Poisson's ratio is 0.5, in which case there is no volume change when compressed or elongated. Materials such as rubber and silicone come close to this limiting value.

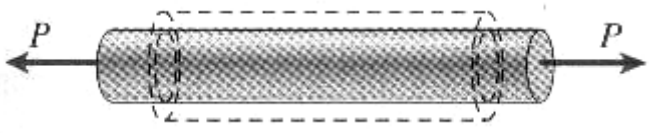

Figure 2-2 Axial elongation and lateral contraction of a bar in tension.

Yielding

Stress-strain diagrams portray the behavior of engineering materials when the materials are loaded in tension or in compression. Figure 2-3 shows the stress-strain diagrams of three materials. Figure 2-3 (a) shows the stress-strain diagram of mild steel. As shown in the figure, point A is the yield point. From this point, considerable elongation of the test specimen occurs with no noticeable increase in the tensile force (from A to B). Furthermore, when the load is removed, a residue strain may remain. Materials undergoing large permanent strains are classified as ductile materials. For most materials, stress-strain diagrams include yield points.

But rubber and silicone maintain a linear relationship between stress and strain up to relatively large strains with no residue strain after unloading. It can sustain large strain repeatedly. Figure 2-3 (b) shows the stress-strain diagrams of two kinds of rubber in tension.

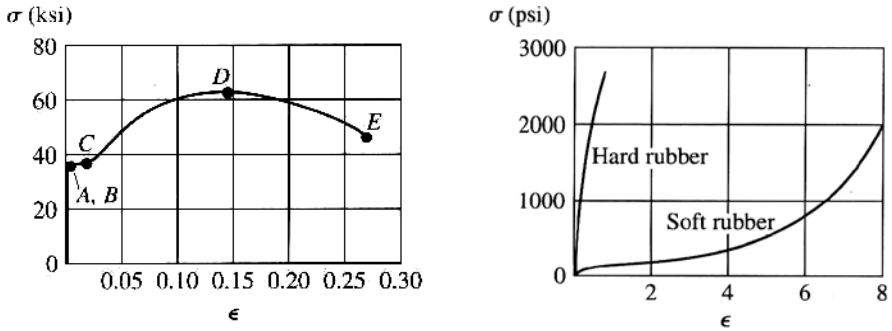

(a) (b)

Figure 2-3 Stress-strain diagrams of (a) mild steel, (b) two rubbers

2-2 Deflection of an Elastic Beam

A cantilever beam with rectangular cross section is common in MEMS application because thin film is deposited uniformly and its side wall can be etched by RIE vertically. Figure 2-4 (a) and (b) show a cantilever beam with length L and its cross section, a rectangle of a in width and b in thickness. For such a beam with one fixed end, if a force of q is applied on its top per unit length, as shown in Figure 2-4 (c), its deflection can be obtained from equation 2-5 [3]：

$$y = -\frac{qx^2}{24EI}(6L^2 - 4Lx + x^2) \tag{2-5}$$

where y is the deflection of the point located at a distance x from the fixed end of the beam, E is the Young's modulus of the material, and I is the moment of inertia of the beam cross section. The deflection is inversely proportional to EI, the flexural stiffness of the beam. For a rectangular cross section of a in width and b in height, the moment of inertia is shown in Equation 2-6 [3].

$$I = \frac{ab^3}{12} \tag{2-6}$$

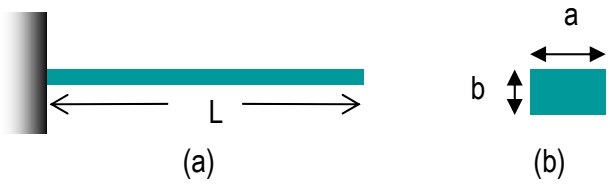

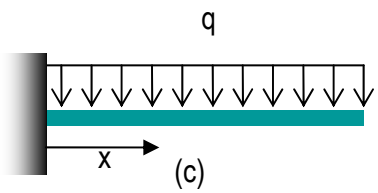

Figure 2-4 Uniform pressure applied on a cantilever beam.

Figure 2-5 shows a cantilever beam above a substrate. If there is a voltage applied between the beam and the substrate, the beam is attracted by the electrostatic force downward. The length of the cantilever beam is L, width is b, thickness is a, and the gap between beam and substrate is z. When a voltage of V is applied between the beam and the substrate, the electrostatic force is shown in Equation 2-7.

$$F = \frac{k\varepsilon_0 A}{2z^2} \times V^2 = \frac{k\varepsilon_0 La}{2z^2} \times V^2 \tag{2-7}$$

where k is the dielectric constant (for vacuum: 1.0, air: 1.00059), and ε_o is permittivity of free space. The electrostatic force can be represented by a uniform pressure when the deflection is small. Therefore, the force per unit length is

$$q = \frac{F}{L} = \frac{k\varepsilon_0 a}{2z^2} \times V^2 \tag{2-8}$$

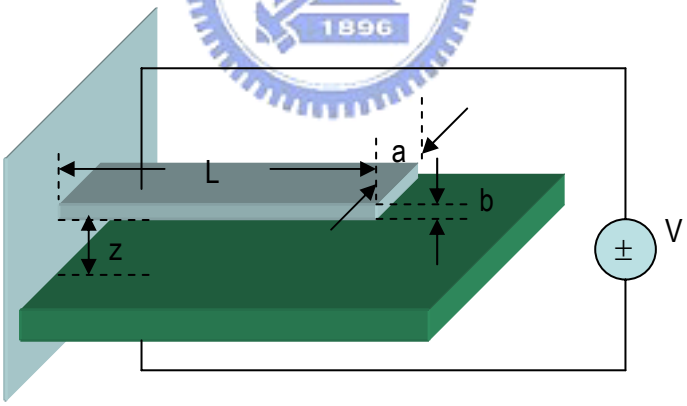

Figure 2-5 Cantilever beam above a substrate

For such an applied voltage, the deflection of the beam can be obtained by substituting Equation 2-8 into Equation 2-5

$$y = -\frac{aV^2}{EI}\frac{k\varepsilon_0 x^2}{48z^2}(6L^2 - 4Lx + x^2)V^2 \tag{2-9}$$

To further realize relationship between the deflection and the dimensions, Equation 2-6 can be substituted into Equation 2-9,

$$y = -\frac{V^2}{Eb^3} \times \frac{k\varepsilon_0 x^2}{4z^2} \times (6L^2 - 4Lx + x^2) \tag{2-10}$$

Therefore,

$$y \propto \frac{V^2}{Eb^3} \tag{2-10}$$

For a certain deflection, the required voltage is related to the Young's modulus and the thickness:

$$V \propto E^{\frac{1}{2}} b^{\frac{3}{2}} \tag{2-11}$$

For a polysilicon cantilever beam and a PDMS cantilever beam with the same dimensions, the difference in required voltages is related to their Young's moduli.

$$\frac{V_{polysilicon}}{V_{PDMS}} = \left(\frac{E_{polysilicon}}{E_{PDMS}}\right)^{\frac{1}{2}} = \left(\frac{170GPa}{750KPa}\right)^{\frac{1}{2}} = 476$$

For a polysilicon film deposited by LPCVD, the thickness is generally about 1μm. But the thickness is about 8μm for a spun on PDMS film. If the thickness is taken into account, the difference in required voltages is:

$$\frac{V_{polysilicon}}{V_{PDMS}} = \left(\frac{E_{polysilicon}}{E_{PDMS}}\right)^{\frac{1}{2}} \left(\frac{b_{polysilicon}}{b_{PDMS}}\right)^{\frac{3}{2}} = 476 \times \left(\frac{1}{8}\right)^{\frac{3}{2}} = 20.04$$

Therefore, the voltage applied to the PDMS beam is about 20 times less than that to the polysilicon beam and the PDMS beam can be driven with a much lower voltage.

2-3 Nonlinear Restoring Force

Figure 2-6 shows an elastic bar with length l and cross section area A. when a compressive load P is applied on its top surface, the bar deformed from L to L-δ in length. The elastic coefficient of the bar can be denoted as:

$$k = \frac{P}{\delta} \tag{2-10}$$

If the Young's modulus of the bar is E, then substitute Equations 2-1, 2-2, and 2-3 into Equation 2-10, the elastic coefficient can be denoted as:

$$k = \frac{A}{L}E \tag{2-11}$$

As shown in the equation, the elastic coefficient of the bar is proportional to the ratio of cross section area to the length (A/L).

For behaviors of PDMS structures in compression, Figure 2-7 (a) shows a quarter cross section of a PDMS post sandwiched between two rigid plates. The post is 3μm in height and 2μm in radius. As shown in Figure 2-7 (b), the shape of the post changes a lot after it is compressed, and its side surface is brought into contact with the plates. When the PDMS post is compressed more, the contact area would get increased, and results in the increasing of the cross section area, as shown in Figure 2-7 (c). When the PDMS post is compressed, the ratio of cross section area to the length get increased, and results in the increasing of the elastic coefficient. Therefore, the relationship between the elastic restoring force and the compressive displacement is nonlinear. The behavior of a PDMS post undergoing a large deformation involves hyperelasticity, and will be simulated with the finite element analysis software, ANSYS, in this study.

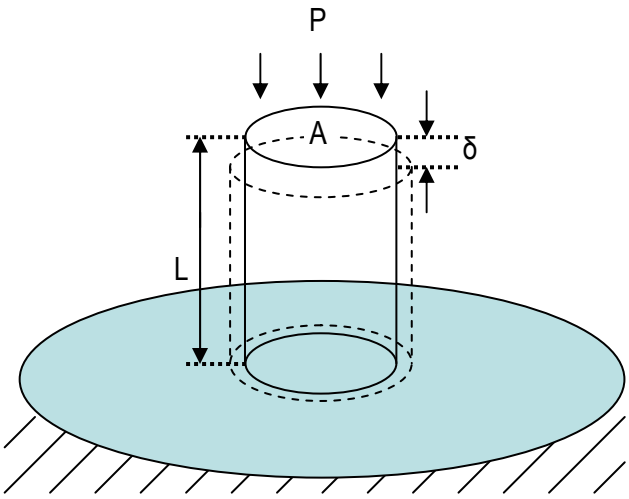

Figure 2-6 A bar in compression.

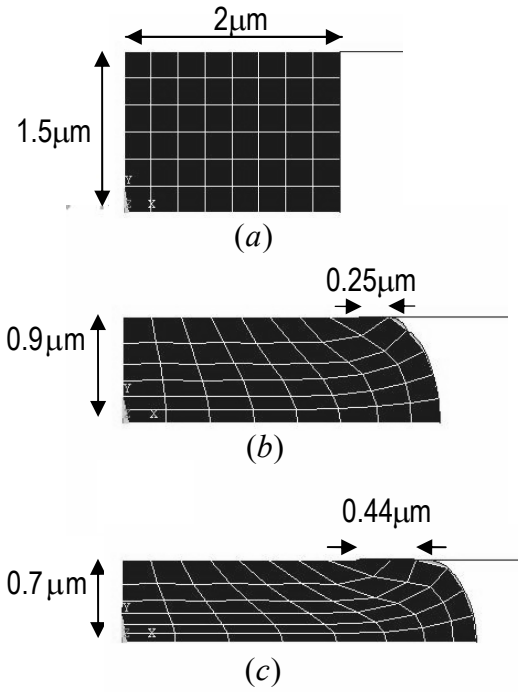

Figure 2-7 Quarter cross section of PDMS post. (a) The original height is 3μm, (a) 1.8μm in height after loaded (b) 1.4μm in height after loaded.

2-4 Device Design

The schematic of the device is shown in Figure 2-8. As shown in the figure, the proposed device is composed of a top electrode, a bottom electrode, and PDMS structures between them. Figure 2-9 shows the fabrication process. First, the substrate is heavily doped and will be used as the bottom electrode. Then, SiO_2 is deposited on the substrate to form the sacrificial layer. Then the sacrificial layer is patterned to form the cavities for PDMS to fill. PDMS is then cast on the SiO_2 layer. After the PDMS on the surface is removed, the PDMS remaining in the cavity forms the elastomer structures. The SiO_2 layer is then patterned to define the anchor of the top electrode. The structure layer is then deposited and patterned. Finally, the device is released by removing the SiO_2 layer.

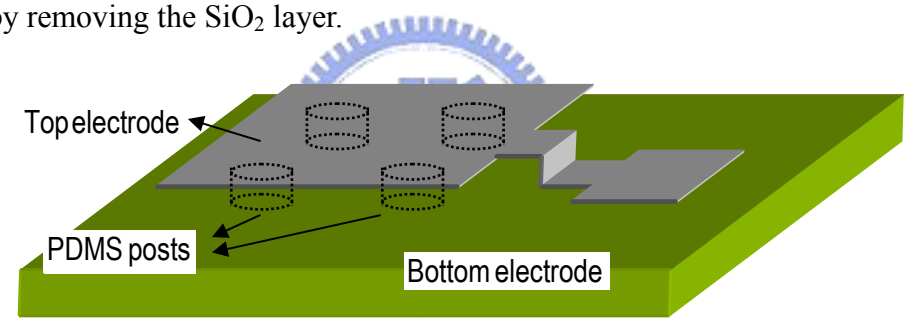

Figure 2-8 The schematic of gap-closing actuator with PDMS posts

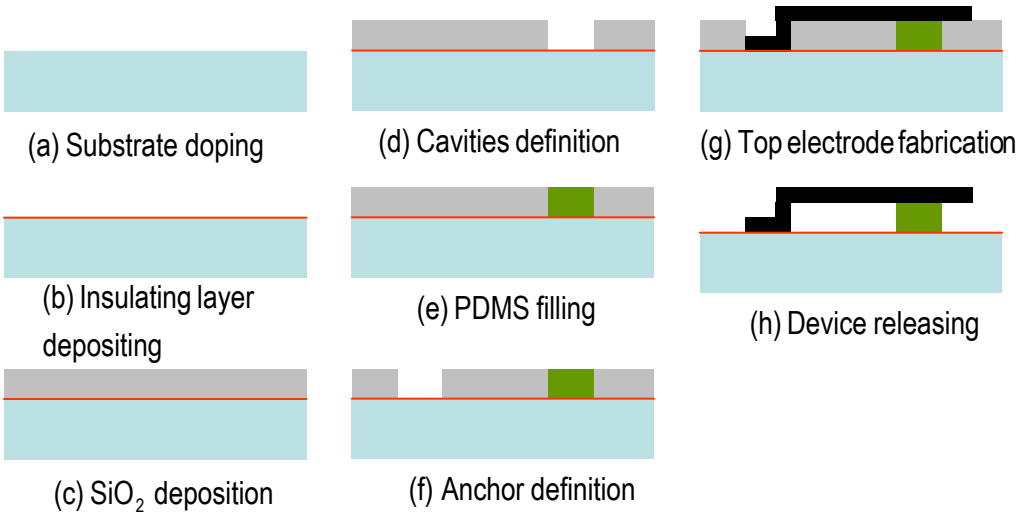

Figure 2-9 Schematic fabrication processes

2-4-1 PDMS Posts

The PDMS was molded into the shape of a post. The height of PDMS is the thickness of the sacrificial layer. The thickness must be reasonable for the deposition process of the sacrificial layer, which is the typical PECVD SiO_2. The thickness, and therefore the gap between two electrodes, should also be reasonable to provide enough electrostatic force. Therefore, a height of 3μm of the PDMS post is chosen in this study.

The radius of the PDMS post is related to the elastic restoring force. The elastic restoring force is calculated with the finite element analysis software, ANSYS. Some element types in ANSYS have the function to simplify a 3D axi-symmetric simulation to a 2D simulation with equivalent behavior. With such a function, 3D axi-symmetric model can be simplified into its half cross section. Besides, ANSYS has the function to simulate the behavior of contact. When the PDMS post is compressed, its lateral expansion should be constrained by top and bottom electrodes. The behavior of contact between the electrode and the lateral surface of PDMS can be simulated with the condition of a contact pair applied on them. The simulation result of compressed PDMS without and with the condition of a contact pair are shown in Figure 2-10 (a) and (b) respectively.

To obtain the relationship between the elastic restoring force and displacement, displacement boundary condition was set on the top electrode, and the deformation and reaction force of PDMS post was simulated by the software, as shown in Figure 2-11. The simulation of the PDMS post includes large deformation and contact pair. To simulate its behavior with a 3D model would be time consuming. So a 2D cross section of the post was built as the model. With the 2D model, the calculation will be much more efficient, and the finite element model can be meshed finer for more

accurate results.

For simulation, 750KPa as Young's modulus and 0.4 as Poisson's ratio was set. Four models with radius 2μm, 3μm, 4μm, and 6μm and height of 3μm were simulated. The model and boundary conditions are shown in Figure 2-12. Since the PDMS post is axi-symmetric, its model can be substituted by a half cross section, which is shown in Figure 2-12 (b). In addition, since the upper part and lower part of the cross section is symmetric, the half cross section can be further simplified into a quarter cross section, which is shown in Figure 2-12 (c). The contact pair is applied to the side wall of the PDMS post and the electrode plate, so the expansion of PDMS post is constrained by the electrode plate.

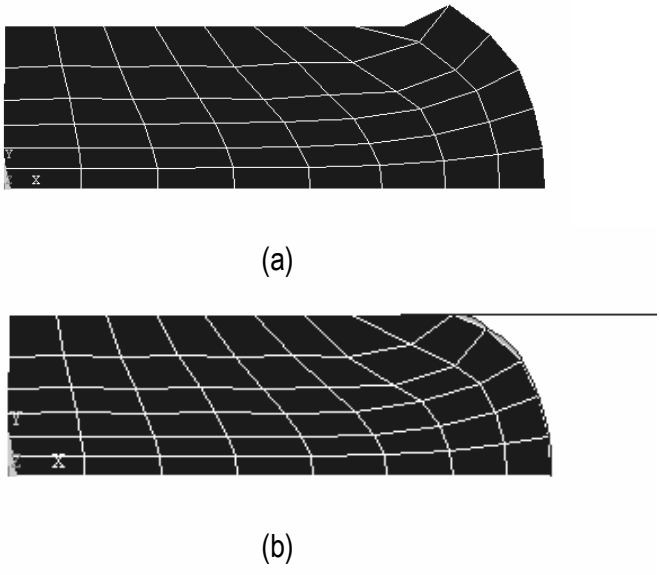

(a)

(b)

Figure 2-10 Simulation result (a) Without, and (b) With the contact pair.

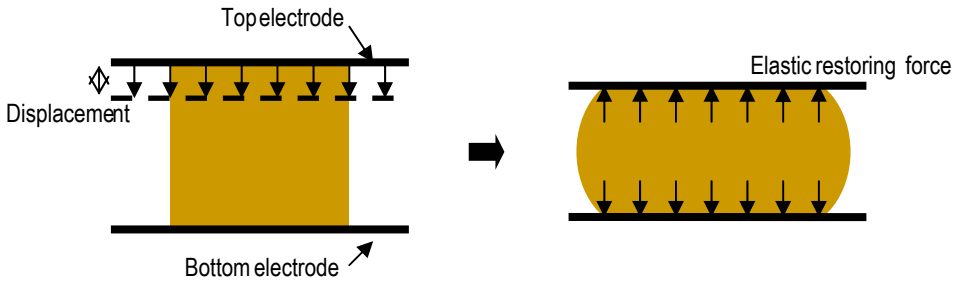

Figure 2-11 The concept of applying load on the model of PDMS post

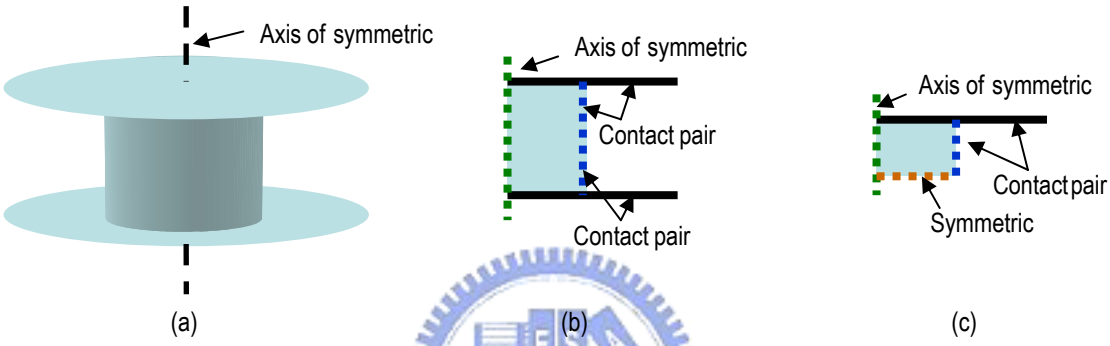

Figure 2-12 The concept of simplifying the model of PDMS elastomer post to its quarter cross-section.

The finite element model and simulation results of a PDMS post with radius 2μm and height 3μm are shown in Figure 2-13. The 3D expansion of the cross section is shown in Figure 2-13 (d). To obtain the curve of the elastic restoring force vs. the displacement, the displacement boundary condition was increased step by step, and corresponding elastic restoring force was calculated by ANSYS. The curve of elastic restoring force vs. displacement is shown in Figure 2-14.

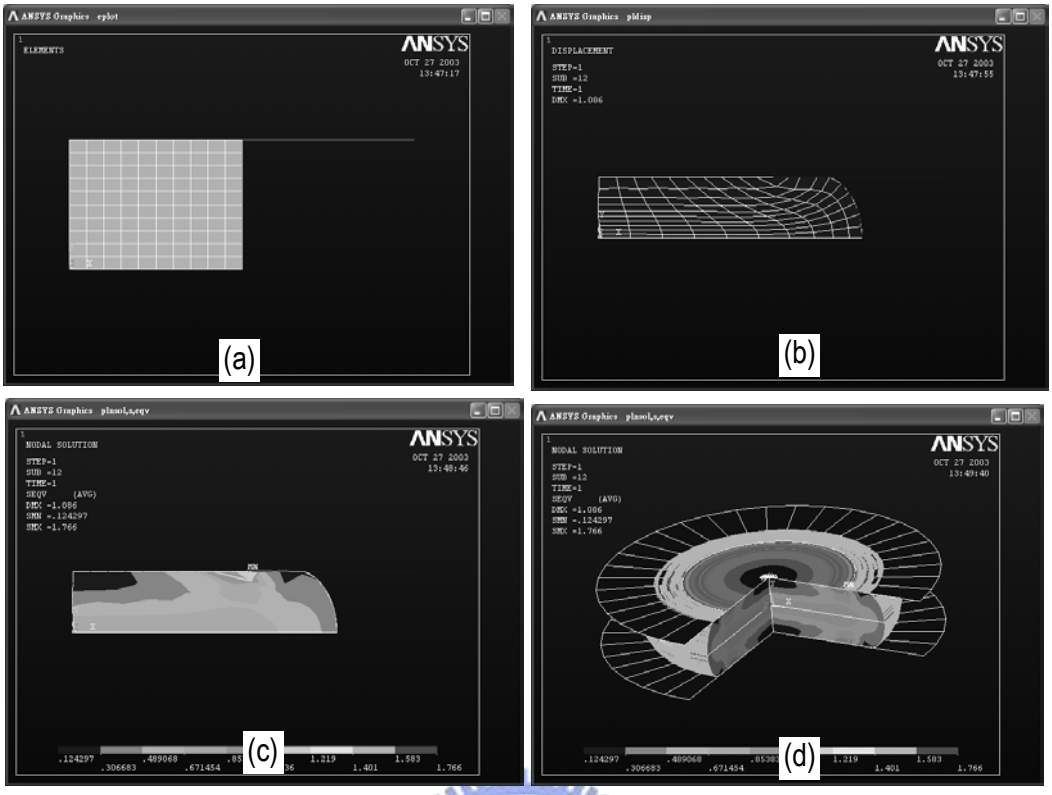

Figure 2-13 For the simulation of PDMS post, (a) Finite element model (b) Deformation and strain distribution (c) Strain distribution (d) 3D expansion

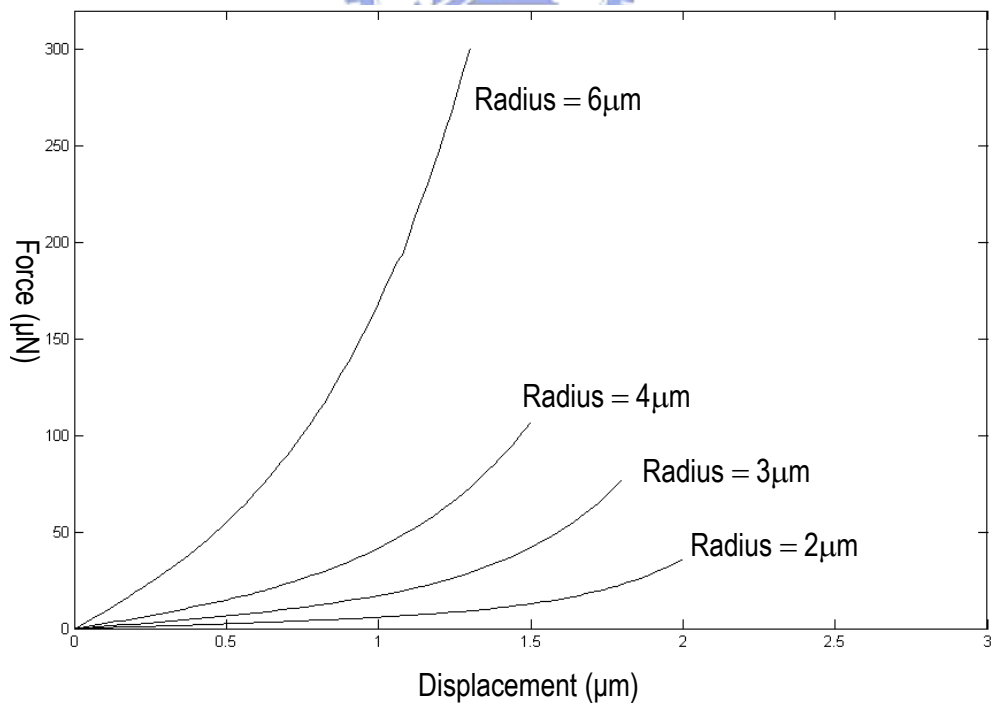

Figure 2-14 Elastic restoring forces of PDMS posts vs. displacement

As shown in the figure, the elastic coefficient is larger for larger displacement. So the simulation results show that the elastic restoring force of the PDMS post is nonlinear. The force to compress the PDMS post with a radius of 6μm is too large and such a PDMS post will not be placed in the device. Therefore, the PDMS posts placed between electrodes are determined to have height of 3μm and radii ranges from 2μm to 4μm.

Furthermore, two imaginary devices can be used to compare the actuators with linear and nonlinear elastic restoring forces. As shown in Figure 2-15, top electrodes in both actuators are 120μm×120μm. The spring in the Figure 2-15 (a) are composed of two polysilicon beams with length of 100μm, width of 20μm, thickness of 1μm, and Young's modulus of 170GPa. The elastic coefficient of such a beam can be obtained by the Equation 2-12 [18].

$$k = \frac{E \times \text{thickness}^3 \times \text{width}}{\text{length}^3} = 6.8 \, N/m \qquad (2\text{-}12)$$

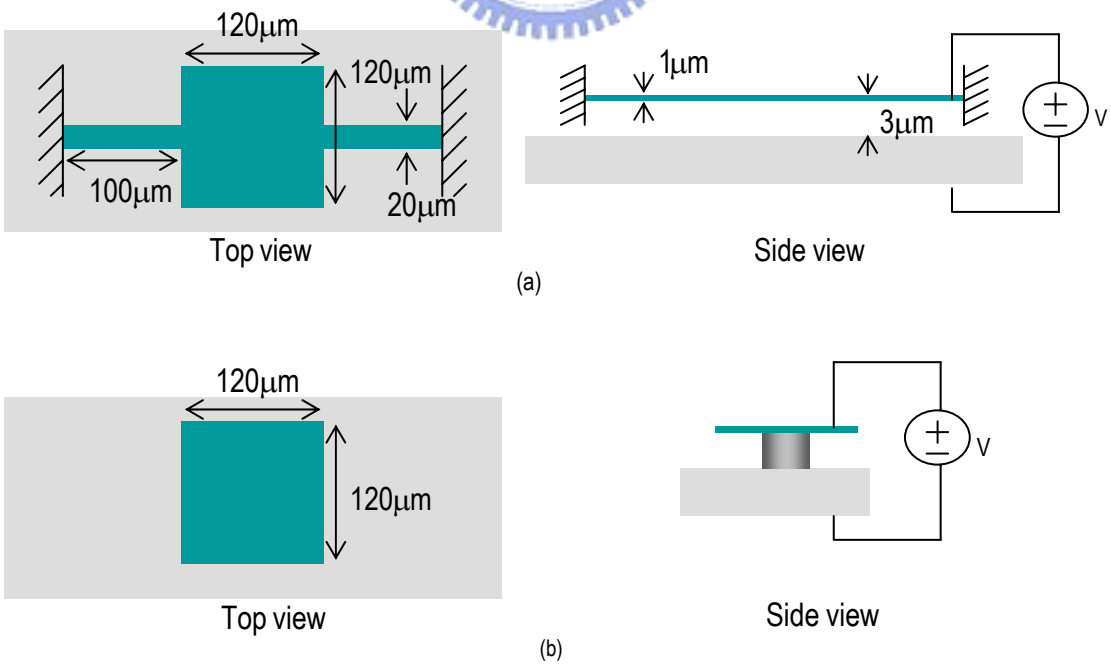

Figure 2-15 Two gap-closing actuators with (a) a linear structural restoring force, and (b) restoring force provided by PDMS post.

The PDMS post with a radius of 2μm is used as a comparison. The linear and nonlinear elastic forces are compared to the electrostatic force, as shown in Figure 2-16 (a) and (b), respectively.

The intersection of the elastic restoring force and the electrostatic force is the equilibrium point and the corresponding displacement is where the electrode is displaced at that voltage. As shown in Figure 2-16 (a), the electrostatic forces due to voltages lower than 6.4V have intersections with the elastic restoring force. Therefore, the actuator is controllable below this voltage. Above 6.4volt, there is no intersection. The elastic restoring force is less than the electrostatic force, and the pull-in effect occurs. The equilibrium displacement at 6.4V is the limit of controllable displacements, which is 1/3 of the original gap.

In Figure 2-16 (b), the electrostatic forces from 2.4V to 7.4V have intersections with the elastic restoring force. The equilibrium displacement at 7.4V is 1.92μm, which is the 64% of the original gap. Therefore, the graph reveals that the actuator with a PDMS post placed between electrodes can move for at least 64% of the original gap. Compared with the actuator with linear restoring force, the actuator with the PDMS post greatly extends the controllable displacement.

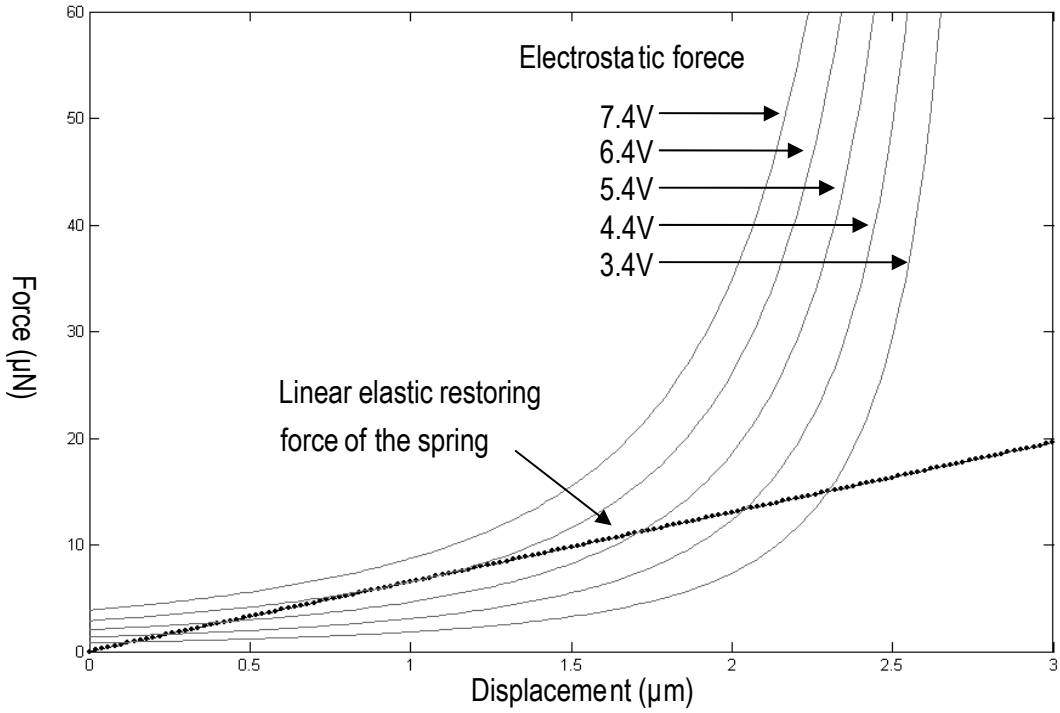

(a) Linear elasticity

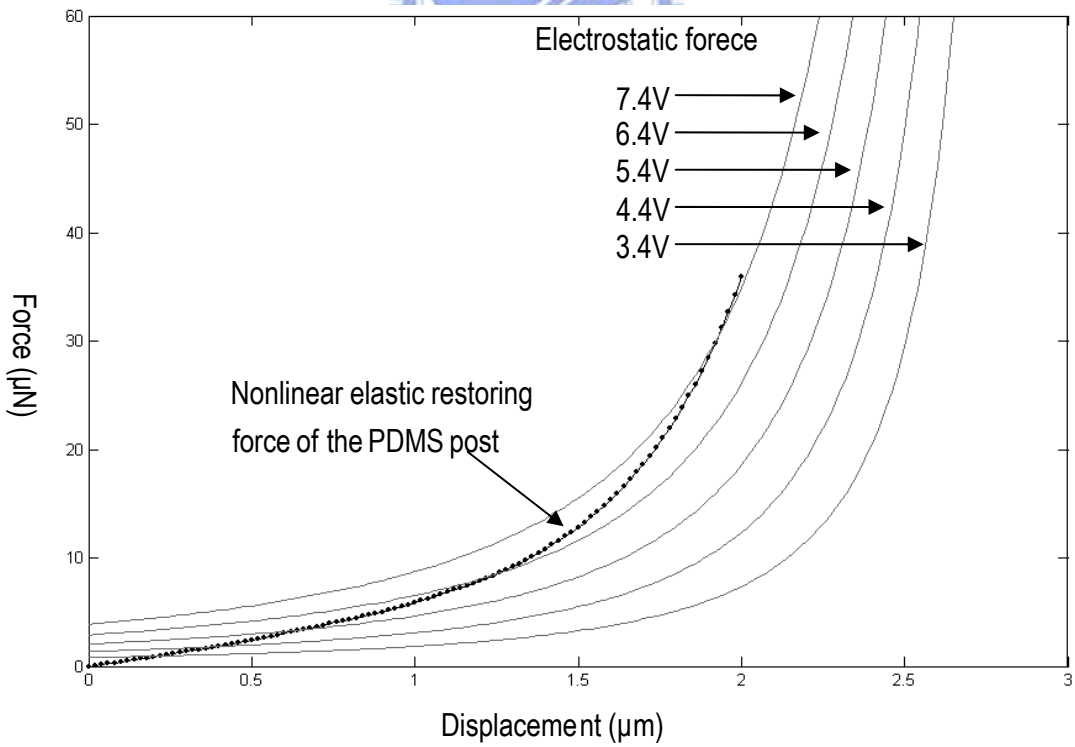

(a) Nonlinear elasticity

Figure 2-16 Elastic restoring force and electrostatic force

2-4-2 Top Electrode

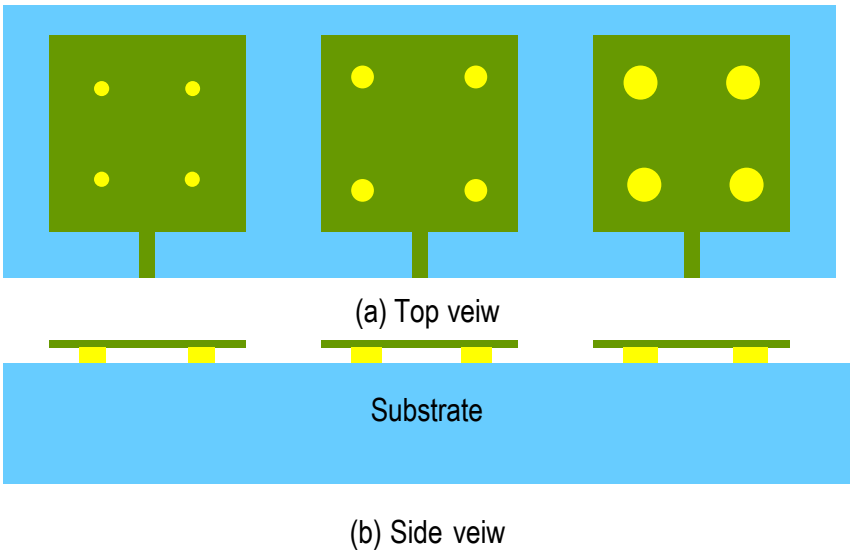

Figure 2-17 Schematic layout and side view of the devices.

As shown in Figure 2-17, PDMS posts with various radii would be placed between the top electrode and the substrate. As mentioned in Section 2-2-1, the radii of PDMS posts would be in the range from 2μm to 4μm. When voltage is applied, the electrostatic force and the elastic restoring force should be balanced. The electrostatic force can be obtained by the Equation 2-7. On the other hand, the elastic force is obtained from Figure 2-14. The elastic restoring force of PDMS posts with radius of 3μm would be used as the example.

It is assumed that the applied voltage is 80V when the top electrode displaces 1.5μm. From Figure 2-14, the elastic restoring force provided by the four PDMS posts would be 168μN for the above displacement, Therefore, to obtain an electrostatic force of 168μN for the remaining gap of 1.5μm at the applied voltage of 80V, an area of 13323μm^2 is needed from Equation 2-7. A square top electrode with the dimension $120 \times 120\,\mu m^2$ is then determined, for which the area (14400 μm^2) is close to 13323μm^2.

2-4-3 Position of PDMS Posts and Thickness of Top Electrode

As shown in Figure 2-17, the top electrode is supported by four PDMS posts. However, the position of PDMS posts influences the performance of device. As shown in Figure 2-18, if the PDMS posts are placed too close to center, the edge of the top electrode may be pulled down more than the center. On the other hand, if the PDMS posts are placed too close to the edge, the center of the top electrode may be pulled down more.

Figure 2-18 Schematic of (a) PDMS posts are placed too close to center. (b) PDMS posts are placed too close to the edge

To find out the appropriate position to place the PDMS posts with ANSYS simulation, the top electrode was modeled as an elastic plate with the shell element. It is a 2D element and is used to simulate the deformation of plates. The Young's modulus and the effective thickness were set as 170GPa and 1μm, respectively. The electrostatic force was modeled as uniform pressure, for which the value is 20KPa, and the position of PDMS was modeled by four areas on the elastic shell which were fixed in the z direction. Figure 2-19 shows the concept of this simulation.

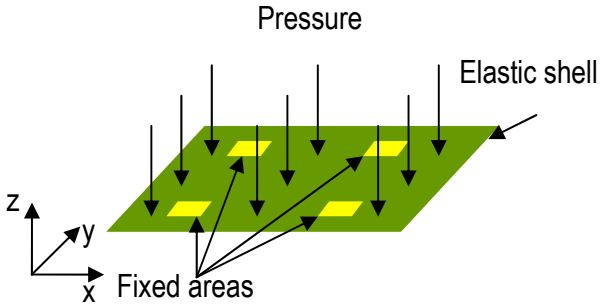

Figure 2-19 Schematic of this simulation of deflection of top electrode

As shown in Figure 2-20, this model was symmetric in x and y direction, so it could be simplified by a quarter model. Symmetric boundary conditions were set on the left-hand side and downside. By changing the position of the fixed area, the simulation would reveal the appropriate position to place the PDMS posts.

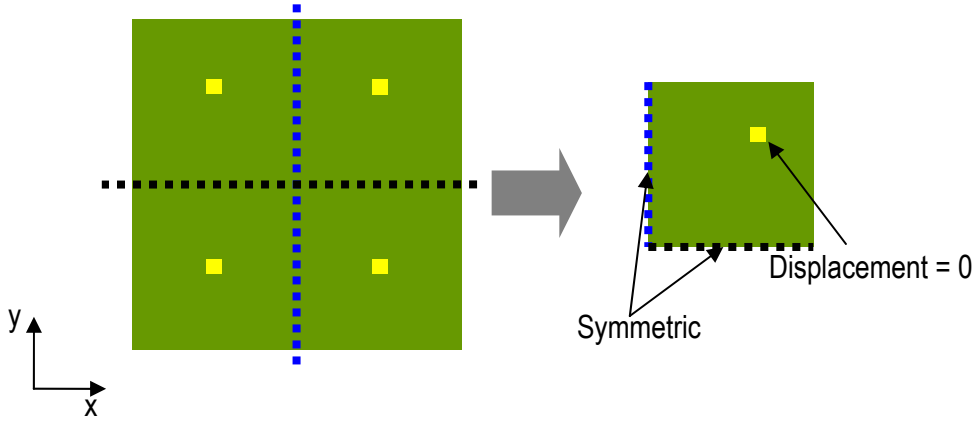

Figure 2-20 Schematic of simplifying the top electrode to the quarter model

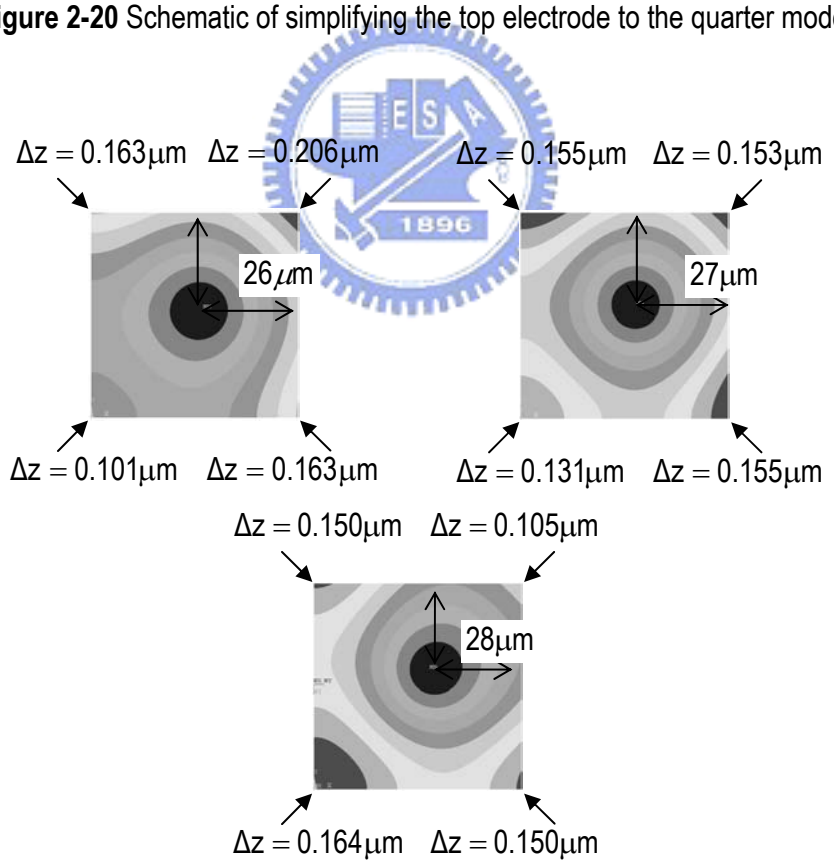

Figure 2-21 Z-direction displacement distributions for various positions of the PDMS posts.

Figure2-21 shows the influence of the position of the PDMS posts on the deformation of the top electrode. In this model, the top right corner represents the corner of top electrode, and the bottom left corner represents the center of top electrode. The left and bottom edges are the symmetric axes of the square plate. Therefore, in Figure 2-20 (a), the center and edges of the top electrode are pulled down more; in Figure 2-20 (b), the center, edges, and corners of top electrode are about the same distance from the bottom; in Figure 2-20 (c), the edges and corners of top electrode are pulled down more. This result shows that the PDMS posts should not be placed too close to the corner or center of top electrode. Otherwise some part of the top electrode would be pulled down more. Therefore, 27μm would be the appropriate distance to place the PDMS posts away from the edges. The position of PDMS post was then determined as 27 micron from edge of top electrode.

As shown in Figure 2-22, when a voltage is applied between two electrodes, both the PDMS posts and the top electrode deform due to the electrostatic force. Deformation of top electrode would decrease the gap between two electrodes and increase the electrostatic force. Therefore, to achieve a certain displacement, the required voltage was less than expectation. So, if the top electrode may deform due to insufficient stiffness, the relationship between displacement and applied voltage is not only governed by the elastic restoring force, the deformation of top electrode should also be taken into account. To ensure that the displacement of the top electrode is not influenced by its deformation, it is assumed that when the compression displacement of PDMS post is 1.8μm, the deformation of the top electrode is within 0.1μm. The elastic restoring force of PDMS post with 3μm in radius is taken as reference.

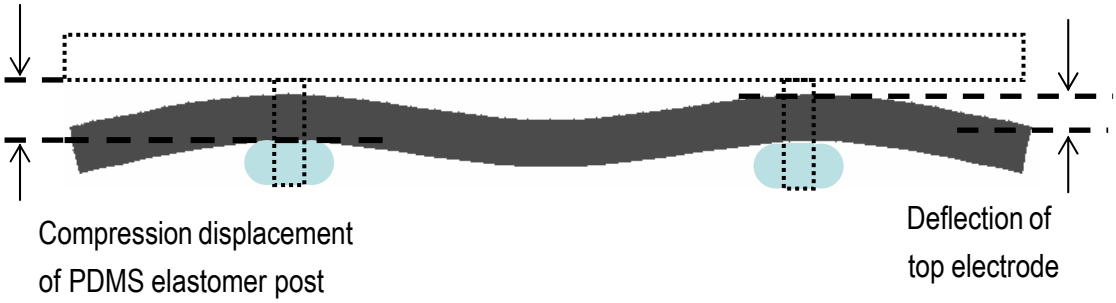

Figure 2-22 Deformation of the top electrode and the PDMS post when a voltage is applied

To observe the difference between devices with an elastic top electrode and a rigid top electrode, an imaginary device composed of rigid top and bottom electrodes and a PDMS post sandwiched between them was built. The area of the top electrode is $60\times60\mu m^2$, and the PDMS post is 3μm in height and 2μm in radius. When the displacement of the top electrode is 1.8μm, the elastic restoring force of the PDMS post is 77μN from Figure 2-14. To balance such a force for the remaining gap of 1.2μm, the applied voltage between these two electrodes is 83V obtained from Equation 2-7. On the other hand, if the elasticity of the top electrode is taken into account, the voltage needed to achieve such displacement would be less. The behavior of the top electrode was analyzed by ANSYS.

Figure 2-23 shows the concept of simulation. In this model, the top electrode and the bottom electrode were built. The top electrode was a quarter model with symmetric boundary conditions on the left and bottom edges. The support of PDMS was substituted by an area, on which we set displacement of -1.8μm in z-direction in simulation. Voltage was applied between two electrodes, and the top electrode was deformed by the electrostatic force. The Young's modulus and Poisson's ratio of 140GPa and 0.3 were set respectively for the top electrode, and the bottom electrode was assumed to be rigid.

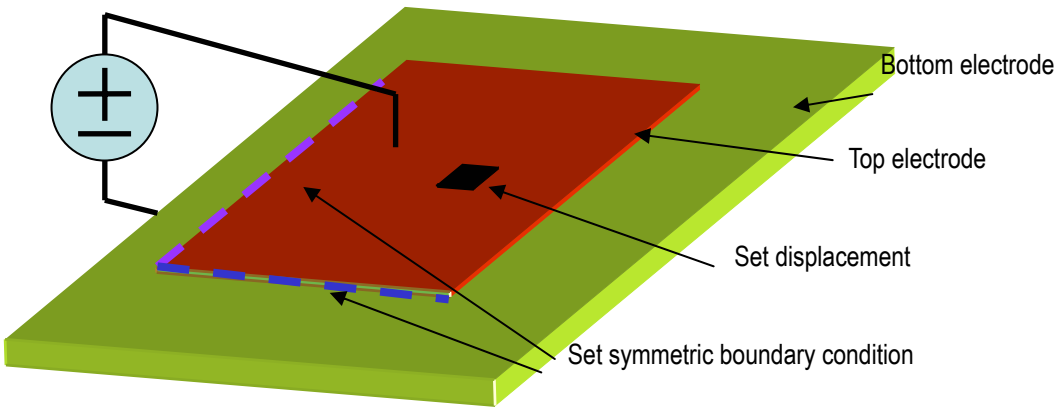

Figure 2-23 Schematic of the simulation of thickness of top electrode

For a top electrode with thickness of 0.8μm, the voltage needed to achieve the electrostatic force of 77μN is 71.4V, but the deflection of top electrode is 0.33μm. On the other hand, for a top electrode with thickness of 1.2μm, the voltage needed is 80.6V and the deflection of top electrode is 0.095μm, which is within the requirement mentioned above. Therefore, the thickness of top electrode is determined as 1.2μm. Figure 2-24 (a) and (b) show the simulation results of top electrodes with 0.8μm and 1.2μm in thickness.

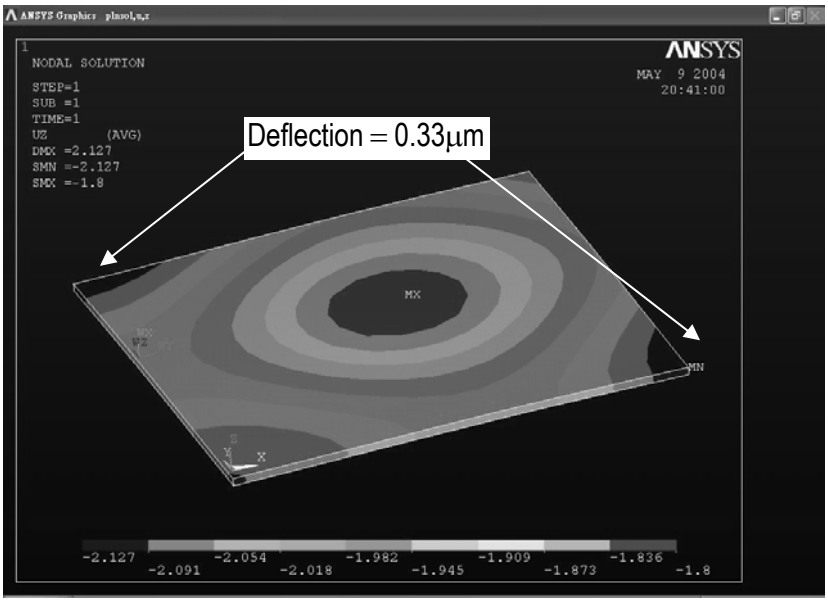

(a) 0.8μm-thick electrode

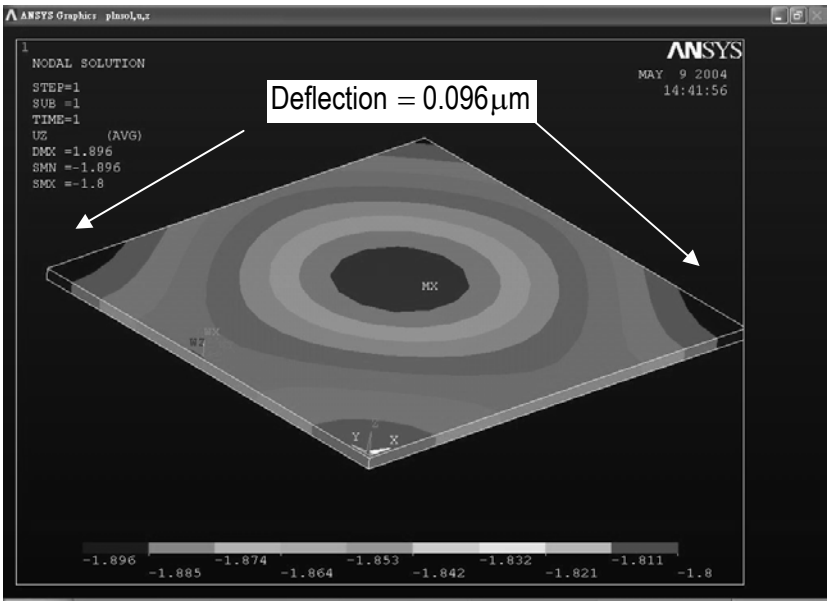

(b) 1.2μm-thick electrode

Figure 2-24 Simulation of the top electrodes with different thickness.

2-4-4 Connecting Beam

In the device, the beam connecting the top electrode and the anchor also provides an elastic restoring force. But the force should be insignificant, or it will influence the performance of the device.

Figure 2-25 shows the dimensions of the connecting beam. As calculated by ANSYS, when the top electrode displaces 1.8μm downward, such a connecting beam would provide restoring force of 7.36μN. But the elastic restoring force provided by the four PDMS posts is 308μN from Figure 2-14. Therefore, the elastic restoring force of the connecting beam can be ignored.

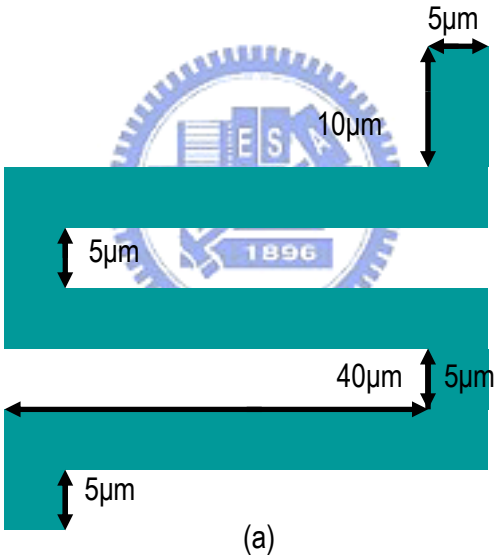

Figure 2-25 Dimensions of the connecting beam.

2-4-5 Full Device

Figure 2-26 (a) shows a part of the layout. And Figure 2-26 (b) shows the 3D model of the device. To estimate the displacement vs. applied voltage of the actuator, an imaginary device was built, as shown in Figure 2-27. Suppose that the top electrode is rigid, to actuate the device for a certain displacement, the elastic restoring force of PDMS posts can be obtained from Figure 2-14. The voltage required to

provide the equivalent electrostatic force for such a gap and area can be obtained from Equation 2-7. Therefore, the displacement vs. applied voltage of the top electrode can be obtained. Figure 2-28 shows the displacement vs. applied voltage of devices with various radii PDMS posts.

As shown in the Figure, the relationship of voltage and displacement is nearly linear in the later part of the curve. But for the device with PDMS post of 2μm in radius, the displacement vs. voltage is relatively nonlinear. As shown in the figure, the slope of the curve increases gradually for applied voltage less than 40V, but after the voltage exceeds 40V, the slope seems starting to decrease. One possible reason is that before the lateral surface of posts are contact with the electrodes, the elastic restoring force is nearly linear, therefore, the top electrode displaces faster and faster. After the surfaces are contact, the elastic restoring force increases rapidly and nonlinearly, therefore, the top electrode displaces slower.

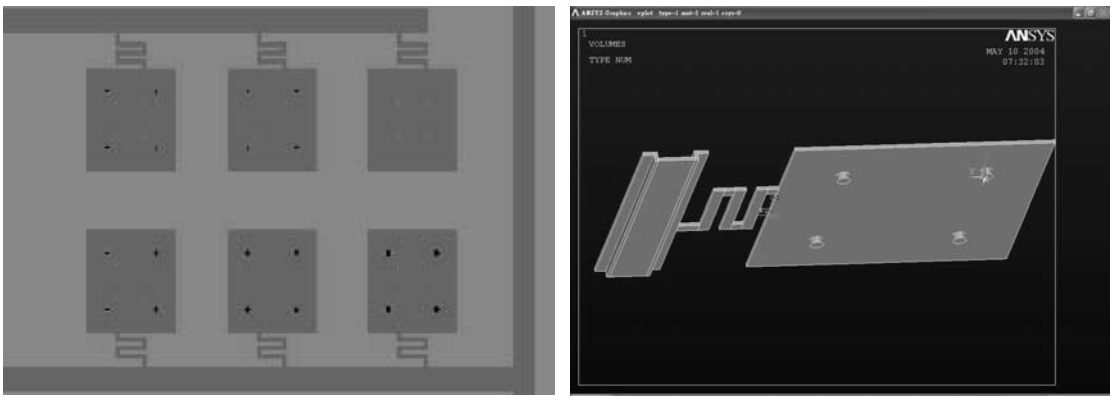

(a) (b)

Figure 2-26 (a) A part of layout (b) 3D Model.

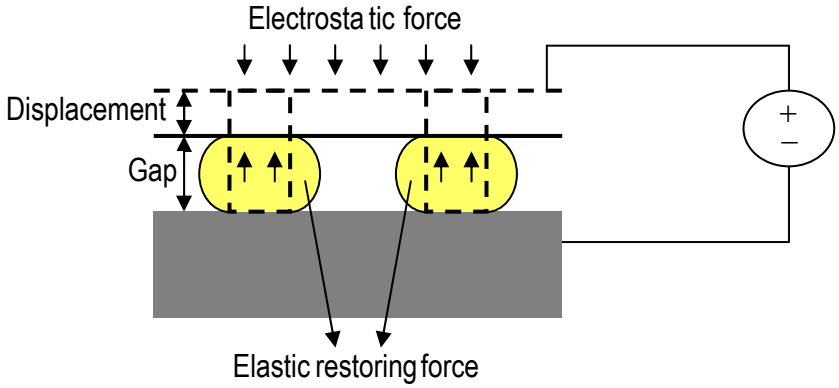

Figure 2-27 The schematic of the device for estimation of the displacement.

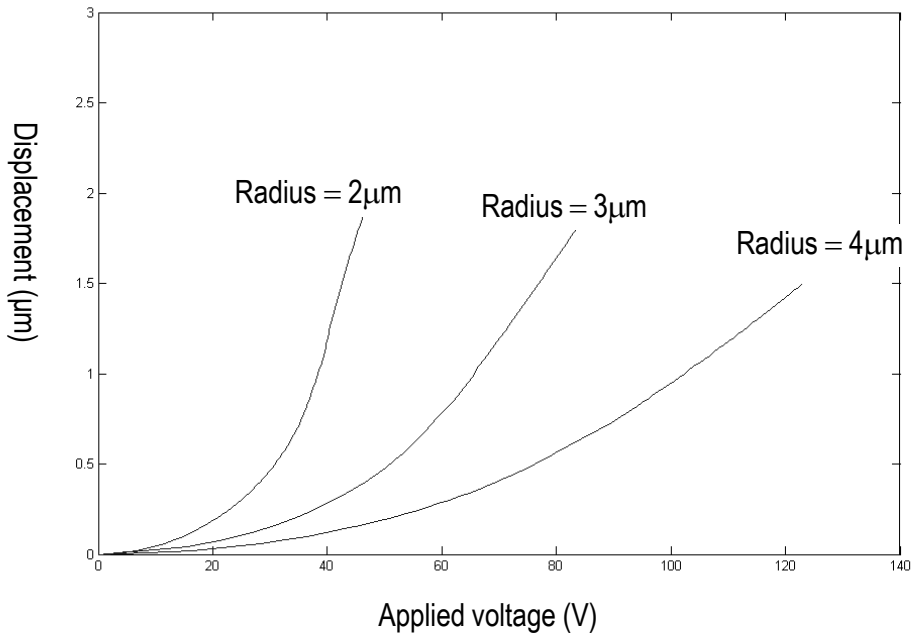

Figure 2-28 Displacement vs. applied voltage for various PDMS posts

Ⅲ、Fabrication Process

There are two devices in this study: one is a gap-closing actuator with PDMS posts placed between two electrodes; the other is a PDMS cantilever beam. Their process flows will be introduced in this chapter. Results and issues related to fabrication will be discussed.

3-1 Gap-closing Actuator with PDMS Posts

The schematic of a gap-closing electrostatic actuator with PDMS elastomer posts placed between the two electrodes is show in Figure 2-8. The device is composed of the top and bottom electrodes and the PDMS posts.

The first step is to form the bottom electrode by heavily doping the substrate, as shown in Figure 3-1 (a). The n type substrate has a sheet resistance of about 35.2Ω/□ measured by the 4-point probe method. To prevent the formation of p-n junction in the substrate, the surface was doped with phosphorous by diffusion; the process gases of PCl_3 and O_2 were delivered into the diffusion furnace by N_2 at 900℃ for half an hour to form a thin SiO_2 layer on the surface with phosphorous, and wafers were then annealed for half an hour to drive the dopant in. The sheet resistance of the n^+ region was measured as1.83Ω/□.

After the doping step, a thin SiO_2 film remained on the surface. This layer was removed by BOE. Then a LPCVD Si_3N_4 layer of 2500Å was deposited for insulation between the top and bottom electrodes, as shown in Figure 3-1 (b). The process gases of 35sccm SiH_2Cl_2 and 105sccm NH_3 were delivered into the furnace at 180mTorr at 800℃ for 45min. With an ellipsometer, the thickness of the Si_3N_4 layer was measured as 2750Å.

Then the Si_3N_4 layer was patterned to define the contact window of the bottom

n^+ region (mask #1), as shown in Figure 3-1 (c). Through this contact window, the n^+ region of substrate and the external circuit were connected. The window was defined with RIE with process gases of 30sccm SF_6 and 10sccm CHF_3 and chamber pressure of 50mTorr.The RF power was 100watt and the etching time was 90seconds.

After the contact window was defined, a layer of 3μm-thick SiO_2 was deposited on the Si_3N_4 layer by PECVD, as shown in Figure 3-1 (d). Process gases of 400sccm O_2 and 10sccm TEOS were delivered into the chamber at 300mTorr at 300℃. The RF power was 200watt and the deposition time was 28minutes. With an ellipsometer, the thickness of SiO_2 layer was measured as 2.85μm. Cavities on this SiO_2 layer would be defined subsequently. The cavities would be filled by PDMS to form the PDMS structures. This SiO_2 layer would also be taken as the sacrificial layer for the top electrode.

The layer of 3μm SiO_2 was patterned with RIE (mask #2) to form the cavities for PDMS to fill, as shown in Figure 3-1 (e). The SiO_2 layer was patterned with RIE rather than BOE wet etching because wet etching causes under cut. Process gases of 30sccm SF_6 and 10sccm CHF_3 were delivered into the chamber at 50mTorr. RF power was 100watt and the etching time was 25 minutes. The cavities defined by mask #2 were then filled with PDMS, as shown in Figure 3-1 (f). The process steps to fill the cavities with PDMS will be discussed later.

The SiO_2 layer was then patterned with BOE wet etching (mask #3), as shown in Figure 3-1 (g). Anchors of the top electrode were defined in this step. BOE wet etching was used rather than RIE due to its good etching selectivity between SiO_2 and Si_3N_4.

To determine the material of the top electrode, several processing issue should be considered. The first issue is temperature. The tolerable temperature of PDMS is

250℃. LPCVD poly silicon is used as structure layer in many MEMS applications. But its processing temperature exceeds 500℃ and PDMS will be destroyed at such a high temperature. The processing temperature of PECVD amorphous silicon is 250℃, which is tolerable for PDMS, but its conductivity and adhesion to the substrate is poor. Conductivity of metal is much better than that of amorphous silicon, and the processing temperature is close to room temperature. To deposit a metal layer, sputter, evaporation, and electroplate processes are available. The second issue is the resistance to HF. Materials that resist HF include chromium, tungsten, platinum, copper, gold, and silver [19]. After the adhesion to substrate and cost are taken into account, chromium is chosen as the material of top the electrode.

After the anchors were defined, a chromium layer of 1.2μm was deposited by sputtering, as shown in Figure 3-1 (h). This chromium layer would be taken as the material of the top electrode. Process gas of 20sccm Ar was delivered into the chamber at 4.5mTorr. The DC current was 1amp and the deposition time was 70minutes.

The chromium layer was then patterned by CR7T wet etching, as shown if Figure 3-1 (i). The thickness was measured as 1.25μm (by an interferometer). The patterning process must be controlled precisely. Otherwise, due to the undercut caused by wet etching, the connecting beam will after releasing. Finally, the devices were released by removing the SiO_2 by HF, as shown if Figure 3-1 (j).

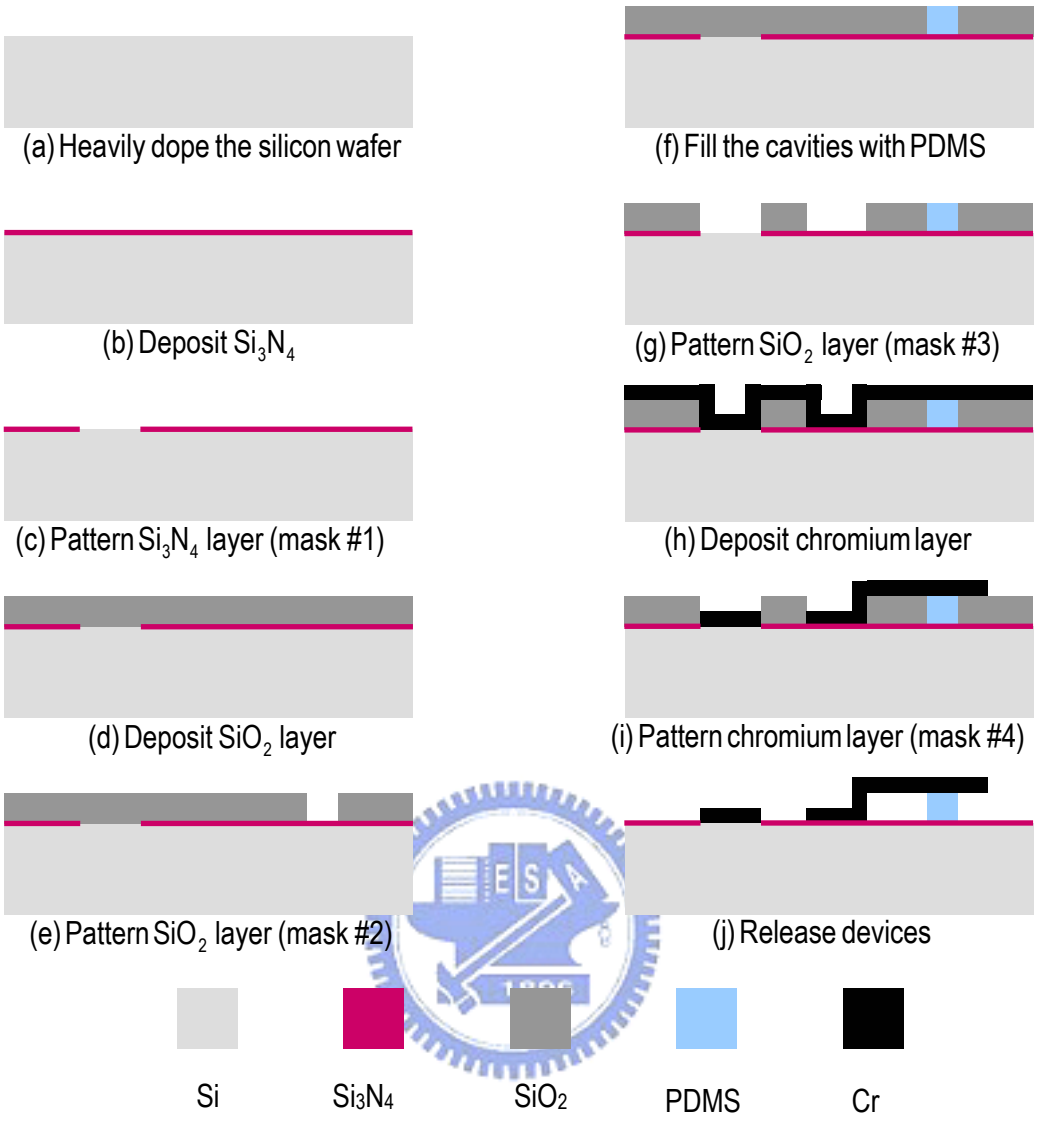

Figure 3-1 Fabrication process of actuator with PDMS elastomer

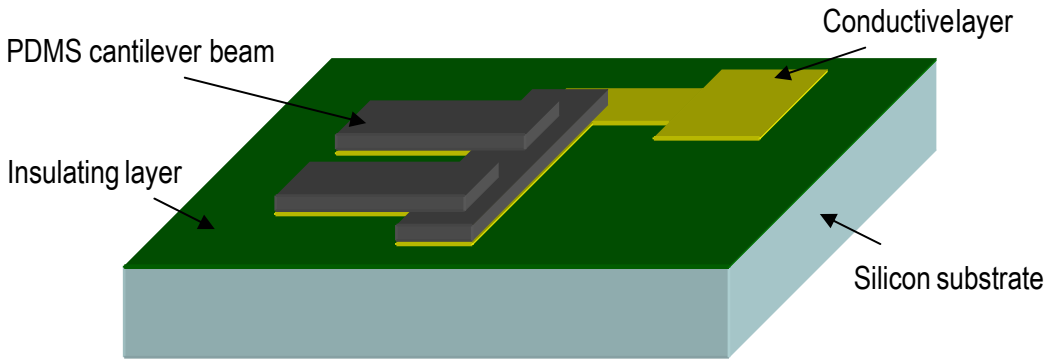

Figure 3-2 Schematic of PDMS cantilever beam

3-2 PDMS Cantilever Beam

This section describes the processes manufacturing for the PDMS cantilever beam. The schematic of the device is shown in Figure 3-2. As shown in the figure, there is a conductive layer below the PDMS cantilever beams to provide electrostatic force to actuate the device. The conductive layer is separated from the silicon substrate with an insulating layer.

The fabrication process is shown in Figure 3-3. The first step was to heavily dope the substrate. A Si_3N_4 layer was then deposited and patterned (mask #1). A SiO_2 layer was then deposited, as shown in Figure 3-3 (a) to (d). The process flows above were the same with the process flows to manufacture the gap-closing actuator with PDMS posts. Then the SiO_2 layer was patterned with BOE wet etching (mask #2), as shown in Figure 3-3 (e). Anchors of the top electrode were defined in this step. A 500Å chromium layer was then deposited by sputtering, as shown in Figure 3-3 (f). Process gas of 20sccm Ar was delivered into the chamber at 4.5mTorr. The DC current was 1 amp and the deposition time was 3minutes. The chromium layer was patterned with CR7T wet etching. The patterned chromium layer was taken as the conductive layer of the PDMS structure. The structural PDMS film was then spun on the substrate, as shown in Figure 3-3 (g). The spin rate parameters were 1000rpm for 30 seconds and 7000rpm for 4minutes. The thickness of the PDMS film was measured as 5.6μm. The surface of PDMS was then treated by O_2 for better adhesion to the later aluminum layer. The O_2 plasma treatment was accomplished in a PECVD chamber. Process gases of 400sccm O_2 was delivered into the chamber at 300mTorr at 250℃, the RF power and treating time were 100watt 10 seconds respectively.

A 1000 Å aluminum layer is then deposited by sputtering. Process gas of 20sccm Ar was delivered into the chamber at 4.5mTorr. The DC current was 1 amp and the

deposition time was 8minutes. The aluminum layer was then patterned with wet etching, as shown in Figure 3-3 (h). The patterned Aluminum layer would be taken as the hard mask for RIE. Then PDMS layer was patterned, as shown in Figure 3-3 (i), the processes will be discussed in detail later. Finally, the aluminum and SiO_2 layer were removed by HF to release the device, as shown in Figure 3-3 (j).

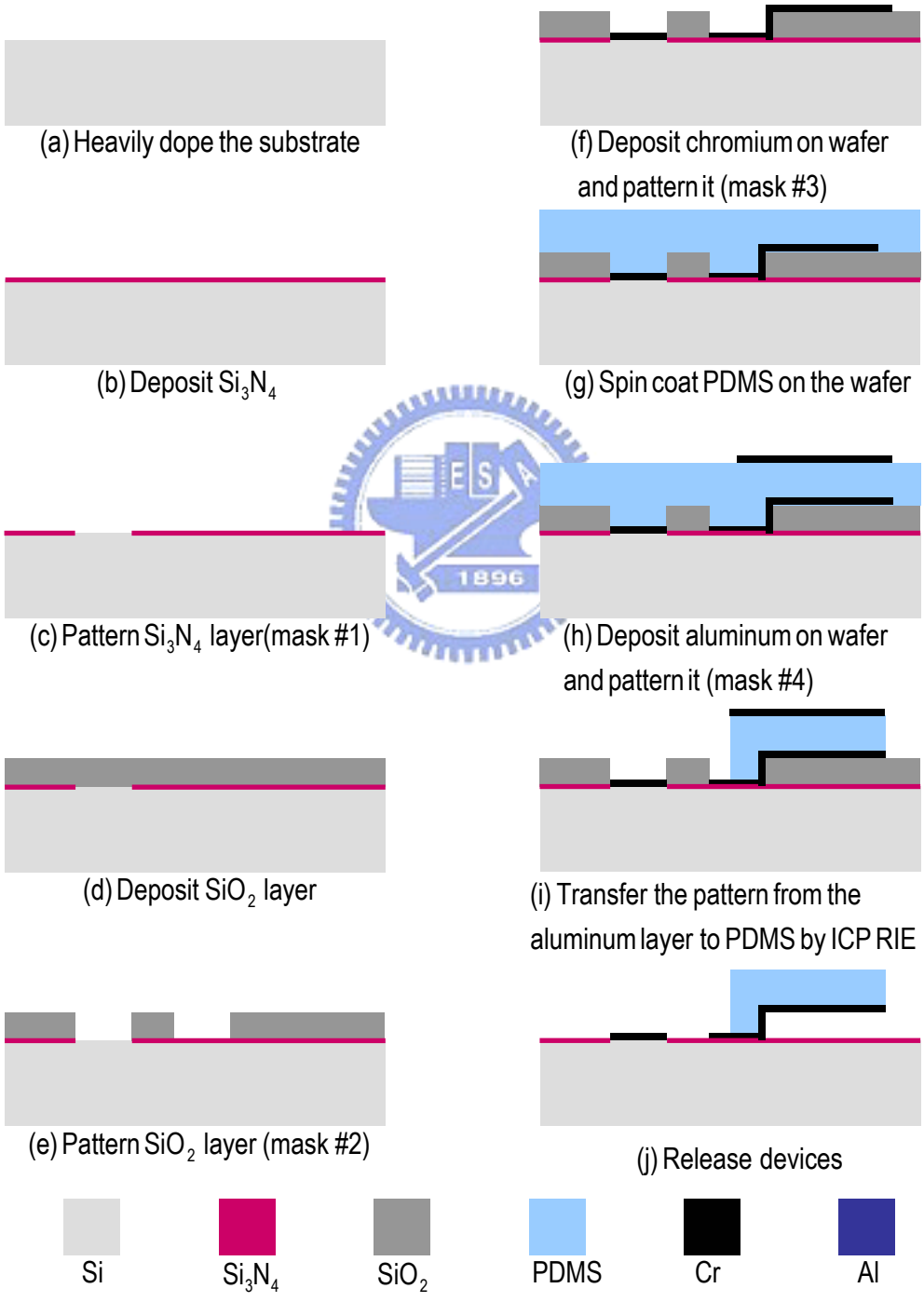

Figure 3-3 Process flow of PDMS cantilever beam.

3-3 Processing Issues

3-3-1 Thickness of PDMS Films vs. Spin Rate

The PDMS used in this study is Sylgard 184 from Dow Corning. The product includes two parts: one is the PDMS base, the other is the curing agent. Both of them are transparent liquids. First these two parts should be completely mixed with the ratio 10:1 by weight. The mixed liquid was then poured into the mold. Because PDMS is viscous, it can trap air during mixing. So after pouring the mixed liquid into mold, the trapped air should be removed vacuum degassing. To cure PDMS, it can be just left intact for 24 hour at room temperature. The curing time can be reduced by increasing the temperature. It takes 1 hour to cure PDMS completely at 100℃.

Test experiments were performed to obtain the relationship between the thickness of PDMS and the spin parameters. The result is shown in Figure3-4, the PDMS layer were spun on with the first spin of 1000rpm for 30sec. and parameters of second spin are shown in figure.

When the device was fabricated, the parameters of PDMS spin coating was 1000rpm for 30sec. and 6000rpm for 4min. From Figure 3-4 this parameter should have resulted in a thickness of 6.7μm. However, the measured thickness was 5.6μm. Since test experiments were carried out about one hour after PDMS mixing and in device fabrication it was about 30minutes after mixing, one possible reason could be that the viscosity of PDMS increases with time after mixing because of the cross linking reaction. Therefore, the thickness is not only related to the spinning parameters but also time interval between mixing and spinning.

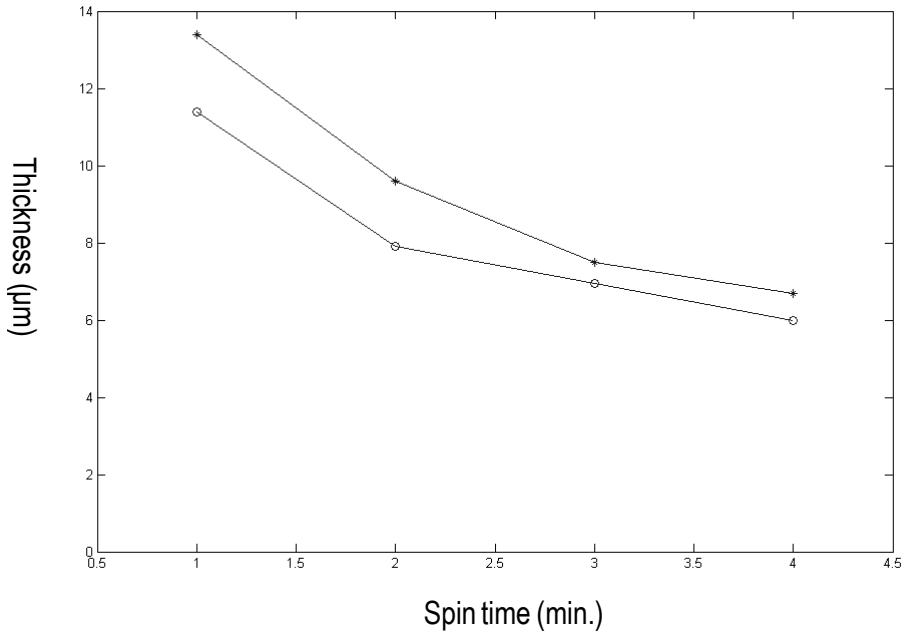

Figure 3-4 Thickness of PDMS vs. spin time for spin rate of 7000rpm and 6000rpm.

3-3-2 Cavity Filling with PDMS

In this study, two methods were used to fill the cavities with PDMS. The first method was modified from that reported by X. Yang [14]. PDMS is difficult to remove once it is coated on the substrate. So the filling of PDMS in the cavities was achieved by a wet lift off process, as shown in Figure 3-5. After the SiO_2 layer was patterned by RIE (Figure 3-5(a)).

The mixed PDMS was cast on the substrate, which was then placed in a vacuum chamber to remove the air trapped in PDMS (Figure 3-5 (b)). The surface of the substrate was wiped by a piece of cotton paper before PDMS was cured (Figure 3-5 (c)). A thin PDMS film would remain on the surface after wiping. The substrate was then flipped over and dipped into acetone immediately. The remaining PDMS would be lifted off (Figure 3-5 (d)).

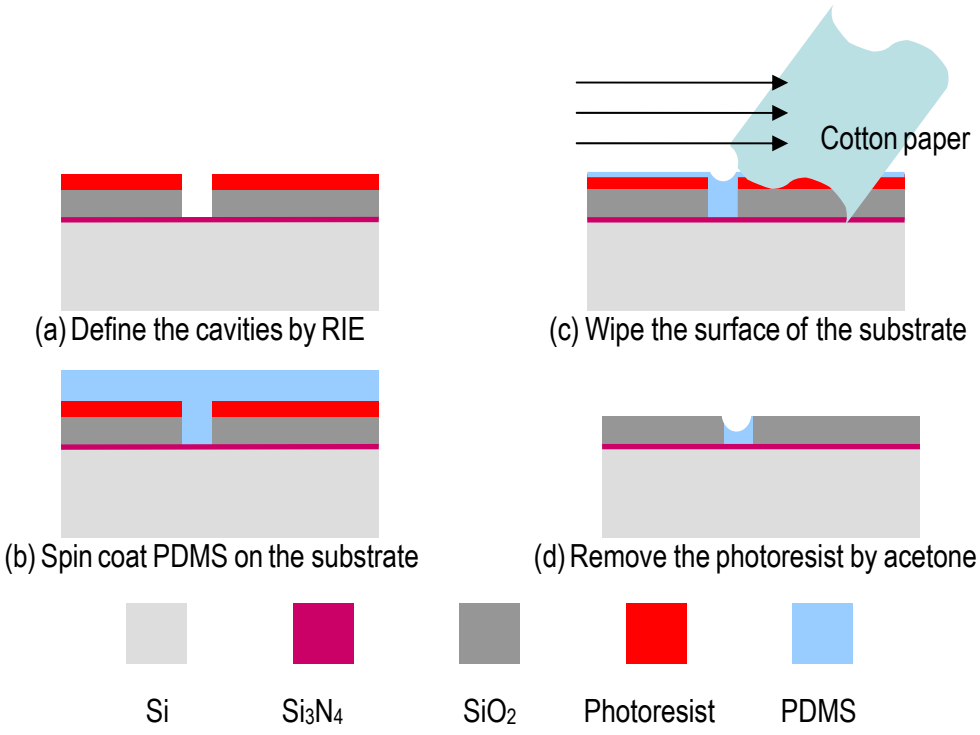

Figure 3-5 The first method to fill the cavities with PDMS.

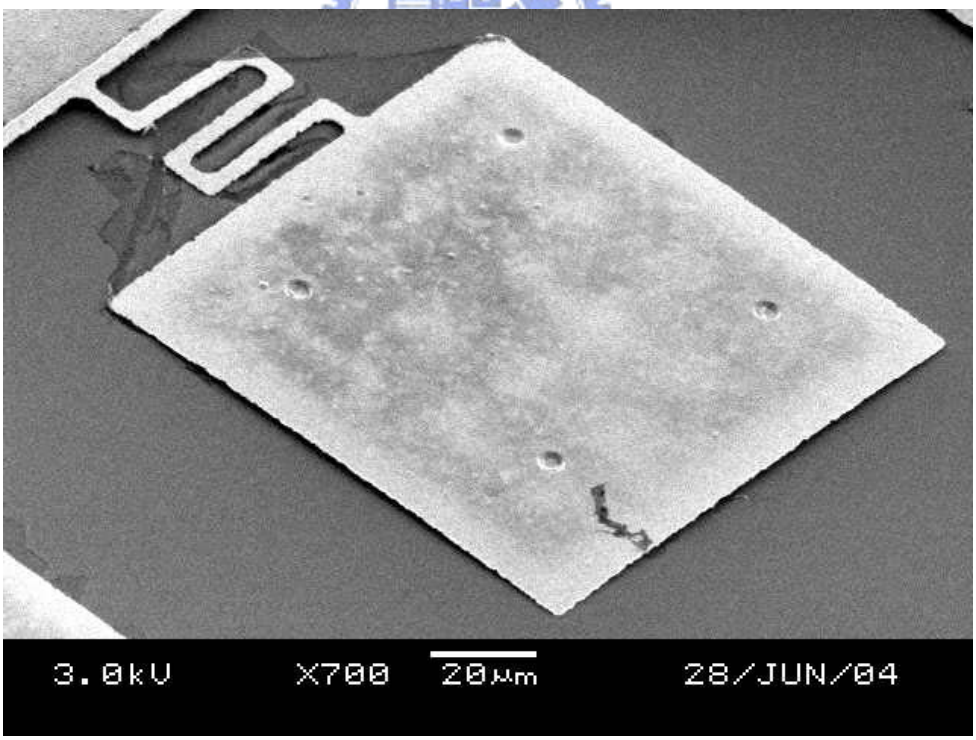

Figure 3-6 The dimples on the top electrode

Figure 3-6 shows the device in which the PDMS posts were formed by this method. The dimples on the top electrode were where the PDMS posts were placed. It is shown that the cavities were not fully filled by PDMS by this method. The depth of the dimples range from 1μm to 1.5μm.

In the second method, PDMS was removed by RIE, as shown in Figure 3-7. After the mixed PDMS was cast on the substrate and degassed, it was cured at 100℃ for 1hour. The thickness of PDMS on the photoresist was measured as 4.8μm. To remove the PDMS film by ICP RIE, process gases of 75sccm $CF_4$and 25sccm O_2 were delivered into the chamber at 30mTorr. The ICP power and the etching time were 200watt and 8 minutes, respectively. Then the photoresist was removed by acetone. If there was any PDMS remained on the photoresist, it could be cleared in this step.

Figure 3-8 shows the device in which the PDMS elastomer posts were formed by the second method. The dimples on the top electrode reveal that the cavities were filled better than in the first method. The depth of the dimples range from 0.5μm to 1μm.

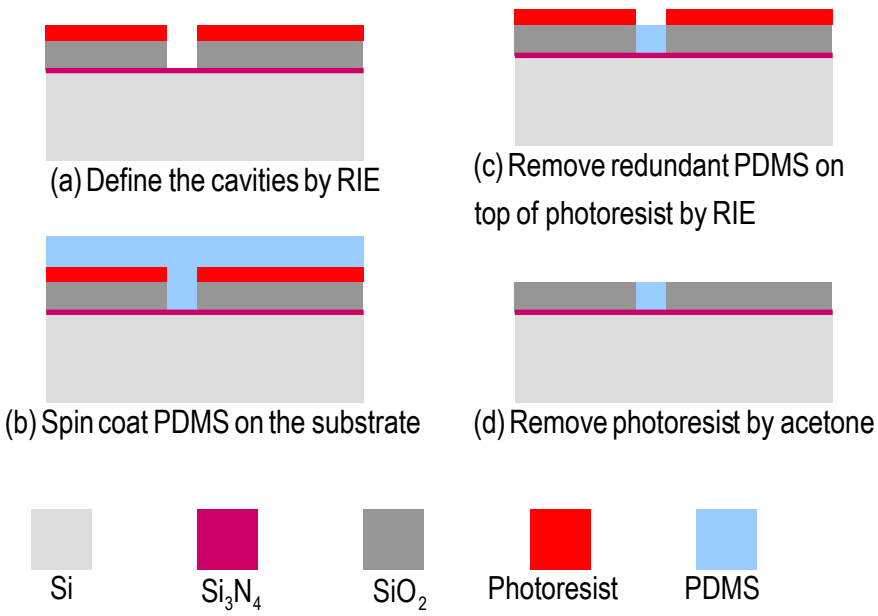

Figure 3-7 The second method to fill the Cavities with PDMS.

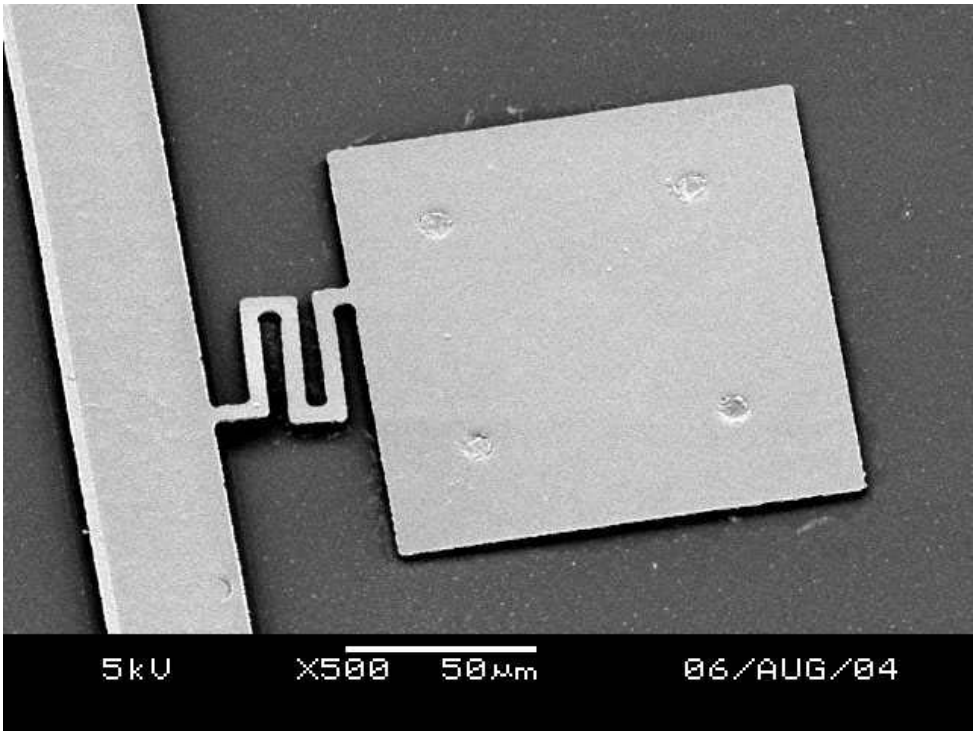

Figure 3-8 Dimples on the top electrode reveal that the cavities were filled better with second method.

3-3-3 O_2 Plasma Treatment

In this study, the positive photoresist AZP 4620 was used in photolithography. Figure 3-9 shows the photoresist spun on PDMS. It can be seen that photoresist tends to shrink to reduce the contact area and form circular holes, as shown in Figure 3-9 (a). Figure 3-9 (b) shows the photoresist which was spun on PDMS and soft baked at 90℃ for 90sec.Cracks in photoresist can be observed. The results show that the adhesion between photoresist and PDMS is extremely poor.On such a PDMS layer, the photolithography is not able to be performed.

The adhesion can be improved by the treatment of O_2 plasma. O_2 plasma treatment oxidizes the surface of PDMS, and converts the $-OSi(CH_3)_2O-$ groups at surface to $-O_nSi(OH)_{4-n}$ groups [9, 10]. The property of oxidized PDMS surface will be similar to that of SiO_2, which is hydrophilic. In addition, HMDS is also necessary to

obtain good adhesion between photoresist and PDMS. Figure 3-9 (c) shows the patterned photoresist on the surface of PMDS which was treated by O_2 plasma and coated with HMDS.

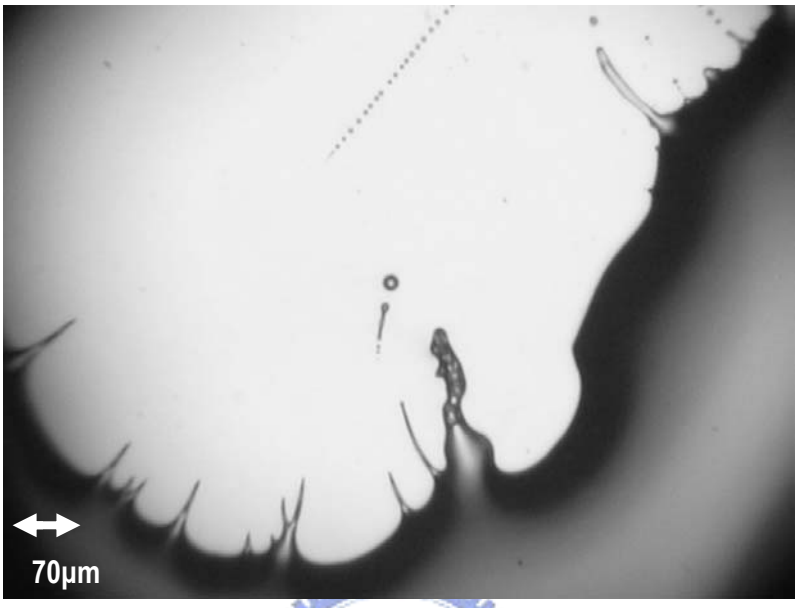

(a) Spun photoresist on PDMS

(b) After photoresist was spun on PDMS and soft baked, it split.

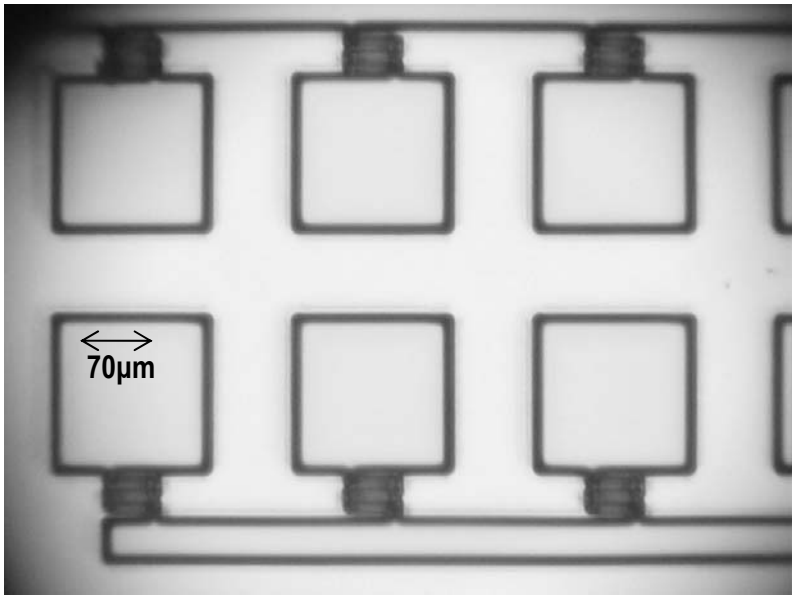

(c) After the surface of PDMS was treated with O_2 plasma and coated by HMDS, photolithography can be performed on it.

Figure 3-9 The relationship between photoresist and PMDS. PDMS in (a) and (b) was not treated with O2 plasma, but PDMS in (c) was treated with O2 plasma.

To fabricate the gap-closing actuator with PDMS posts, after the cavities are filled with PDMS, the next step is to define the anchor (mask #3), as shown in Figure 3-1 (g). However, the untreated PDMS has poor adhesion with subsequent photoresist layer. It is necessary to treat the PDMS with O_2 plasma to enhance adhesion.

When the photolithography was performed without the O_2 plasma treatment, the photoresist would peel off during developing the pattern on it. The peeling of photoresist is caused by the poor adhesion between photoresist and PDMS, even though the PDMS only occupies very small area. Figure 3-10 (a) shows the patterned photoresist on an untreated surface. Figure 3-10 (b) shows the patterned photoresist on the treated with O_2 plasma suface.The O_2 plasma treatment can effectively improve the adhesion, so that photolithography can be facilitated.

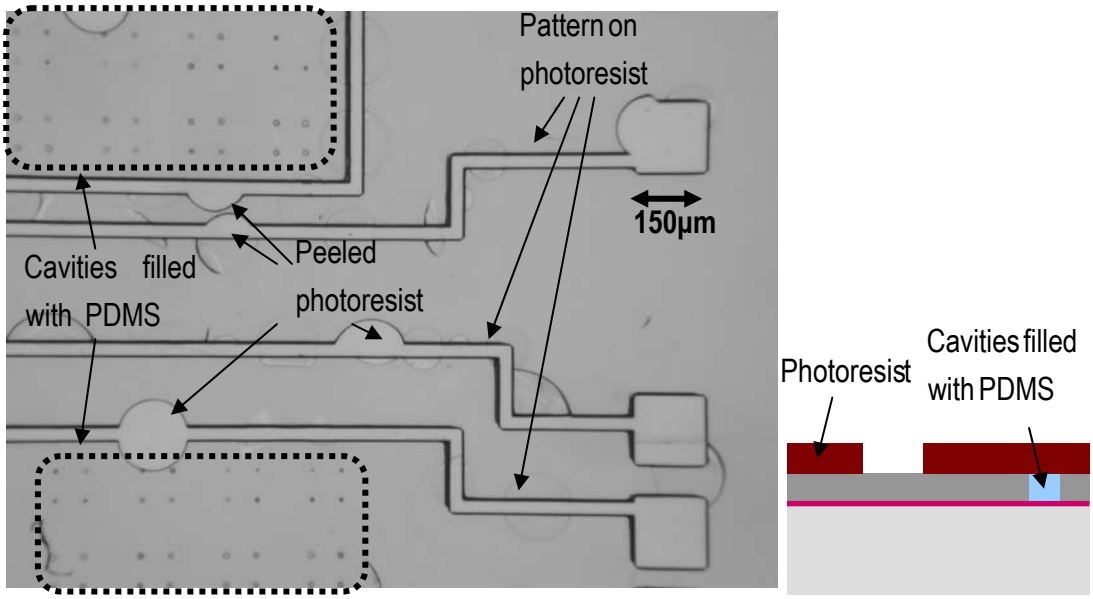

(a) Without the treatment of O_2 plasma

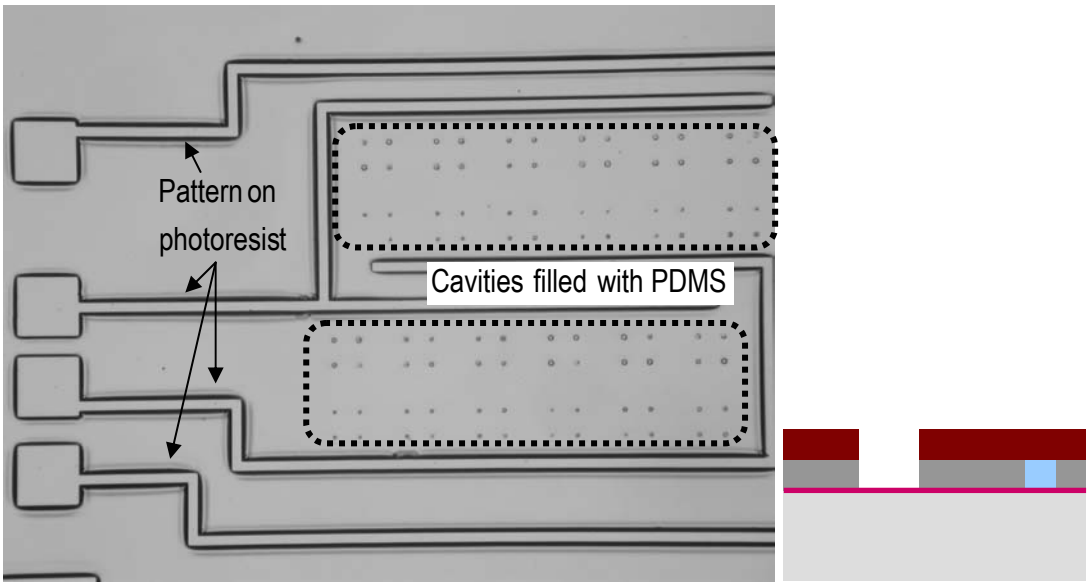

(b) With the treatment of O_2 plasma

Figure 3-10 Pattern of photoresist after cavities were filled with PDMS.

Figure 3-11 (a) shows an aluminum layer deposited on PDMS. As shown in the figure, the quality of the aluminum film sputtered on the untreated PDMS was very bad. It was badly wrinkled. Besides, the adhesion between aluminum and PDMS was very poor and photolithography and wet etching were not able to be performed. To improve the aluminum film quality on PDMS, the surface of PDMS can be treated by

O_2 plasma. Figure 3-11 (b) shows the aluminum film deposited on O_2 plasma treated PDMS. As shown in the figure, the film was a little rough but not wrinkled. After the treatment of O_2 plasma, the adhesion good is enough to perform photolithography and wet etching.

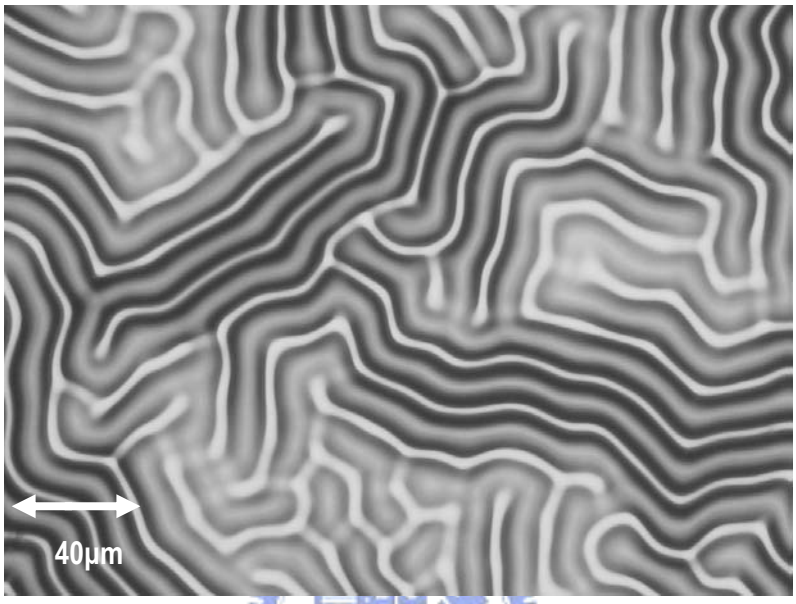

(a) Aluminum film deposited on PDMS.

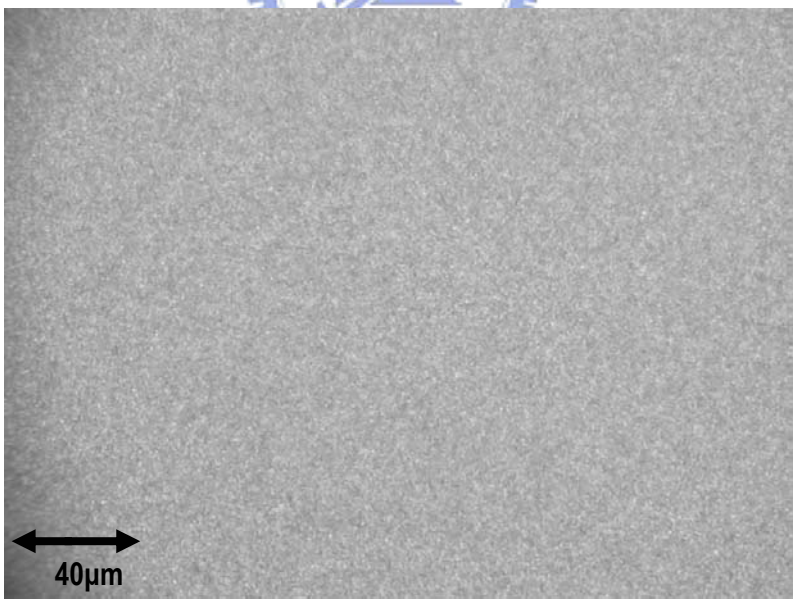

(b) Aluminum film deposited on O_2 plasma treated PDMS.

Figure 3-11 Aluminum film deposited on PDMS.

3-3-4 Patterning of Chromium Layer

The connecting beam is the least strong part in the device. If the connecting beam is too narrow due to processing errors, it will easily break when the device is released. In the fabrication process of the gap-closing actuator with PDMS posts,

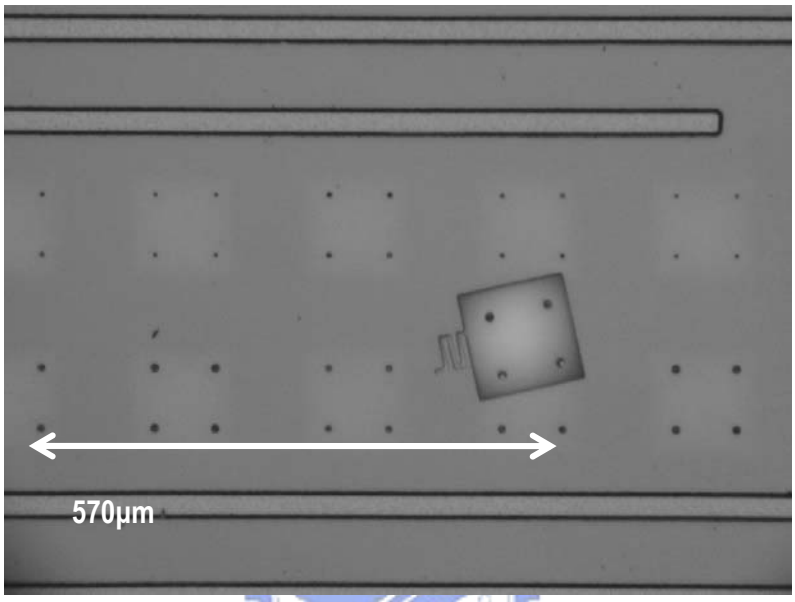

(a) Without filter lens

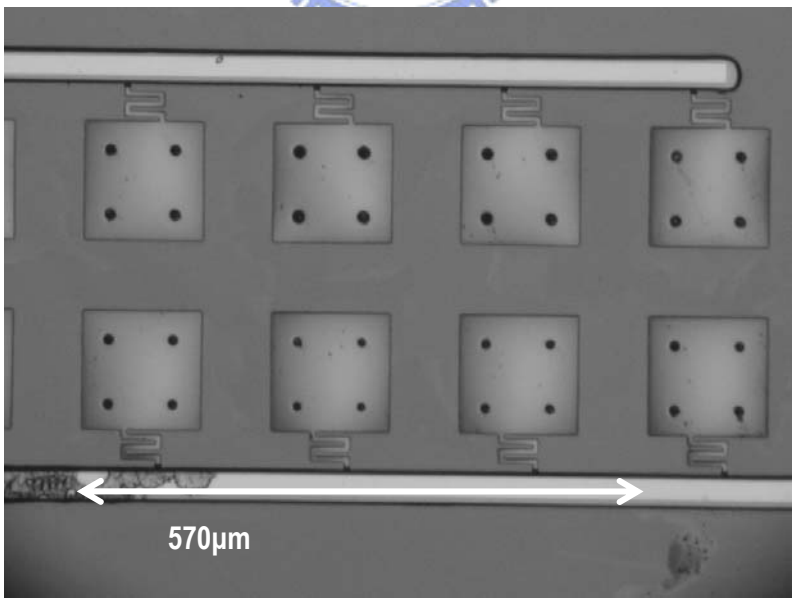

(b) With filter lens

Figure 3-12 Effect of the exposure filter on the process yield.

the chromium layer was patterned by photolithography and wet etching. The photoresist used in the photolithography was AZP 4620 with thickness of 7μm, and the chromium layer was etched with CR7T. Both of these two steps introduced errors. Figure 3-12 (a) shows the released device whose connecting beams were broken during releasing. As shown in the graph, the yield of process is very poor. Since wet etching always introduces undercut, light source in photolithography plays an important role to improve the process yield. To obtain better exposure, a filter lens was added during exposing. The filter lens will filter out the light with wave length longer then 365nm. Therefore, the width of the connecting beam can be maintained. Figure 3-12 (b) shows the released devices fabricated by adding a filter during exposure.

3-4 Fabrication Result

3-4-1 PDMS Posts

Figure 3-13 (a) shows the SEM photograph after SiO_2 cavities were filled with PDMS by the second method mentioned in Section 3-3-2. As shown in the figure, the PDMS posts are little higher than the surface of SiO_2. Figure 3-12 (b) shows the PDMS posts after removing SiO_2 layer. As shown in the figure, PDMS posts are not a perfect cylinder. The top surface of the PDMS post is rough. The rough surface of PDMS caused by RIE was mentioned in the study of Garra et al. [12]. Besides, there is a ring around the PDMS post. A possible reason is shown in figure 3-14. Before SiO_2 was removed, the cavities were slightly overfilled with PDMS. After SiO_2 was removed, the overhanging part had no support and dropped to the substrate and, therefore, formed the ring.

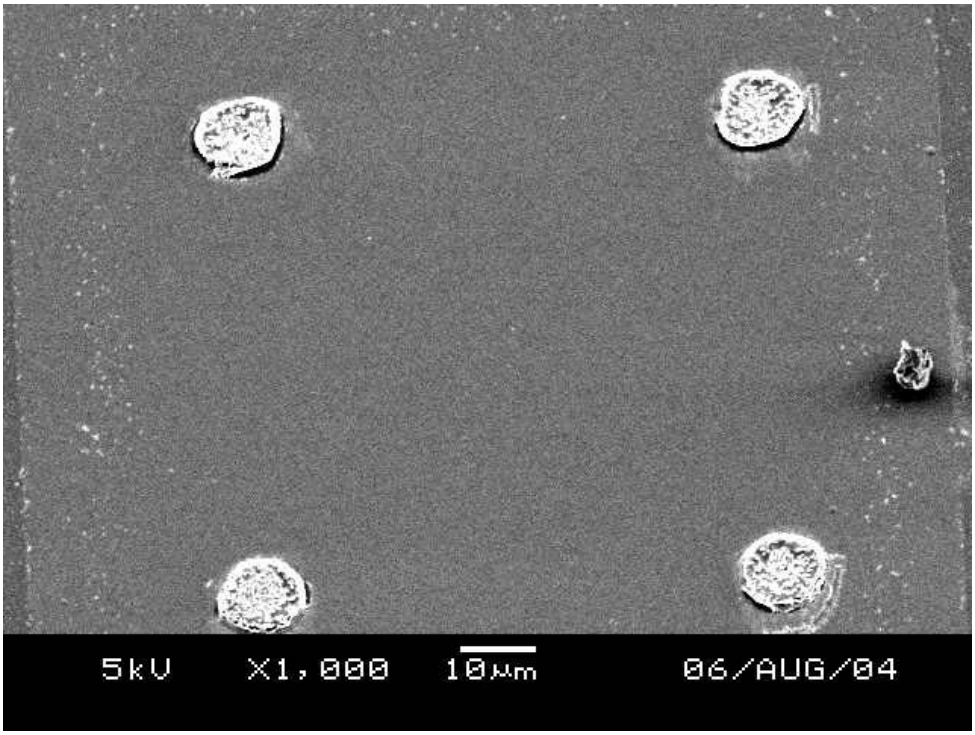

(a) PDMS posts in the SiO2 cavities.

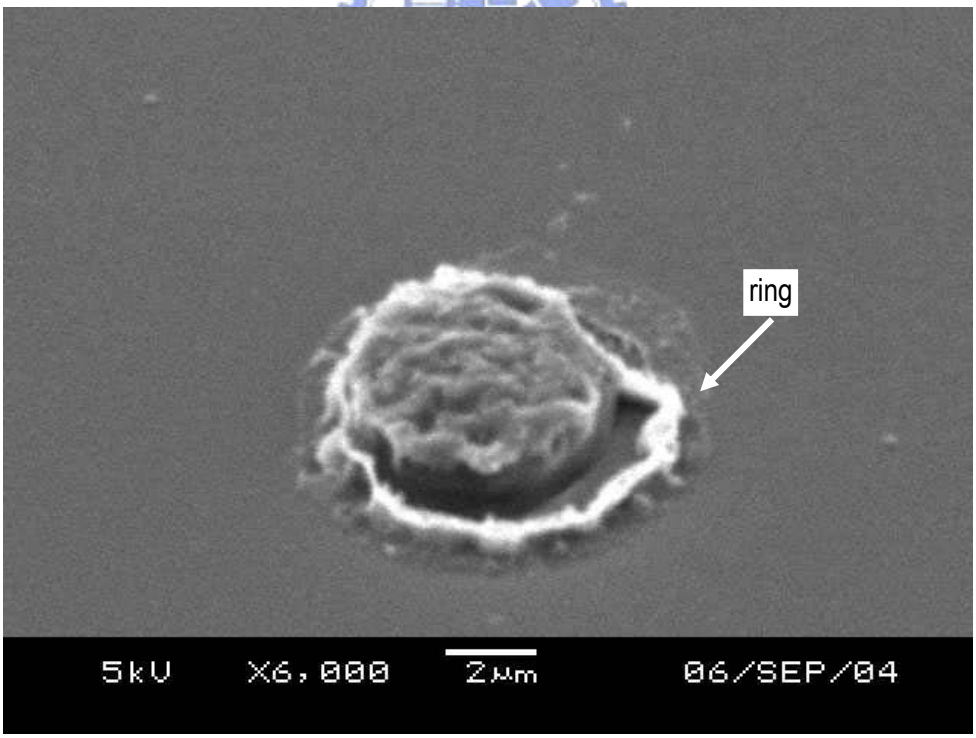

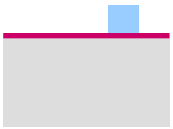

(b)PDMS posts with the SiO_2 layer removed.

Figure 3-13 PDMS posts

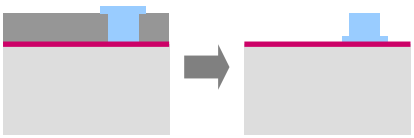

Figure 3-14 Schematic of the ring formed around the PDMS post

3-4-2 Chromium Structure Layer

After the device was released, the chromium layer was taken as the top electrode. Figure 3-15 shows the SEM photograph of a device. To observe the suspension of the top electrode, the surface profiles were measured by a WYKO NT1100 interferometer. The profile image of a device is shown in Figure 3-16. As shown in the figure, the top electrode is curled, which indicates a residual stress in the deposited film.

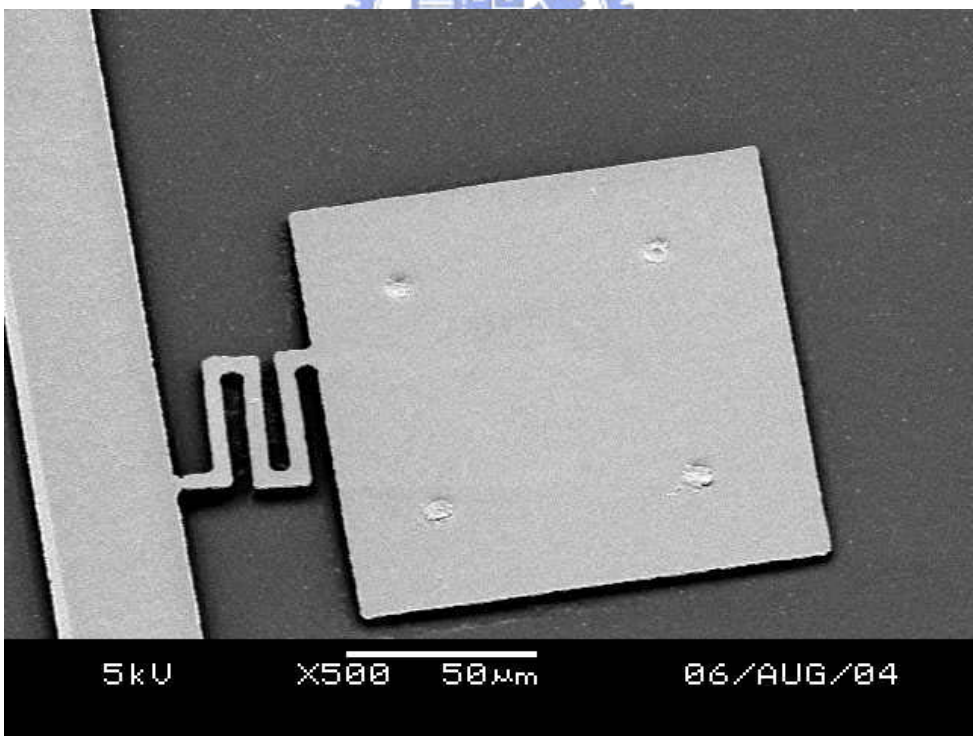

Figure 3-15 SEM photograph of the device.

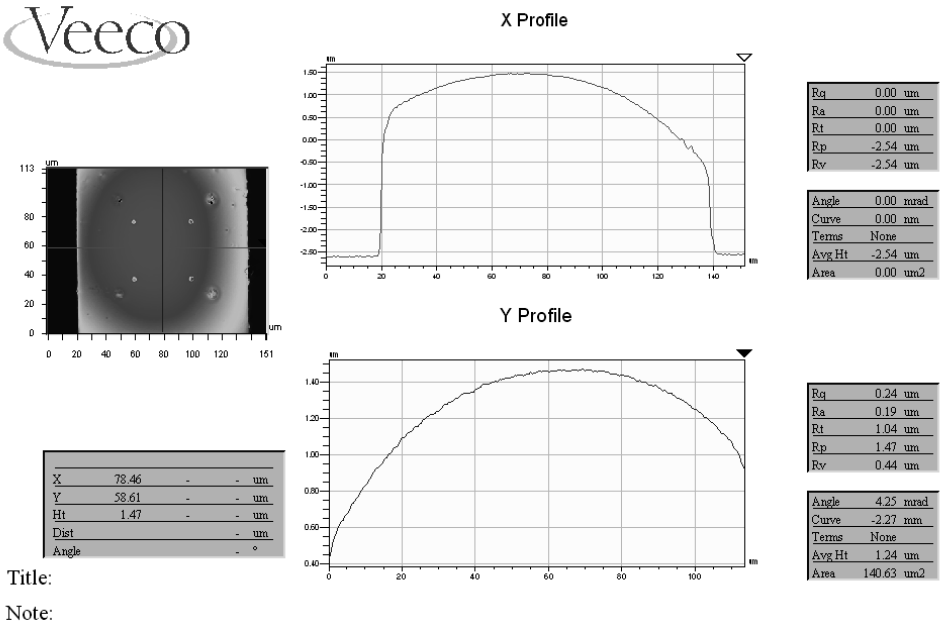

Figure 3-16 Profile image obtained from WYKO NT1100 interferometer.

Residual stress in a thin film is composed of a uniform component and a gradient component, as shown in Figure 3-17. The uniform residual stress causes slight elongation or shortening of the structure, but the value can not be measured. Gradient residual stress causes curling and its value can be obtained by measuring the radius of curvature of the film. Relationship between gradient residual stress and radius of curvature of a cantilever beam is shown in the following equation [20],

$$\sigma_1 = \frac{1}{2} \times \frac{EH}{\rho_x} \tag{3-1}$$

where E is Young's modulus, H is the thickness, and ρ_x is the radius of curvature of the film.

To obtain the residual stress, the surface profile of a cantilever beam was measured by the interferometer, as shown in Figure 3-18. Radius of curvature of the beam is about 1600μm. With the Young's modulus of 140GPa and thickness of

1.25μm, the value of σ_1 is calculated as 54.7MPa.

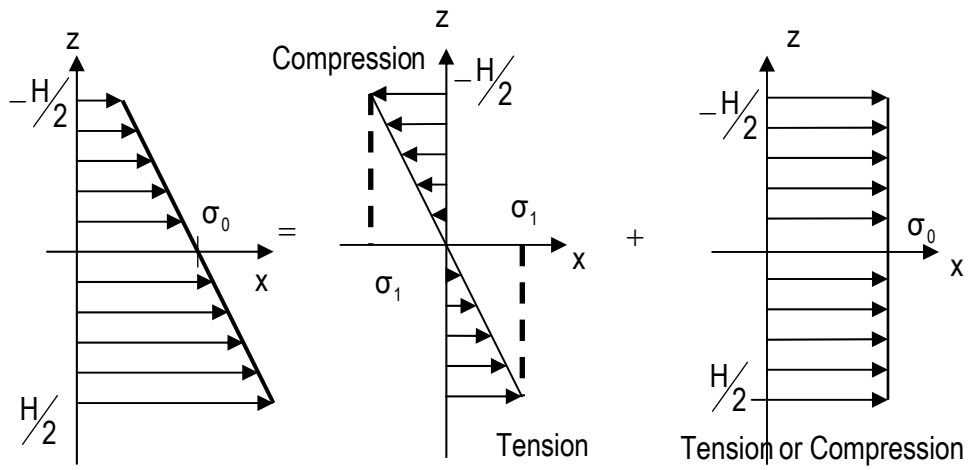

Figure 3-17 Residual stress in a cantilever beam.

Due to the gradient residual stress, the top electrode is not flat; the gap between top electrode and the substrate is larger at the center and smaller at the corners. The gap at the center of top electrode is 2.66μm, and is 1.74μm at corner. The radius of the top electrode is about 2200μm from Figure 3-16. This value is greater than the cantilever beam. The radius of curvature of the plate can be obtained by the Equation 3-2.

$$\rho_x = \frac{1}{2}\left(\frac{E}{1-\nu}\right)\frac{H}{\sigma_1} \qquad (3\text{-}2)$$

where ν is the Poisson's ratio. For chromium ν is 0.3. By substituting σ_1 calculated from the cantilever beam, a radius of curvature of 2285μm was obtained from Equation 3-2, which is close to the measured value in Figure 3-16. However, the variations in radii of curvature for chromium structures are large. The radii of curvature of the top electrodes range from 1500μm to 2500μm, and for cantilever beams, the radii range from 600μm to 1500μm. One possible reason is that the distribution of residual stress in the chromium film is not uniform.

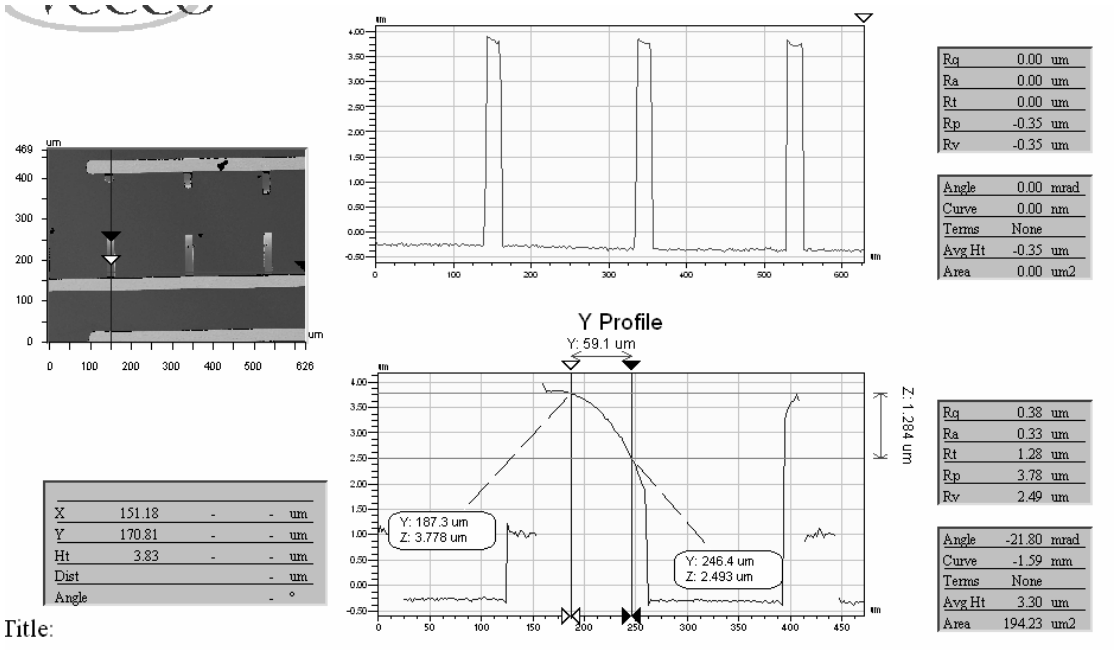

Figure 3-18 Surface profile of a cantilever beam

3-4-3 PDMS Cantilever Beam

The patterning of the PDMS layer was completed by ICP RIE and PECVD with the process parameter of chamber cleaning. In this process, an aluminum film was used as the masking layer. RIE process gases include 75sccm $CF_4$and 25sccm O_2, and the chamber pressure is 30mTorr. The PDMS film was etched for 12minutes and 30seconds with an ICP power of 200watt. Figure 3-19 shows the SEM photograph of the device after RIE, in which the aluminum film was removed. As shown in the figure, a 8000Å-thick of PDMS layer remained on the substrate after RIE. The remained PDMS was etched in the chamber of PECVD with the process parameter of chamber cleaning. Process gases of 400sccm CF_4 and 100sccm O_2 were delivered into the chamber at 250℃. The RF power and process time were 300watt and 30min. After the process, there was a layer of ashes remaining on the SiO_2, which is shown in Figure 3-20. The SEM photograph of the device after the PDMS layer was completely etched is shown in Figure 3-21.

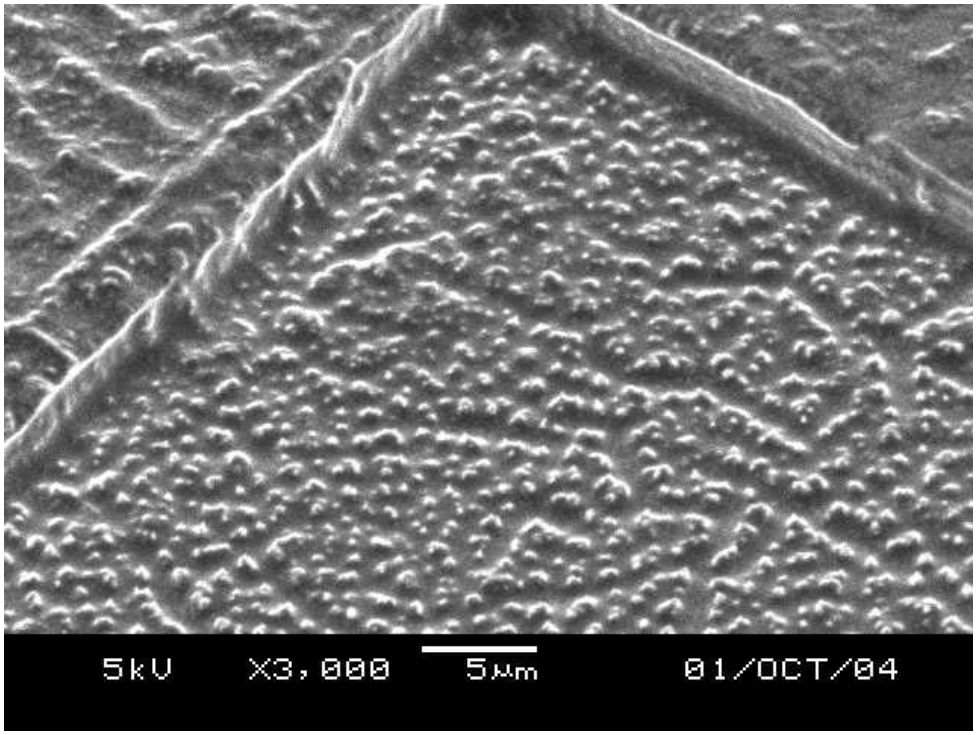

Figure 3-19 SEM photograph of the devices after the PDMS layer was first etched by RIE.

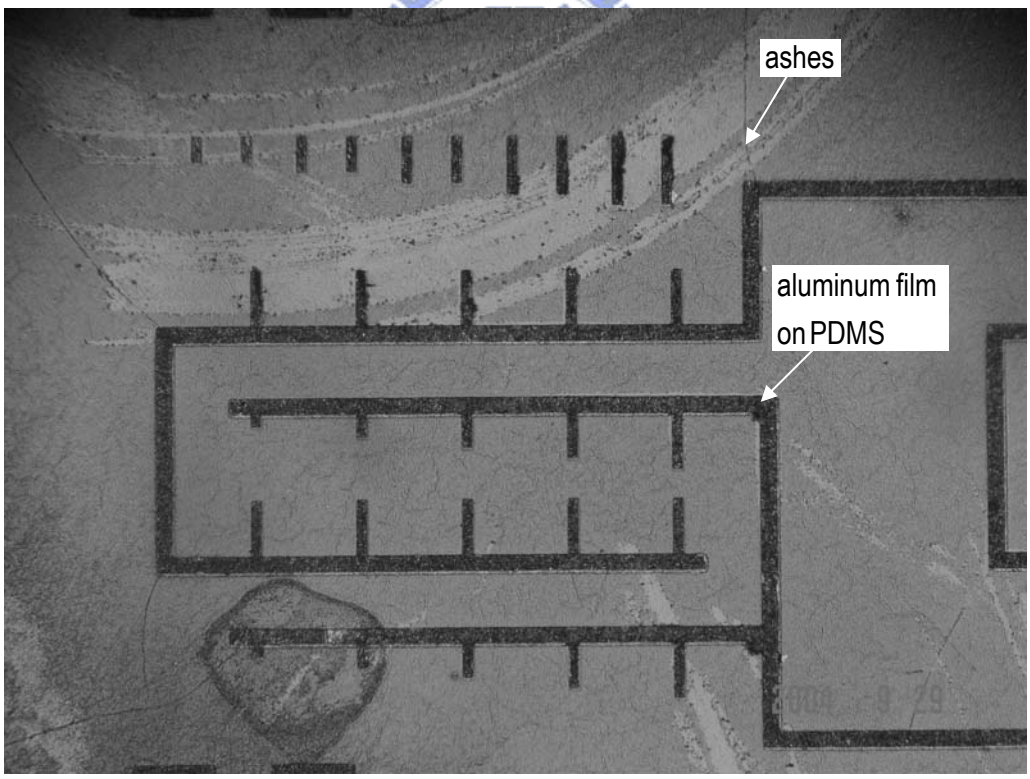

Figure 3-20 The photograph of the devices after the PDMS layer was patterned.

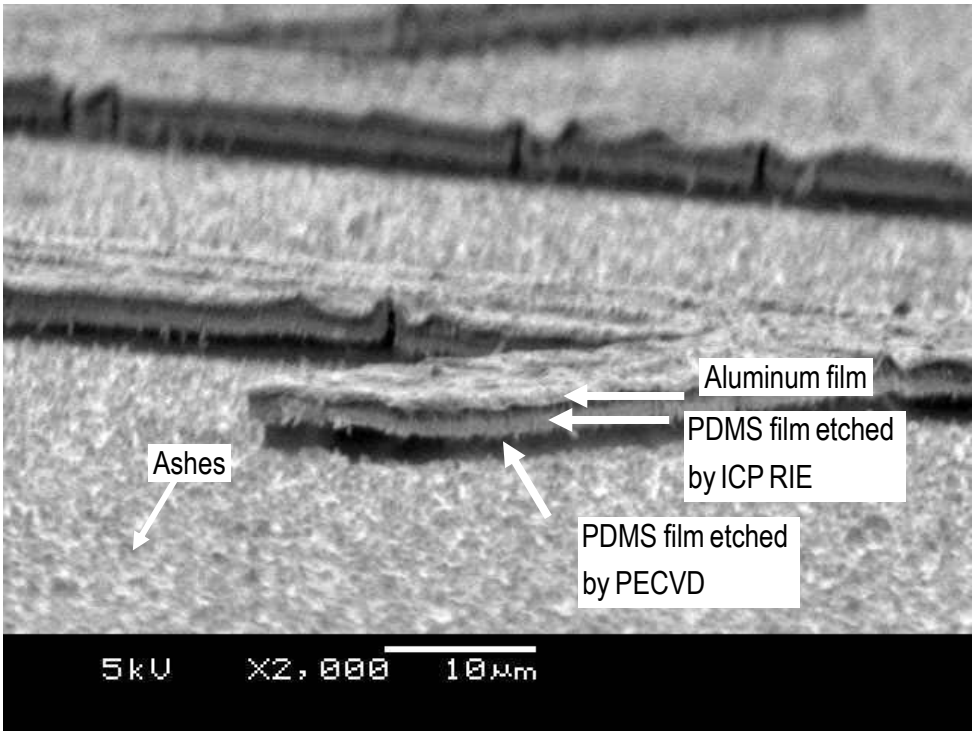

Figure 3-21 SEM photograph of the devices after the PDMS layer was completely etched

After the PDMS film was etched, the aluminum hard mask and the SiO_2 layer were removed simultaneously by 49% HF. Figure 3-22 shows the photograph of the released device. As shown in Figure 3-22, despite the ashes on the surface, the SiO_2 layer was easily etched. Figure 3-23 shows the SEM photograph of a cantilever beam. As shown in the figure, the PDMS cantilever beam was stuck on the substrate. So the structural force of the PDMS cantilever beam and the underneath chromium layer were not enough to suspend itself. Therefore, the actuation of the device would not be performed. Compare Figure 2-23 to Figure 2-21, the PDMS structure seemed to reflow and became smooth. A possible reason is that when the PDMS was freed, its structure tends to cohere to achieve a state with lower energy.

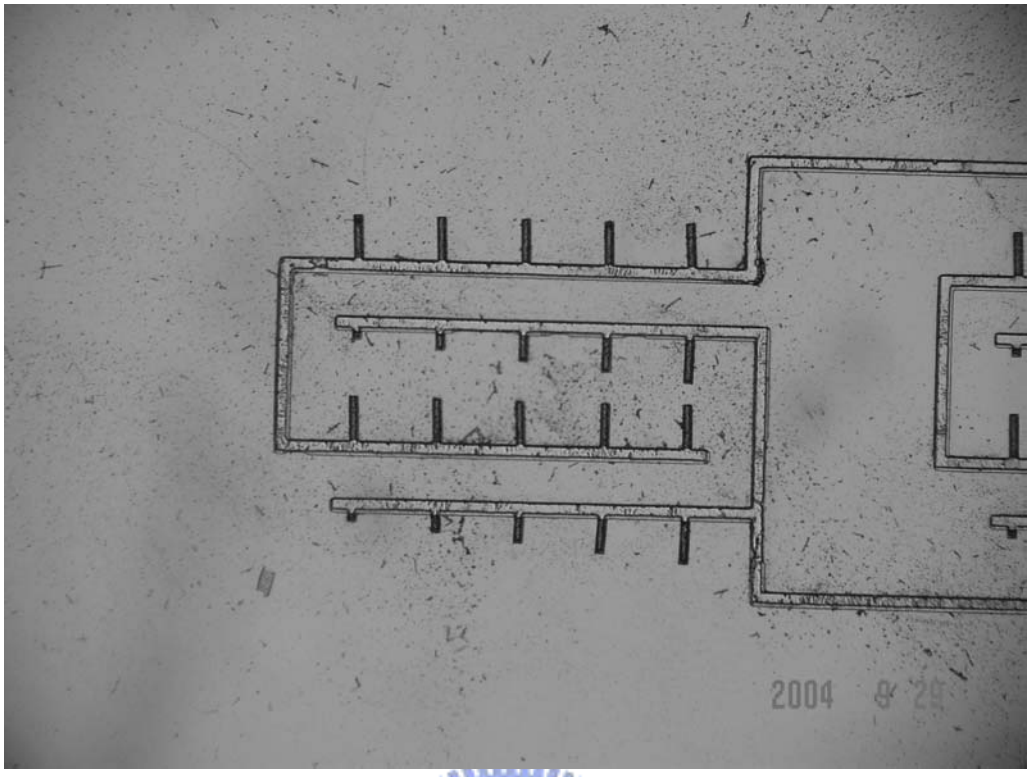

Figure 3-22 Released PDMS cantilever beams.

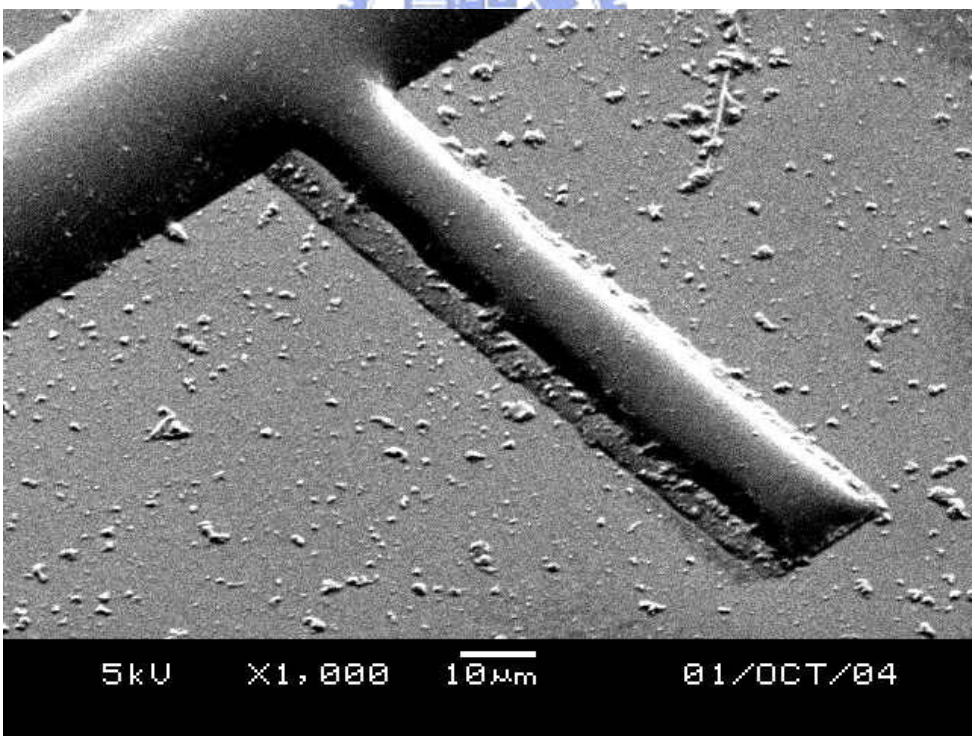

Figure 3-23 SEM photograph of released a PDMS cantilever beams.

Ⅳ、Measurement and Discussion

In this chapter, the instrument setting and measured are first presented. The actual behavior of the device is then discussed.

4-1 Measurement Setting

Figure 4-1 shows the schematic of the measurement platform. As shown in the figure, a DC voltage is supplied by the power supply and delivered to the device through the probe station. The displacement is measured by a WYKO NT1100 interferometer and the data are collected by the computer. Figure 4-2 shows the photograph of the instrument setting.

4-2 Measured Data

In this section, the measured data of test devices are presented. The test devices are used to verify the function of the PDMS posts. Then the measured data of gap-closing actuators with PDMS posts are presented.

4-2-1 Cantilever Beams

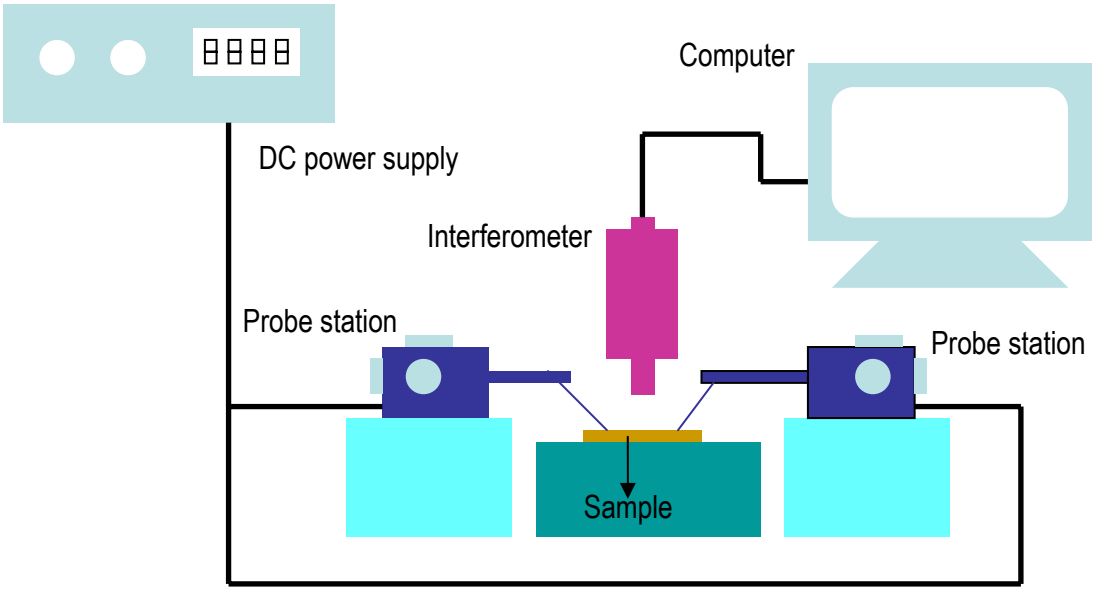

Figure 4-1 Schematic of measuring platform.

Figure 4-2 Instrument setting

To compare the behaviors of gap-closing actuators with and without PDMS posts, test devices were fabricated. As shown in Figure 4-3, one is a pure chromium cantilever beam, which is called as "beam 1", and the other is a chromium cantilever beam with a PDMS post, which is called as "beam 2". Figure 4-4 shows the surface images of beam1 and beam 2 obtained by the interferometer. In the figure, the data of profile a-a' (beam 1) and b-b' (beam2) were recorded for various applied voltages, and are shown in Figure 4-5.

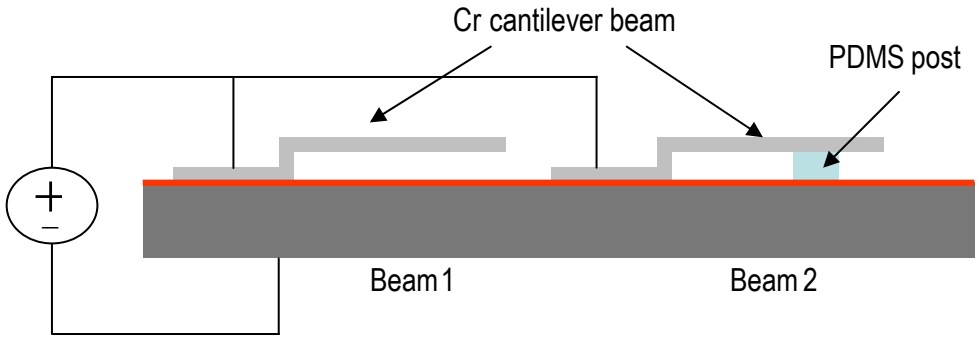

Figure 4-3 Test devices for verifying the functions of PDMS posts.

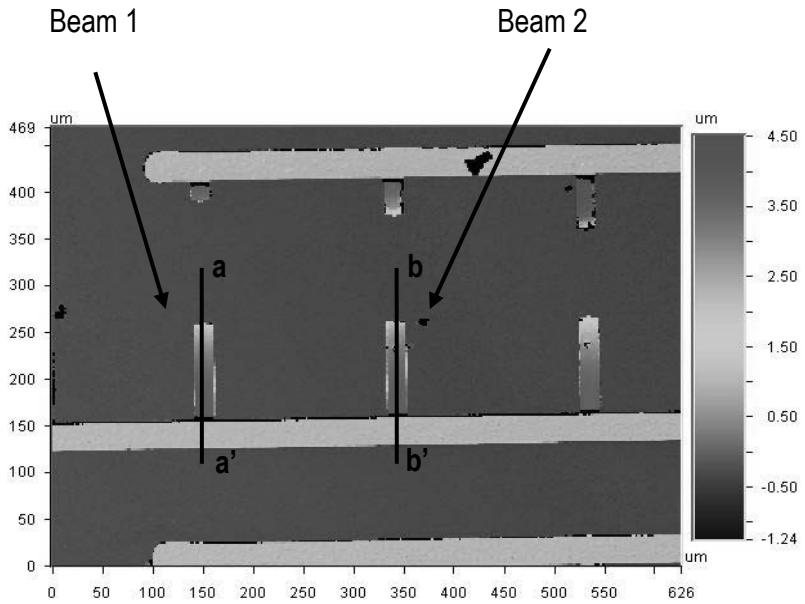

Figure 4-4 The surface images of beam 1 and beam 2.

From the displacement in Figure 4-5 (a) and 4-5 (b), the pull-in of beam 1 can be seen, and at the point 70μm from the fixed end of the beam, the controllable displacement is about 0.5μm. But for beam 2, the displacement of the corresponding point is larger than beam 1. As showed in the figure, the maximum displacement is 0.75μm for an applied voltage of 95V. Figure 4-5 (c) shows the displacement of the point 70μm from the fixed end of the beams. Therefore, the controllable displacement of beam2 is extended with the nonlinear elastic restoring force of PDMS posts.

From Figure 4-5 (b), the result of the filling of PDMS can be seen. The profile b-b' passed through where PDMS post is placed. There was a sunken part on the profile at about 72μm from the fixed end, which reveals that the cavity was not fully filled by PDMS.

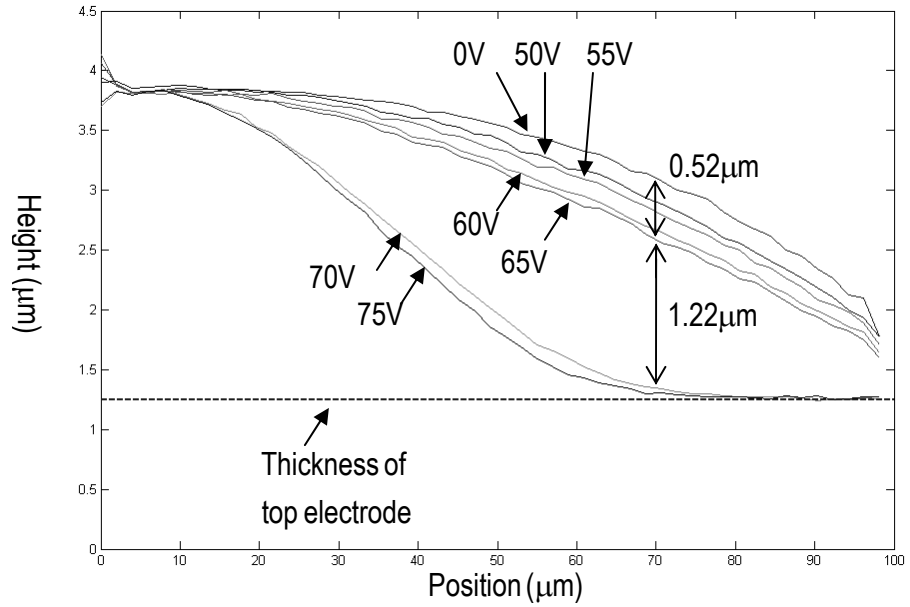

(a) Surface of profile a-a' for various applied voltages

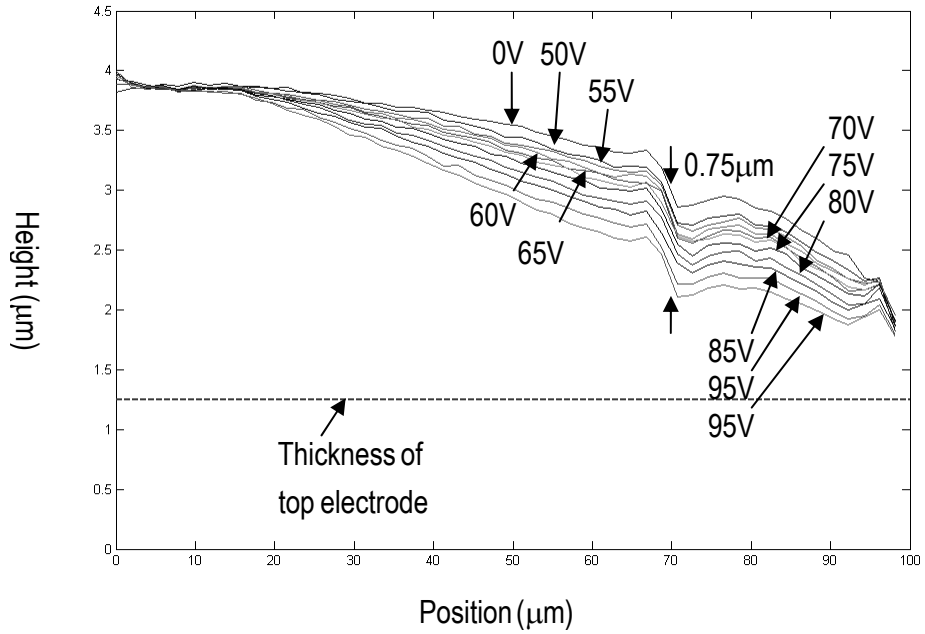

(b) Surface of profile b-b' for various applied voltages

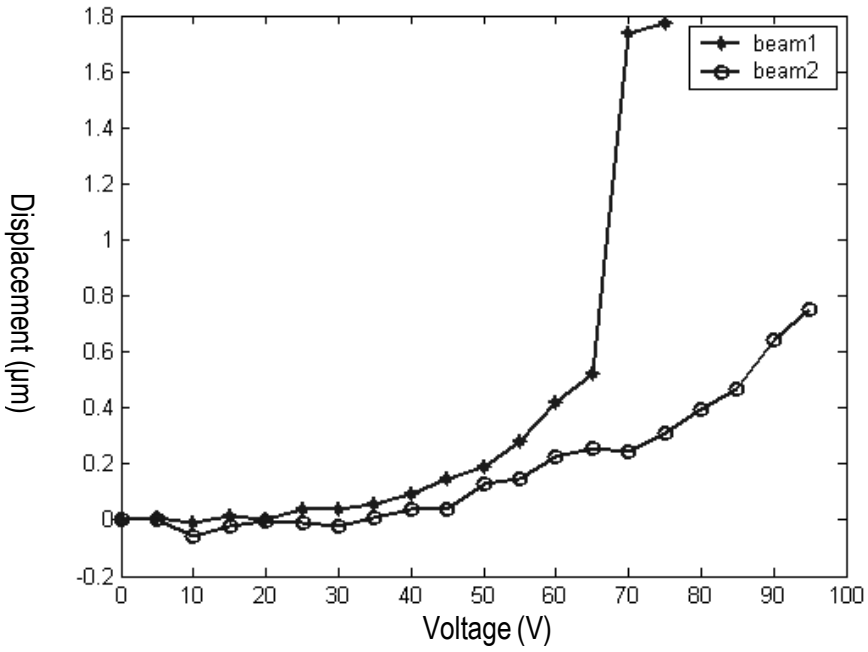

(c)Displacement of beam1 and beam2 vs. voltage.

Figure 4-5 Profile data and displacement of beam 1 and beam 2.

4-2-2 Gap-closing Actuator with PDMS Posts

Figure 4-6 shows layout of six devices in which have PDMS posts with radii from 2μm to 4.5μm. The top three devices are connected to the same pad, so they would be actuated simultaneously. The bottom three devices are connected to another one. The six devices are assigned from "device 1" to "device 6", as is shown in figure. In this measurement, surface profiles were obtained by the interferometer every 5V. Figure 4-7 shows the surface image of the six devices with no applied voltage. The data of the profile a-a' and b-b' in Figure 4-7 were recorded for various applied voltages, and are shown in Figure 4-8 (a) and (b).

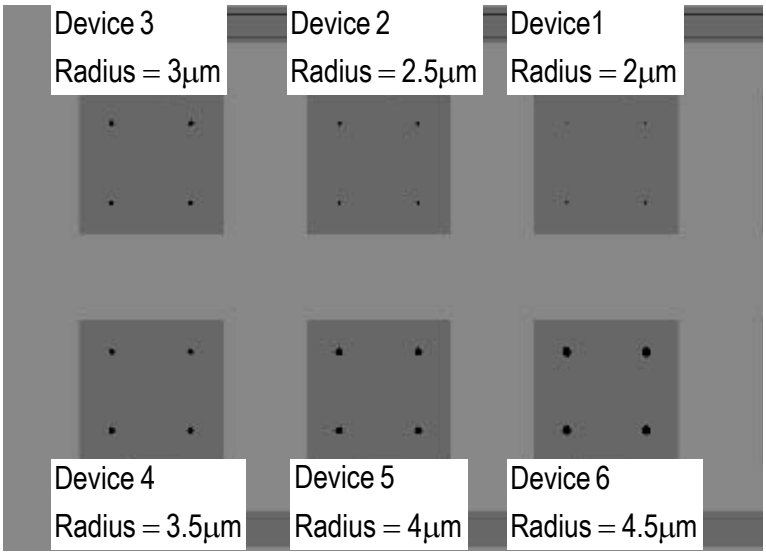

Figure 4-6 The layout of the devices. The diameters of the PDMS posts are shown in the figure.

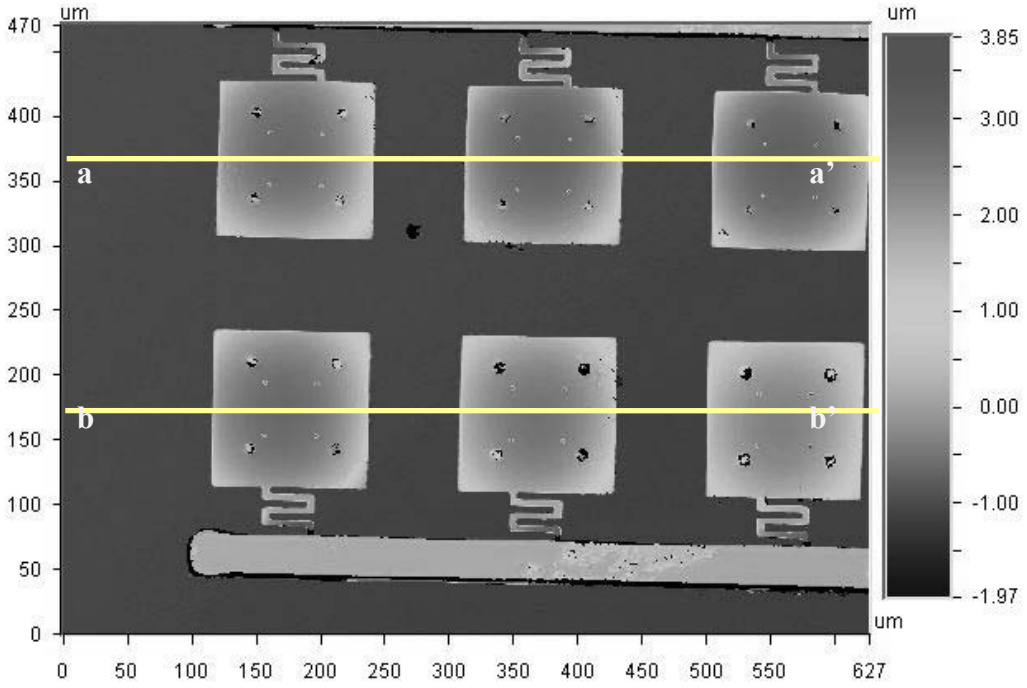

Figure 4-7 The surface image of the six devices when the applied voltage is 0.

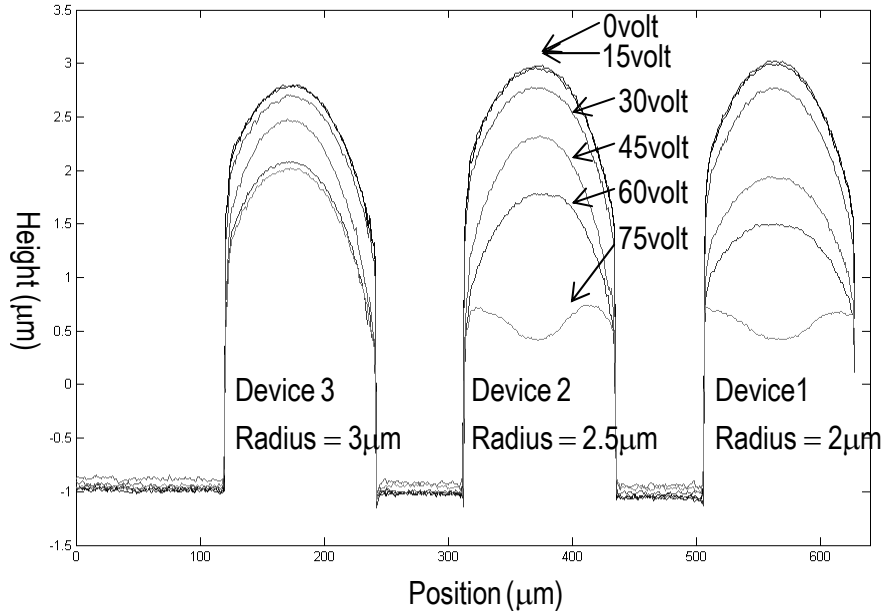

(a) Profile a-a' for various applied voltages. (Device 1-3)

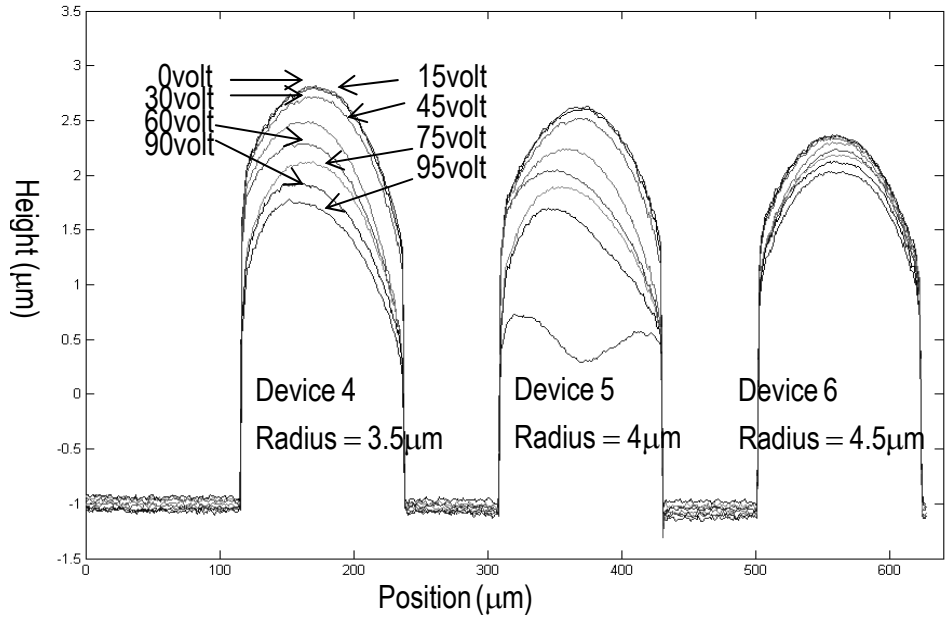

(b) Profile b-b' for various applied voltages. (Device 4-6)

Figure 4-8 The profile data of test devices

The displacement of five points on the top electrodes are plotted in Figure 4-9.They are the center point and four points right above the PDMS posts.

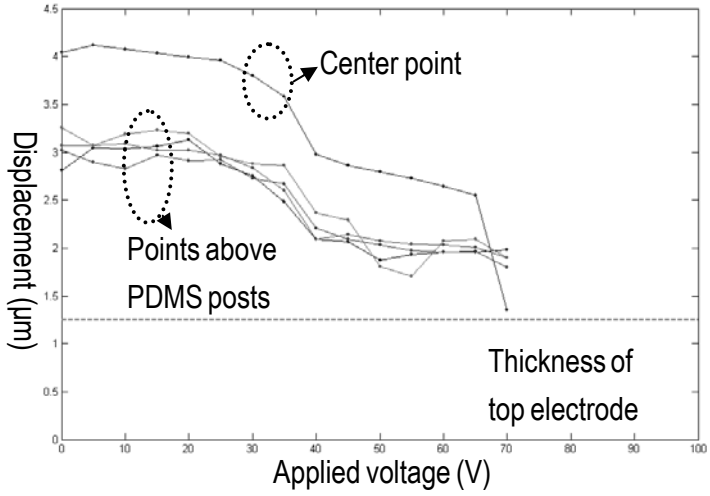

(a) Device 1 (r=2μm)

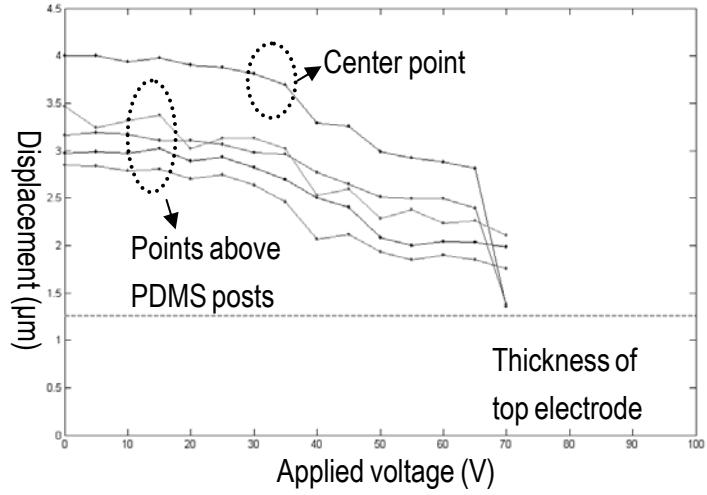

(b) Device 2 (r=2.5μm)

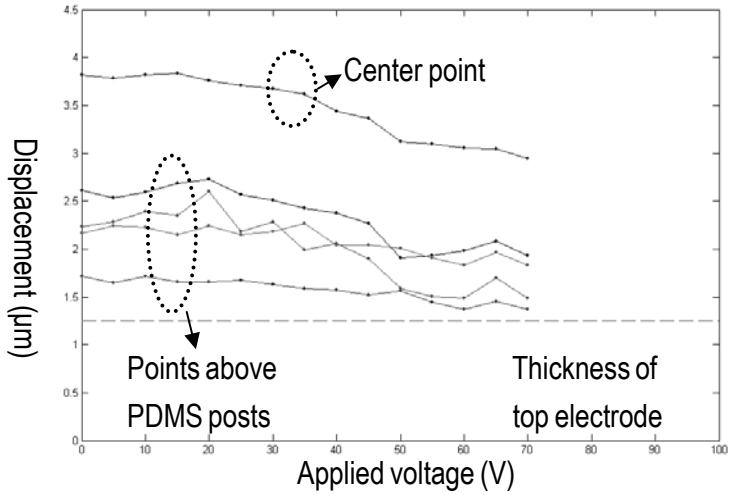

(c) Device 3 (r=3μm)

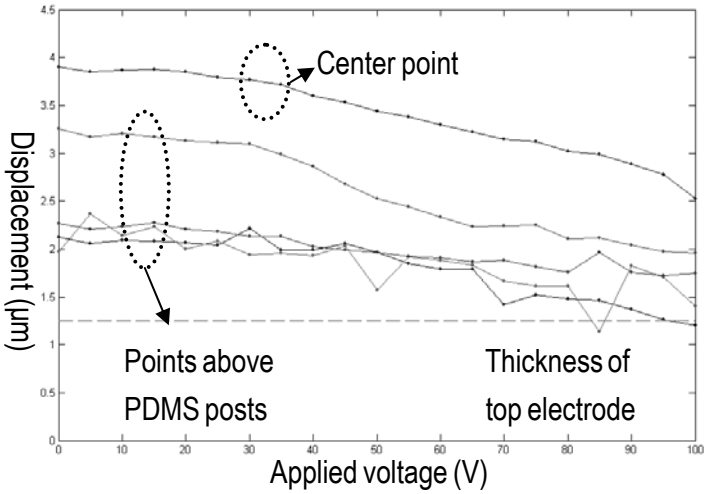

(d) Device 4 (r=3.5μm)

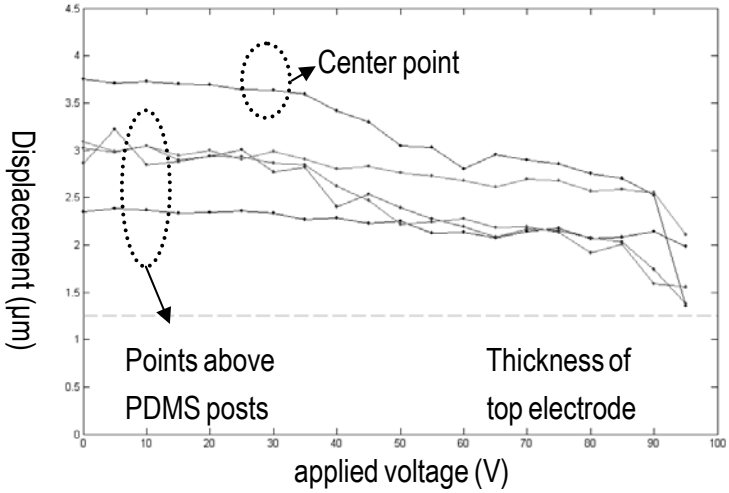

(e) Device 5 (r=4μm)

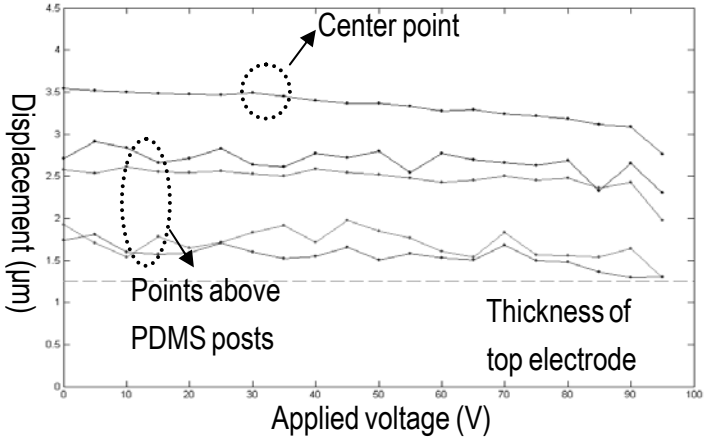

(f) Device 6 (r=4.5μm)

Figure 4-9 Displacement of top electrodes

4-3 Discussion

As shown in Figure 4-9 (a), device 1 pulled in at 70V. Therefore, the maximum displacement at center is (the original height) - (height at 65volt) = 4.042μm -2. 554μm =1.488μm. The original gap between top electrode and substrate is 2.77μm, so a displacement of 54% of the original gap is achievable. The related data of the six devices are listed in Table 4-1.

Table 4-1 The percentage of achievable displacement of six devices.

	Pull in voltage (V)	Original gap(μm)	Center displacement at pull in or max applied voltage (μm)	%
device 1	70	2.77	1.49	54%
device 2	70	2.73	1.19	44%
device 3	Not yet	2.54	0.77	30%
device 4	Not yet	2.65	1.37	52%
device 5	90	2.50	1.22	49%
device 6	Not yet	2.29	0.78	34%

Variations in Fabrication Processes

For these six devices, the relationship between the pull in voltage and the radius of PDMS post is not quite regular. One possible reason is that the flexural stiffness of the top electrode is different for different devices. The residual stress of the chromium film causes the top electrodes to curve. As mentioned in Section 3-4-2, the variations in radii of curvature are large. The shapes of the curved top electrodes are different, which results in the different flexural stiffness. Therefore, when a voltage is applied, the deflections of top electrodes for different devices are different. In addition, due to the process uncertainty, there are variations PDMS posts. The relationship between the displacement and the applied voltage should be governed by the dimensions of

PDMS posts, However, as shown in Figure 4-9 (d) and (e), for a same applied voltage, the displacement of device 5 is larger than device 4, but the elastic restoring force of PDMS posts in device 5 was designed to be larger than that in device 4. Figure 4-10 shows the measured data of another three devices, the radii of the PDMS posts are shown in the figure. It can be seen that the elastic restoring force in the center was designed to be smaller than that in the center, but the displacement was measured to be less. These results indicate that the elastic coefficient may get larger or less due to the variation in PDMS posts.

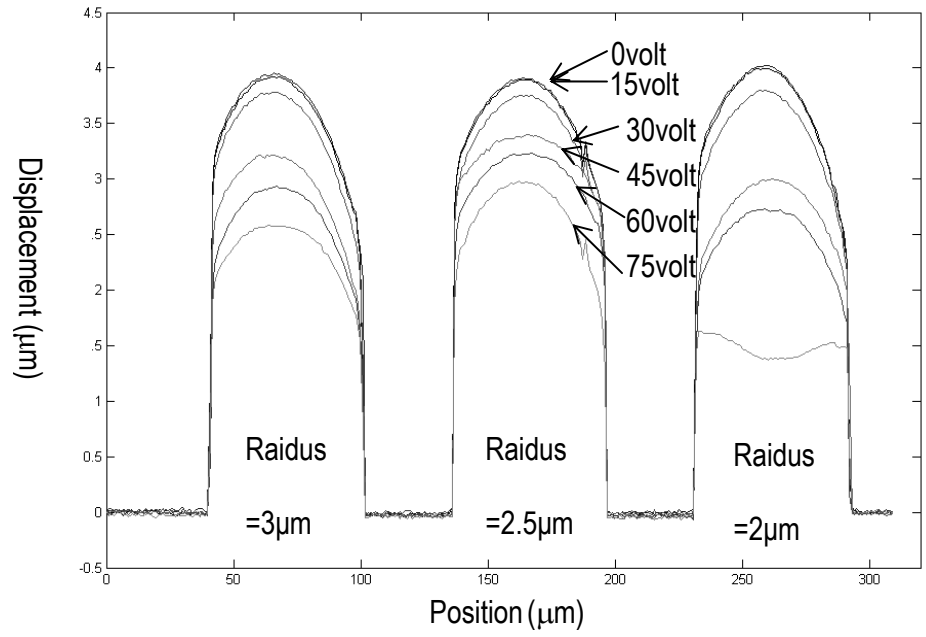

Figure 4-10 Profile data of another three devices for various applied voltage

Performance of Each Device

Figure 4-11 (a) and (b) show the displacement of the six test devices. From Figure 4-11(a), the three curves indicate that the three devices tend to displace faster vs. applied voltage before 40V, and displace slower vs. applied voltage after 40V. Such a behavior is already mentioned in Section 2-4-5, but it is much more obvious for the actual devices, especially for the devices with the PDMS posts smaller in radius. For the actuators with PDMS posts with smaller radius, although the required applied voltage is less, but the behavior is relatively nonlinear. From Figure 4-11 (b), the displacement of Device 4 is nearly linear for the applied voltage from 40V to 100V. In addition, the controllable displacement achieves the 52% of the original gap. Therefore, the PDMS post with dimension of 3.5μm in radius and 3μm in height is the most suitable elastomer structure for gap-closing actuator.

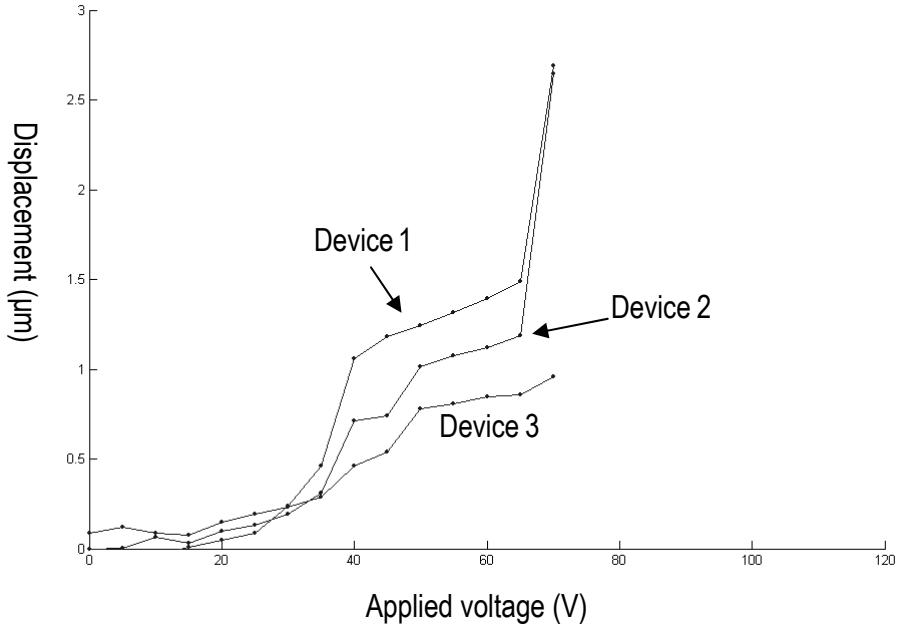

(a) Measured displacement vs. applied voltage from device 1 to device 3

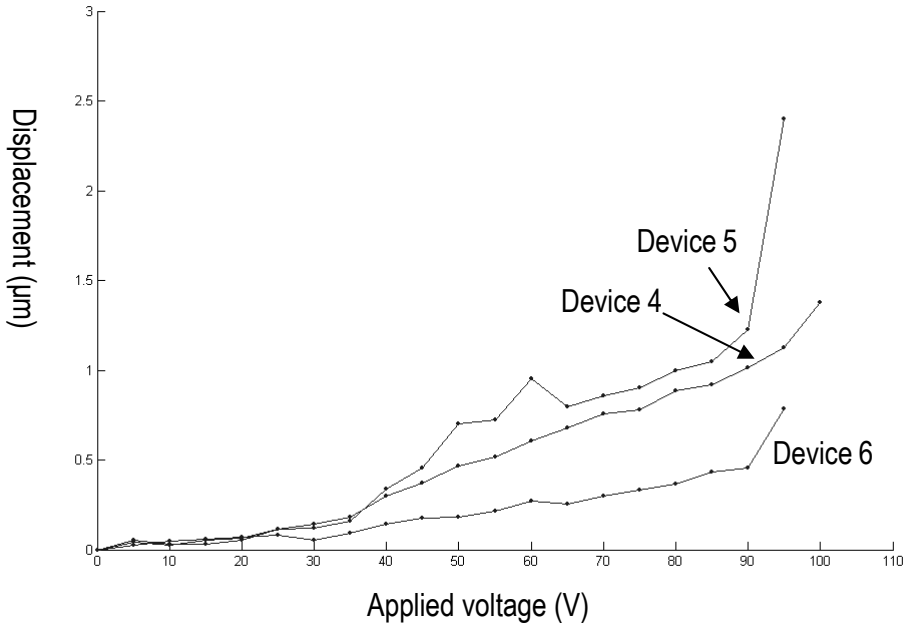

(b) Measured displacement vs. applied voltage from device 4 to device 6

Figure 4-11 Displacement of top electrode vs. applied voltage

Ⅴ、Conclusion and Future Work

The measured results reveal that the nonlinear elastic force is able to reduce the pull-in effect caused by the electrostatic force. However, there are still rooms for improvement. The improvement can be carried out from design and processing.

Design:

1. The mixing ratio of PDMS base and the curing agent affects the stiffness of the cured PDMS. A series of experiments can be carried out to obtain the relationship between the mixing ratio and the Young's modulus of the result elastomer. With such data, the device with PDMS posts with appropriate stiffness can be fabricated.
2. The flexural stiffness of the top electrode can be improved by increasing the thickness and changing the geometry. For example, it was reported that the stiffness of a plate can be enhanced with reinforced folded frames [21]. Top electrode with sufficient flexural stiffness can resist the deformation and increase the controllable displacement.

Processing:

1. To obtain PDMS posts with better shape, the processes to fill the cavities with PDMS can be improved. For example, a better top surface of PDMS posts may be obtained by adjusting the RIE recipe.
2. For polysilicon, the Young's modulus is larger and the residual stress is smaller compared with chromium. Therefore, the stiffness and flatness can be improved if the top electrode is fabricated with polysilicon. The schematic of fabrication process is shown in Figure 5-1. First, the substrate is heavily doped. A Si_3N_4 layer and a SiO_2 layer are then deposited to be the insulating layer and sacrificial layer, as shown in (a). The sacrificial layer is then patterned to define the anchor, as

shown in (b). The polysilicon layer is then deposited and patterned, as shown in (c). Then the cavities for PDMS to fill are then patterned, as shown in (d). the polysilicon and SiO_2 layers are both etched in this step. The cavities are then filled by PDMS, as shown in (e). A chromium layer is then deposited and patterned to encapsulate the PDMS, as shown in (f). The device is then released in HF, as shown in (g). Because the polysilicon layer is deposited before PDMS is filled, so PDMS will not be destroyed in the high temperature. In addition, the polysilicon is deposited before the cavities are defined, so the flatness of the top electrode will not be influenced by the cavities. The performance will be effectively improved through this device.

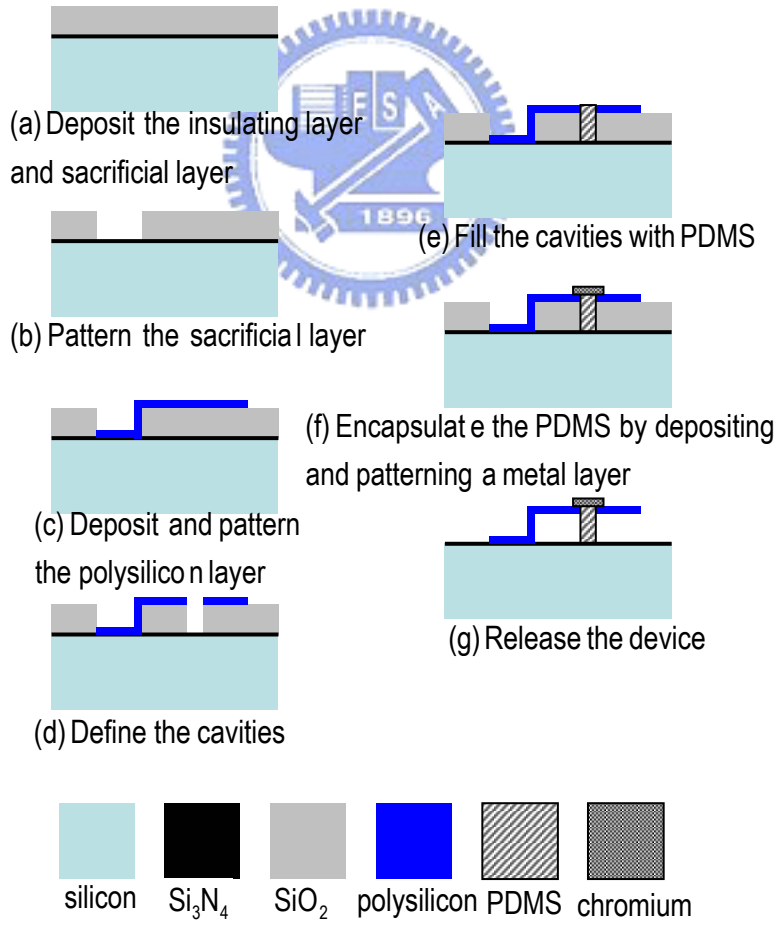

Figure 5-1 Schematic of fabrication processes of the improved device.

Reference

1. W. C. Tang, T.-C. H. Nguyen, and R. T. Howe, “Laterally driven polysilicon resonant microstructures”, Proceedings, IEEE Micro Electromechanical Systems Workshop, February 1989, pp. 53-59.
2. J. E. Mark and J. Lal, “Elastomer and Rubber Elasticity”, 1982, ACS symposium series, pp. 309-328.
3. J. M. Gere, and S. P. Timoshenko, “Mechanics of Materials”, 4th edition, 1997, PWS Publishers, pp.3-26, 609-610, 890.
4. L. J. Hornbeck, “From cathode ray to digital micromirrors: A history of electronic projection display technology”, TI Technical Journal, July-September 1998, pp. 7-46.
5. R. K. Gupta, S. D. Senturia, ”Pull-in time dynamics as a measure of absolute pressure”, Proceedings, IEEE Micro Electromechanical Systems Workshop, January 1997 pp. 290 - 294
6. E. K. Chan and R. W. Dutton, ”Electrostatic Micromechanical Actuator with Extended Range of Travel”, Journal of Microelectromechanical Systems, Vol. 9, No. 3, September 2000, pp. 321-328.
7. R. Nadal-Guardia, A. Dehe, R. Aigner, and L. M. Castaner, “Current Drive Methods to Extend the Range of Travel of Electrostatic Microactuators Beyond the Voltage Pull-In Point”, Journal of Microelectromechanical Systems, Vol.11 No. 3, June 2002, pp.255-263.
8. O. Degani, and Y. Nemirovsky, “Design Considerations of Rectangular Electrostatic Torsion Actuator Based on New Analytical Pull-in Expressions”, Journal of Microelectromechanical Systems, Vol.11 No.1, February 2002,

pp.20-26.

9. D. C. Duffy, J. C. McDonal, O. J. A. Schueller, and G. M. Whitesides, “Rapid Prototyping of Microfluidic Systems in Poly(dimethylsiloxane)”, Analytical Chemistry, Vol.70, No. 23, December 1,1998, pp.4979-4984.
10. D. C. Duffy, O. J. A. Schueller, S. T. Brittain, and G. M. Whitesides, “Rapid Prototyping of Microfluidic Switches in Poly(Dimethyl Siloxane) and Their Actuation by Electro-Osmotic Flow”, Journal of Micromechanics and Microengineering. Vol.9, No.3, 1999, pp.211-217.
11. B.-H. Jo, L. M. V. Lerberghe, K. M. Motsegood, and D. J. Beebe, “Three-dimensional Micro-Channel Fabrication in Polydimethylsiloxane (PDMS) Elastomer”, Journal of Microelectromechanical Systems, Vol. 9, No.1, March 2000, pp.76-81.
12. J. Garra, T. Long, J. Currie, T. Schneider, R. White, and M. Paranjape, “Dry etching of polydimethylsiloxane for microfluidic systems”, Journal of Vacuum Science & Technology A-Vacuum Surfaces & Films, Vol.20, No.3, May 2002, pp.975-982.
13. E. Leclerc, Y. Sakai, T. Fujii, “Perfusion Culture of Fetal Human Hepatocytes in PDMS Bioreactors”, Engineering in Medicine and Biology Society, Proceedings of the 25th Annual International Conference of the IEEE, Vol. 2, September, 2003, pp.1211-1214
14. X. Yang, C. Grosjean, and Y.-C. Tai, “Design, Fabrication, and Testing of Micromachined Silicone Rubber Membrane Valves”, Journal of Microelectromechanical Systems, Vol.8, No. 4, December 1999, pp. 393-402.
15. J. C. Lotters, W. Olthuis, P. H. Veltink, P. Bergveld, “Polydimethylsiloxane, a photocurable rubberelastic polymer used as spring material in micromechanical

sensors", Microsystem Technologies, Vol. 3, No. 2, February, 1997, pp. 64-67.

16. J. C. Lotters, W. Olthuis, P. H. Veltink, P. Bergveld, "Characterisation of a Highly Symmetrical Miniature Capacitive Triaxial Accelerometer", Transducers '97, 1997 International Conference on Solid-State Sensors and Actuators, June, 1997, pp. 1177-1180.
17. Y. Xia, E. Kim, X.-M. Zhao, J. A. Rogers, M. Prentiss, and G. M. Whitesides, "Complex Optical Surfaces Formed by Replica Molding Against Elastomeric Masters", Science, Vol. 273, July 1996, pp. 347-349.
18. F.-G. Tseng, lecture notes of Micro System Design.
19. K. R. Williams, K. Gupta, and M. Wasilik, "Etch Rates for Micromachining Processing-Part II", Journal of Microelectromechanical Systems, Vol.12, No.6, December 2003, pp. 761-778.
20. S. D. Senturia, "Microsystem Design",2001, Kluwer Academic Publishers, pp. 222-224.
21. A. Tomanek, "Silicones & Industry, A compendium for practical use, instruction and reference", Wacker-Chemie GmbH, Munich Publishers.
22. H.-Y. Lin and W. Fang "The Improvement of the Micro Torsional Mirror by a Reinforced Folded Frame," the ASME Proceedings of the 2000 International Mechanical Engineering Congress and Exhibition (IMECE), Orlando, FL, USA.
23. T. Fujii, "PDMS-based microfluidic devices for biomedical applications", Microelectronic Engineering, vol.61-62, July 2002, pp.907-914.